EXOPRIME TECHNOLOGY FOR EXOSOMAL MIRNA ANALYSIS AND IDENTIFICATION OF OXIDATIVE DNA DAMAGE-INDUCED MIRNA REGULATORY NETWORK IN HUMAN ASTROCYTES

by

Chukwumaobim Daniel Obiwulu Nwokwu, M. S.

A Dissertation Presented in Partial Fulfillment
of the Requirements of the Degree
Doctor of Philosophy

COLLEGE OF ENGINEERING AND SCIENCE
LOUISIANA TECH UNIVERSITY

November 2021

LOUISIANA TECH UNIVERSITY

GRADUATE SCHOOL

September 28, 2021
Date of dissertation defense

We hereby recommend that the dissertation prepared by

Chukwumaobim Daniel Obiwulu Nwokwu, M.S.

entitled **ExoPRIME technology for exosomal miRNA analysis and identification of oxidative DNA damage-induced miRNA regulatory network in human astrocytes**

be accepted in partial fulfillment of the requirements for the degree of

Doctor of Philosophy in Molecular Sciences and Nanotechnology

gergana nestorova
Gergana G. Nestorova
Supervisor of Dissertation Research

gergana nestorova
Gergana G. Nestorova
Head of Molecular Sciences and Nanotechnology

Doctoral Committee Members:
Teresa A. Murray
Scott Poh
Jeff Shultz
Prerna Dua

Approved:
Hisham Hegab
Dean of Engineering & Science

Approved:
Ramu Ramachandran
Dean of the Graduate School

ABSTRACT

The high lipid content of the brain, coupled with its heavy oxygen dependence and relatively weak antioxidant system, makes it highly susceptible to oxidative DNA damage that contributes to neurodegeneration. This study assesses and compares the neurotoxic effects of proton and photon radiation on mitochondrial function and DNA repair capabilities of human astrocytes. Human astrocytes received either proton (0.5 Gy and 3 Gy), photon (0.5 Gy and 3 Gy), or sham-radiation treatment. The mRNA expression level of the human base-excision repair protein, 8-deoxyguanosine DNA glycosylase 1 (hOGG1) was determined via RT-qPCR. Radiation-induced changes in mitochondrial mass and oxidative activity were assessed using fluorescent imaging with MitoTracker™ Green FM and MitoTracker™ Orange CM-H_2TMRos dyes, respectively. A significant increase in mitochondrial mass and levels of reactive oxygen species was observed after radiation treatment. This was accompanied by a decreased OGG1 mRNA expression. These results are indicative of a radiation-induced dose-dependent decrease in mitochondrial function, an increase in senescence and astrogliosis, and impairment of the DNA repair capabilities in healthy glial cells. Photon irradiation was associated with a more significant disruption in mitochondrial function and base-excision repair mechanisms *in vitro* in comparison to the same dose of proton treatment.

This study further identifies specific ROS-responsive miRNAs that modulate the expression and activity of the DNA repair proteins in human astrocytes, which could lead

to the development of targeted therapeutic strategies for neurological diseases. Oxidative DNA damage was established after treatment of human astrocytes with 10 μM sodium dichromate for 16 hours. Comet assay analysis indicated a significant increase in oxidized guanine lesions. PCR analysis confirmed that sodium dichromate reduced the mRNA expression levels of hOGG1. Small RNAseq was performed on an Ion Torrent™ system and the differentially expressed miRNAs were identified using Partek Flow® software. The biologically significant miRNAs were selected using miRNet 2.0. Oxidative-stress-induced DNA damage was associated with a significant decrease in miRNA expression: 231 downregulated miRNAs and 2 upregulated miRNAs ($p < 0.05$; > 2-fold). In addition to identifying multiple miRNA-mRNA pairs involved in DNA repair processes, this study uncovered two novel miRNA-mRNA pairs interactions: miR-1248:OGG1 and miR-103a-OGG1. Inhibition of miR-1248 and miR-103a via the transfection of their inhibitors restored the increased expression levels of hOGG1. Therefore, targeting the identified microRNAs could ameliorate the nuclear DNA damage caused by exposure to mutagens. The miRNA candidates identified in this study could serve as potential biomarkers and therapeutics for oxidative stress in the brain to reduce the incidence and improve the treatment of cancer and neurodegenerative disorders.

In a parallel but closely related study, we report a direct, one-step exosome sampling technology, for selective capture of CD63+ exosome subpopulations using an immune-affinity protocol. The ExoPRIME microprobe provides a **P**recise **R**apid **I**nexpensive **M**ild (non-invasive) and **E**fficient (i.e. **PRIME**) alternative to the conventional polymer precipitation-based methods by enriching a comparatively more homogenous exosome population. The tool consists of an inert Serin™ stainless steelz

microneedle (300 μm in diameter × 30 mm in height), pre-coated with a thin-film polyelectrolyte layer that serves as a substrate for covalent bonding of biotin. An anti-CD63 steptavidin-conjugated antibody that selectively binds to the corresponding tetraspanin embedded in the lipid bilayer of exosomes was immobilized to the outer surface of the probe. The feasibility of the ExoPRIME technology was validated using two types of biological samples: conditioned astrocyte medium (CAM) and astrocyte-derived exosome suspension (EXO). The study investigated the impact of the temperature (4°C and 22°C) and incubation duration (2h and 16h) on the capture efficiency of the ExoPRIME tool. A fluorescence-based enzymatic assay for exosome quantification was used to assess the probe's exosomes capture efficiency and the reproducibility of the technology. The low level of non-specific binding initially observed in non-functionalized microneedles was drastically minimized by blocking the ExoPRIME probe with 0.1% BSA. The ExoPRIME microprobe captured exponentially more exosomes than the non-functionalized microneedle that indicates enrichment of CD63-expressing exosomes.

A major advantage provided by the ExoPRIME technology over existing platforms is its applicability over a broad dynamic range of temperature and incubation parameters without compromising the purity and viability of exosomal cargoes. The loading capacity of the probe increased after incubation for 16 h at 4^0C in exosome suspension (24×10^6 exosomes per probe) while the efficiency decreased 10 folds after 2 h at 4^0C (24×10^5 exosomes per probe). The increase in temperature had an impact on the stability of the reagents that contributed to a 2-fold efficiency reduction after incubation in exosome suspension for 16 h at 22^0C (12×10^6 exosomes per probe). However, the 2-hour room-temperature incubation (2 h at 22^0C) of the ExoPRIME probe yielded an increased capture

efficiency (12×10^6 exosomes per probe) when compared to the 2 h at 4°C incubation (24×10^5 exosomes per probe). These results suggest that lower temperatures with extended incubation times constitute the most optimal parameters that ensure high probe loading capacity.

Another advantage of the ExoPRIME microprobe is that it captures antigen-specific subpopulation of exosomes directly from conditioned astrocyte medium (CAM), eliminating the requirements for additional filtration and pre-concentration, and thereby cutting down costs and handling time. Besides the relatively reduced number of enriched exosomes, the CAM results are consistent with the trend obtained for EXO incubations, a phenomenon that could be attributed to the presence of various extracellular proteins and cellular debris, which could mask antibodies and compete physically with exosomes for binding. The capabilities to integrate different incubation times, temperatures, and biofluid type thus present exosome researchers with the flexibility to choose the combined parameters that best suit their purpose, the desired factor in clinical and laboratory applications.

The developed tool requires very low amounts of antibody, permits the use and re-use of minimal sample volumes (≤ 200 μL), can be multiplexed in arrays to diagnostically profile multiple exosome classes and is amenable to integration into a lab-on-a-chip platform to achieve parallel, high-throughput isolation in a [semi]-automated workstation. Moreover, this platform could provide direct exosomal analysis of biological fluids since it can elegantly interface with existing picomolar-range nucleic acid assays to provide a clinical diagnostic tool at the point of care and facilitate fundamental studies in exosomes functions.

APPROVAL FOR SCHOLARLY DISSEMINATION

The author grants to the Prescott Memorial Library of Louisiana Tech University the right to reproduce, by appropriate methods, upon request, any or all portions of this Dissertation. It is understood that "proper request" consists of the agreement, on the part of the requesting party, that said reproduction is for his personal use and that subsequent reproduction will not occur without written approval of the author of this Dissertation. Further, any portions of the Dissertation used in books, papers, and other works must be appropriately referenced to this Dissertation.

Finally, the author of this Dissertation reserves the right to publish freely, in the literature, at any time, any or all portions of this Dissertation.

Author _____

Date _____

DEDICATION

To:

My Beloved Mama, **Obianuju C. Nwokwu** (of Blessed Memory) – whose spirit has been my staying power in my biomedical research adventures. Each time I was tempted to quit the rigors of Science, I was spurred by the indelible vivid imagery of her courageous struggle with cancer and by my bedside/graveside commitment to her to work towards a cure to that tormentor of mankind. Nne m oma, uche m ka di ya!

To:

My beautiful and supportive wife, and best friend, **Premina Obianuju Chukwumaobim** – who has made me a proud father! She has also been my backbone through this doctoral journey and helped immensely with the formatting of this dissertation.

And to:

Our unborn baby, **"Chemi"** whose epochal arrival in the wake of notable events and great fortunes is nothing short of the Divine – *Omalubiauwa, Obianuju, Nnemabia*. May your birth herald times of refreshing for Ndigbo worldwide and usher in "the country we deserve".

TABLE OF CONTENTS

LIST OF FIGURES

LIST OF TABLES

ACKNOWLEDGMENTS

My profound gratitude goes to **Chukwu Okike Abiama** (The Most High God) in whom I live and move and have my being. I could not have achieved this feat of bagging a doctorate degree, considered the pinnacle of academic pursuit, without His unseen hands steadying and steering my tempest-tossed ship.

The statement is true that "a teacher affects eternity; he can never tell where his influence stops". So, I would like to acknowledge the efforts of all my teachers and academic mentors in forging me into the well-rounded man I am today. The special icing on this cake is my PhD advisor and mentor, **Dr. Gergana G. Nestorova**, for her scholarly critiquing, legendary patience and understanding, responsible and responsive mentoring, and most importantly, her affability and open-door policy that makes her approachable (I look forward to future research collaborations with her). Her innovative ideas and the grants that she attracted through the course of my scholastic foray made these projects possible. Thus we are thankful to the following funding agencies: the Louisiana Board of Regents through its Research Competitiveness Subprogram (RCS) support fund, NASA EPSCoR, the Center for Biomedical Engineering and Rehabilitation Science (CBERS) and the School of Biological Sciences at Louisiana Tech University.

Under Dr. Nestorova's tutelage and mentorship, I have evolved into a seasoned scientist, gaining a wide array of scientific and professional skills which I believe would be of immense benefit in my chosen career going forward. Furthermore, I would like to

thank other members of my advisory committee, **Dr. Teresa A. Murray**, **Dr. Scott Poh**, **Dr. Jeff Shultz**, and **Dr. Prerna Dua**, for their invaluable inputs to make this dissertation more sound and robust.

I will not fail to recognize members of Nestorova Lab – my research team, past and present; they were angels in laboratory coats. Worthy of mention are **Saif Ishraq Mohammed Bari** and **Ms. Hope Hutson** for their specific contributions to certain aspects of these dissertation projects. My **"Shadow Assistant"** – my lab coat of 18 years – deserves honorable mention, having followed me as I traversed and sojourned in three different continents in pursuit of my Bachelor's, Master's, and now, my Doctorate degrees. Whenever I don this "magical" tuxedo, I am in my elements, firing from all cylinders,

Because every falling leaf rests on its roots, I would like to appreciate my immediate family members: my Papa, **Obiwulu E. Nwokwu** and my stepmother, **Nkechi F. Nwokwu** – both of whom have been my indefatigable cheerleaders; and my siblings, **Eberechukwu Aniagboso**, **Ogochukwu Nwosu**, and **Tochukwu Nwokwu** – whose ceaseless prayers and encouragement infused me with the strength to keep trudging on. I am indebted in no small measure to my American Mum, **Prof. Stephanie Carwile** and her husband, **Prof. Guy Carwile** – who treated me as their adopted son and greatly helped me ease through this phase of my life. Indeed, as the Igbo say, *"Nwanne di na mba"* (Brotherhood knows no boundaries).

Finally, I extend my heartfelt gratitude to every person and/or circumstance that inspired me by their action or inaction, or those whose contribution(s) might have passed unnoticed. God bless you all!

CHAPTER 1

INTRODUCTION

1.1 Goals and Objectives

The overall goal of this study is to investigate the role of short regulatory RNAs in human astrocytes. The scientific work included the following specific objectives: (1) assess and compare the impact of proton and photon irradiation on the mitochondrial function and DNA repair capability of human astrocytes; (2) identify miRNAs that are involved in mediating oxidative stress-induced DNA repair response in human astrocytes; (3) identify and validate the functional relationship between novel regulatory miRNAs and the human base-excision repair protein, hOGG1; and (4) develop a platform for rapid, selective purification and genetic analysis of antigen-specific exosomal miRNAs.

1.2 Significance

Nucleic acids are susceptible to oxidation by environmental and endogenous factors. Impairment and mutations in the DNA repair pathways in glial cells are associated with neurodegenerative disorders and premature aging [1]. Oxidative DNA damage is repaired primarily by DNA glycosylases, part of the base excision repair pathway which removes damaged bases in a substrate-specific manner. One of such enzymes is the human 8-deoxyguanosine DNA glycosylase 1 (hOGG1), a bi-functional 8-OHdG-specific glycosylase that plays an important role in reducing the rate of mutation. By providing the

first line of defense against oxidative DNA damage, OGG1 plays an important role in decreasing the detrimental effects of oxidative DNA damage [2]. Therefore, the expression levels of OGG1 provide an assessment of the cell's DNA repair capability.

The high lipid content of the brain (phospholipids, polyunsaturated fatty acids), coupled with its heavy dependence on oxygen and relatively weak antioxidant system, makes it more susceptible to oxidative stress-induced DNA damage [3]. Astrocytes, a major glial cell type, play a critical role in modulating synaptic transmissions, regulating energy metabolism, water and ion homeostasis, and protecting neurons from oxidative stress [4,5]. Photon and proton radiation therapies are widely used for the treatment of glial cell primary tumors, however, the biological effect of proton radiotherapy versus photon radiotherapy on cellular DNA repair capabilities and mitochondrial response in glial cells is still poorly understood. Astrocytes perform several functions that are essential for normal neuronal activity, including glutamate uptake and release, K+, and H + buffering, and water transport [6]. Therefore, astrocyte function can critically influence the survival and the physiological state of the neurons during radiation-associated brain insults. Previous work indicates that astrocytes have a higher threshold for apoptotic activation when exposed to radiofrequency radiation than neurons [7].

Exposure to high-energy radiation leads to an increased production of reactive oxygen or nitrogen species that are associated with the transmission of radiation damage among mitochondria [8]. Mitochondrial dysfunction is characterized by reduced oxidative capacity and diminished ATP production and is a major hallmark of radiation-induced DNA damage and senescence in neurological tissue [9]. Impaired ability to repair radiation-induced mtDNA damage is associated with reductions in mitochondrial gene

expression and ATP generation [10]. Investigating the impact of ionizing radiation on DNA repair mechanisms and mitochondrial function of healthy human astrocytes is important for the assessment of the secondary risk of radiation-induced injuries (Figure 1-1) [1].

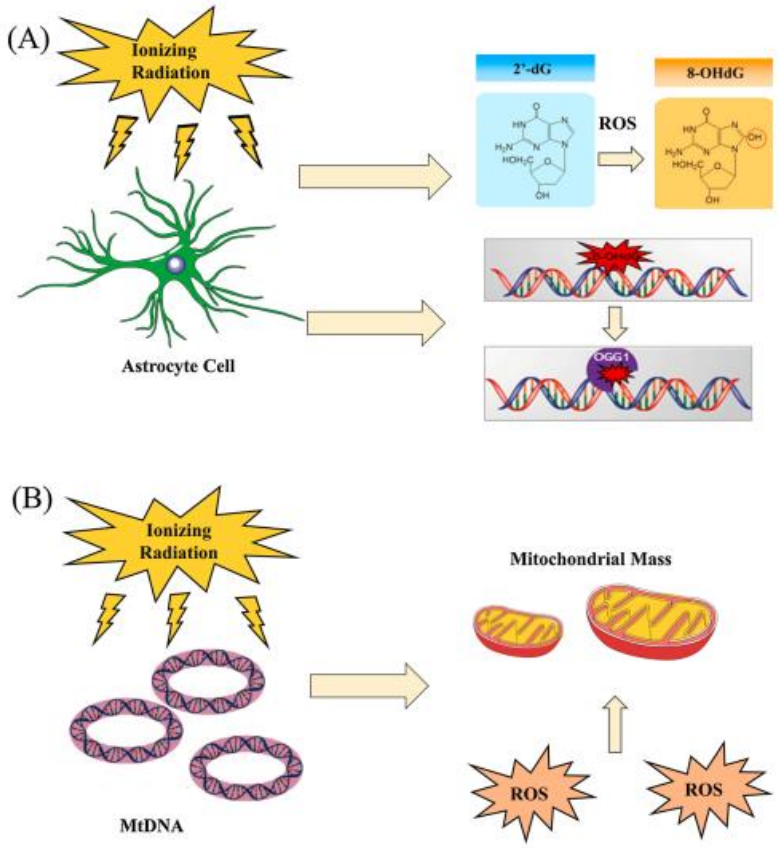

Figure 1-1 Schematic of experimental workflow. Human astrocytes were treated with 0.5 Gy and 3 Gy proton and photon radiation. (A) Gene expression of OGG1; and (B) mitochondrial mass and oxidative activity were assessed 16 h post-treatment [11]

MicroRNAs (miRNAs) are small non-coding RNAs (17 – 25 nts) that inhibit gene expression at the post-transcriptional level [12]. Growing evidence suggests a reciprocal connection between ROS signaling and the microRNA regulatory pathways. It has been

[1] K.H. Hutson, K. Willis, C.D. Nwokwu, M. Maynard, G.G. Nestorova, Neurotoxicology Photon versus proton neurotoxicity : Impact on mitochondrial function and 8-OHdG base-excision repair mechanism in human astrocytes, *Neurotoxicology*. 82 (2021) 158–166. https://doi.org/10.1016/j.neuro.2020.12.011.

reported that ROS are implicated in various steps of miRNA biogenesis via the control of transcription factors [13,14], epigenetic regulatory enzymes, and miRNA maturation proteins [15]. Identification of specific miRNA types with a functional role in modulating the activity of DNA repair proteins could lead to a better assessment of the response of glial cells to ROS-induced oxidative damage. Currently, there are no reports on a high-throughput analysis of miRNA expression following exposure of human astrocytes to oxidative DNA damage. The discovery of ROS-responsive miRNAs provides a potential novel strategy to specifically overcome ROS-mediated pathological conditions. An increased understanding of how miRNAs regulate DNA repair in astrocytes will expand the potential for miRNA-based therapeutics that will substantially improve the outlook for patients with cancer and age-related neurodegenerative disorders (Figure 1-2).

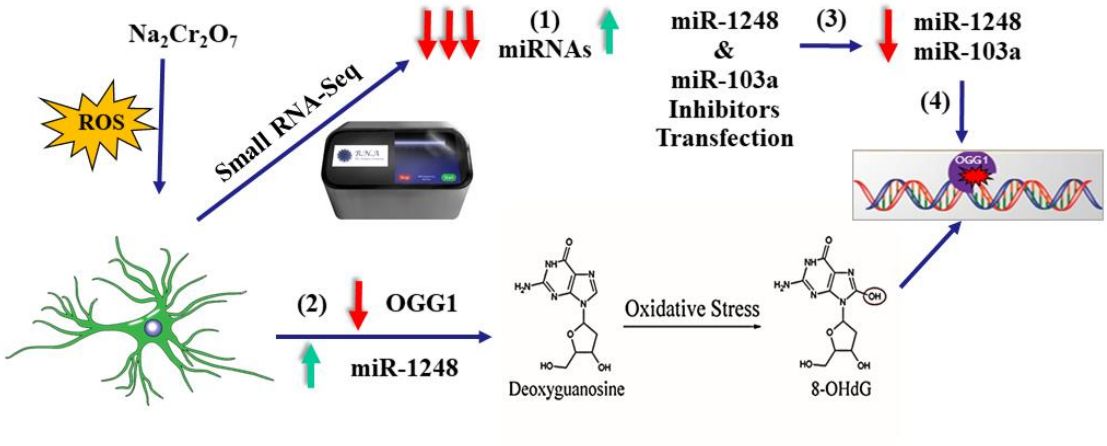

Figure 1-2 Schematic of experimental workflow that includes induction of oxidative DNA damage using sodium dichromate treatment followed by small RNA sequencing, computational analysis of differentially expressed targets, and the restorative effect of miR-1248 and miR-103a inhibition on OGG1-mediated DNA repair mechanism

Exosomes (30 – 150 nm) secreted by host cells play an important role in cell-to-cell communication since they encapsulate a diverse pool of non-coding microRNAs that are capable of reprogramming protein expression in recipient cells [16,17]. Compelling evidence indicates that exosome-mediated transfer of genetic material is superior to direct contact [18]. Thus, exosomes are considered a promising source of biomarkers for disease diagnosis including cancer [19,20], glioblastoma [21], diabetic cardiomyopathy [22], arthritis [23], asthma [24], urinary tract infection [25], and neurodegeneration [26], since their biological cargo reflects the pathophysiological condition of the host cell. Exosomes are released under normal physiological conditions, but their number is often increased upon cellular activation or neoplastic transformation [27]. The ease of access to exosomes from virtually any biological fluid forms the rationale for their use as non-invasive biomarkers for disease diagnostics [28,29].

Exosomal membranes are enriched in tetraspanins (CD63, CD9, and CD81) that are used as biomarkers for disease diagnostics and prediction of therapeutic response [30]. However, the clinical applications of exosomes have not been fully realized due to technical challenges associated with traditional and newer methods for exosome isolation [31,32]. Inefficient purification techniques lead to the extraction of heterogeneous extracellular vesicles that have different sizes, surface proteins, or cellular origins. Selective isolation of surface-protein marker-specific exosomal subpopulations for subsequent genetic analysis is critical in studies to evaluate their clinical relevance [33]. For example, CD63-positive exosomes are present at a higher level in malignant cells compared to healthy ones [34], while exosomes secreted in cerebrospinal fluid carry specific markers such as Alix, syntenin-1, heat shock proteins, and tetraspanins [35] that may provide crucial information for neurodegenerative disorders. Therefore, a technology that can isolate an exosomal subpopulation that expresses a specific surface marker can be used as a biomarker detection platform for disease diagnosis and treatment monitoring, since disease-responsive exosomes encapsulate proteomic and genomic cargoes that are unique to diseased tissues. Such technology is especially relevant for tissues that are not directly accessible, such as the central nervous system, offering a precise and non-invasive approach to liquid biopsy and clinical care.

A solid-phase exosome isolation method circumvents the shear strain from sample-reagent mixing and pelletization that increases the likelihood for specimen destruction. The proposed microneedle-based, antibody-functionalized platform can provide direct enrichment of intact exosomes from all types of biological fluids with high spatial resolution that can be leveraged upon for *in situ* immunofluorescence assays, without

compromising exosome structure. Furthermore, the microprobe has the prospects for integration with microfluidics-based standard systems for genomic and proteomic analysis of exosomal cargoes, thereby offering a potential clinical diagnostic tool at the point of care (Figure 1-3) [2].

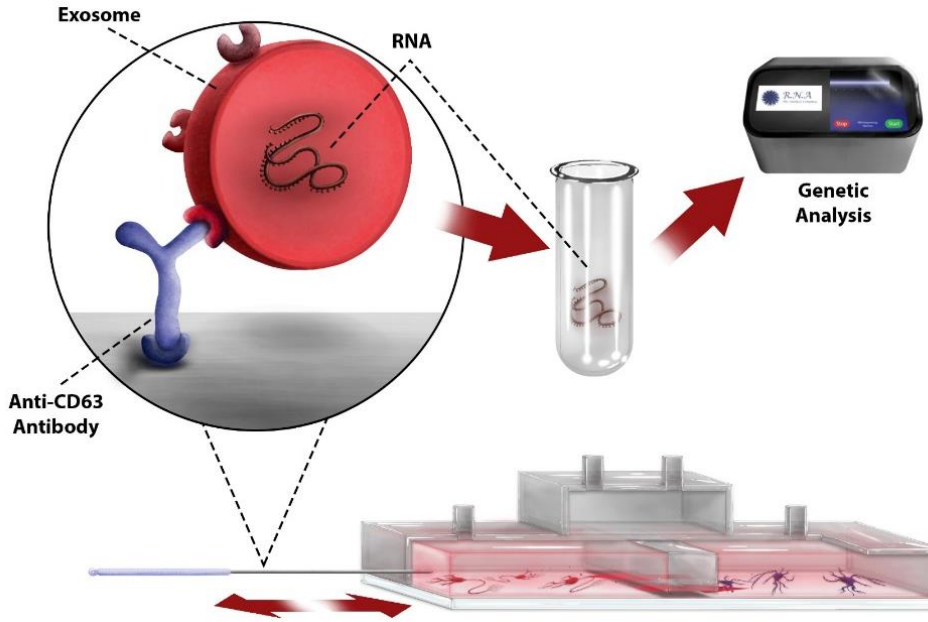

Figure 1-3 A Prototype Design of a Benchtop [Semi-]automated ExoPRIME Technology depicting Integration with Microfluidics and Bioanalytical Platforms [36]

1.3 Non-Coding RNAs

1.3.1 Types and Physiological Roles

The discovery of non-coding RNAs brought the realization that gene expression is a much more intricate phenomenon than initially thought. Non-coding RNAs (ncRNAs) are a class of RNA species that do not encode proteins and so were thought for a long time to be part of the so-called "junk DNA" [37,38]. However, research in the last three decades

[2] C.D. Nwokwu, S.M. Ishraq Bari, K.H. Hutson, C. Brausell, G.G. Nestorova. ExoPRIME: Solid-phase immunoisolation and OMICS analysis of surface-marker-specific exosomal subpopulations, Talanta 236(2022):122870. https://doi.org/10.1016/j.talanta.2021.122870.

has proven that these RNA transcripts give rise to functional RNAs that impact the regulation of transcription, RNA processing, and translation and, therefore, play critical roles in a variety of biological processes [39–41]. The ribosomal RNA (rRNA) directs the catalytic steps of protein synthesis [42], while the transfer RNA (tRNA) serves as an adaptor molecule between the amino acids and the mRNA during protein synthesis [43].

Except for ribosomal rRNAs, small nuclear RNAs (snRNAs), small nucleolar RNAs (snoRNAs), and tRNAs, the remaining ncRNAs are generally grouped into long ncRNAs (lncRNAs) of more than 200 bases, and the small ncRNAs that are usually less than 200 bases and include microRNA (miRNA), short interfering RNA (siRNA), and piwi-interacting RNA (piRNA). Intronic sequences constitute 30% of the human genome and are the major sources for lncRNAs (intronic lncRNAs); so lncRNAs sequences are spread over the entire genome and can be found on all chromosomes [44]. Although their genes are not subject to the same histone modifications (H3K4me3 and H3K36me), the process of lncRNA transcription and maturation is similar to that of messenger RNA (mRNA): transcribed by RNA polymerase II, undergoes 3' poly-(A) tailing and 5'end-capping as well as splicing. Unlike miRNAs that have a well-established mechanism of action, causing translation inhibition or mRNA degradation, lncRNAs have diverse functionalities depending on their subcellular localization and how they interact with proteins as well as with RNA or DNA. In their role in nuclear organization, lncRNAs modulate chromatin function and interfere with signaling pathways. Their association with ribosomes in the cytoplasm suggests an additional role in mRNA metabolism [45]. Interestingly, lncRNAs are reported to have miRNA binding sites that enable them to sequester miRNAs and competitively reverse gene repression by miRNAs [46]. Recent

discoveries point to embedded miRNA sequences within lncRNAs, suggesting that they could be a source of miRNAs [47].

The first small endogenous ncRNAs (lin-4/let-7) were described in *C. elegans* in 1993 by Lee and co-workers [48], and these RNAs were eventually called microRNAs (miRNAs) [49–52]. These single-stranded RNAs are characterized by their size of about 17–25 nucleotides and are highly conserved during evolution [49] in contrast to the poorly conserved and least characterized lncRNA family [53]. Whole-genome and transcriptome analysis estimates that there are about 23,000 lncRNAs, comparable to the number of protein-coding RNAs and much higher than the number of miRNAs (put at approximately 2000) [44,54].

The major classes of small non-coding RNAs, their size, origin, and function are summarized in Table 1-1.

Table 1-1 Major Classes of Small Noncoding RNAs

Class	Size	Biogenesis	Number of Members (Humans)	Function
microRNA (miRNA)	21 – 23 nt	Processed by DICER from 65 to 70 nt precursors	>2500	Regulation of gene expression
piwi-RNA (piRNA)	25–33 nt	Nuclear precursor amplified by ping pong mechanism in the cytoplasm	>20,000	Regulation of retro transposons
Endogenous silencing RNA (endo-siRNA)	21–26 nt	Processed from messenger RNA transcripts	Unknown	Regulation of gene expression
Small nucleolar RNA (snoRNA)	60–300 nt	Processed from messenger RNA introns	>260	Chemical modification of other RNAs
Small nuclear RNA (snRNA)	150 nt	RNA polymerase II and III	9 families	Splicing of other RNAs
Transfer RNA (tRNA)	73–93 nt	RNA polymerase III	>500	Translation of mRNA to protein
microRNA off-setRNA (moRNA)	19–23 nt	Processed from miRNA precursor	Unknown	Unknown
Enhancer RNA (eRNA)	50–2000 nt	Nascent RNA transcription	>2000	Regulate proximal gene expression

[Adapted from [55]]

1.3.2 MicroRNAs (miRNAs)

Among the short regulatory ncRNAs, miRNAs (approximately 17 – 25 nucleotides long) have generated the most interest because they exert a pleiotropic and redundant effect on gene expression, modulating a variety of biological functions, including organismal development, cellular signaling, and disease pathology [56]. A single miRNA can control hundreds of target genes, and multiple miRNAs can target a single gene. There are at least

2000 different kinds of miRNAs and the number is even estimated to be up to 20,000 [57]. It is estimated that more than half of the human transcriptome is under miRNA regulation [58,59]. These small, non-coding RNAs regulate gene expression in a sequence-specific manner by inducing mRNA degradation or translational repression [60].

MiRNAs have recently emerged as important regulators of disease progression and development. MiRNA expression profiles are altered by oxidative stress [61], cancerogenesis [62], age-related neurological disorders [63], and ionizing radiation [64]. Aberrant miRNA expression is associated with cancer development, progression, and response to therapy, suggesting the possible use of miRNAs as diagnostic biomarkers. Moreover, an increasing number of studies demonstrate that miRNAs can function as potential oncogenes or oncosuppressor genes that intervene in the various aspects of cancer development and progression, including apoptosis, angiogenesis, and neoplastic microenvironment (Allegra et al., 2012). While the role of miRNA in carcinogenesis and neurological disorders is a relatively new area of research, due to its therapeutics potential, the field is rapidly growing and numerous miRNAs that modulate disease-related physiological processes have been identified [66].

1.3.2.1 miRNA Biogenesis

Short and long ncRNAs differ in their origin, processing, and mode of action. The canonical miRNA biosynthetic and maturation pathway is a complex multi-step process and begins with their transcription by RNA polymerase II (or III for miRNAs encoded within Alu repeat sequences) [67] into primary miRNAs (priRNAs) from intergenic or intronic/exonic loci, often during transcription of their host genes [68]. The genome-encoded pri-miRNAs are then processed (cleaved) in the nucleus by an enzyme, Drosha to

generate approximately 70-nucleotide long precursor miRNAs (pre-miRNAs) which is hairpin-shaped [69]. Exportin-5, a Ran-GTP-binding nuclear transporter mediates the transport of pre-miRNAs from the nucleus to the cytoplasm where the RNAse III-like enzyme Dicer and TARBP2 (TAR binding protein 2) cleaves pre-miRNAs into a transient duplex of around 17 – 25 nt in size, made up of the functional miRNA strand (guide strand) and the passenger strand [70,71]. Of these two strands, the "passenger" strand is degraded, while the other active "guide" strand becomes the mature miRNA that is loaded onto an Argonaute protein in the RNA-Induced Silencing Complex (RISC).

An alternative, non-canonical pathway for miRNA biogenesis, also called the Mirtron pathway [72], involves the splicing of intronic sequences and debranching of the primary miRNA (priRNA) by a lariat debranching enzyme (Ldbr) after which they are folded into precursor miRNA (pre-miRNA) hairpins, and becomes merged with the canonical pathway. So, essentially, as short hairpin RNA molecules that are derived from spliced introns, they bypass the nuclear Drosha-DGCR8 micro compressor complex and become cleaved by Dicer in the cytoplasm into mature miRNAs. A schematic of the distinct stages in miRNA processing is depicted in Figure 1-4.

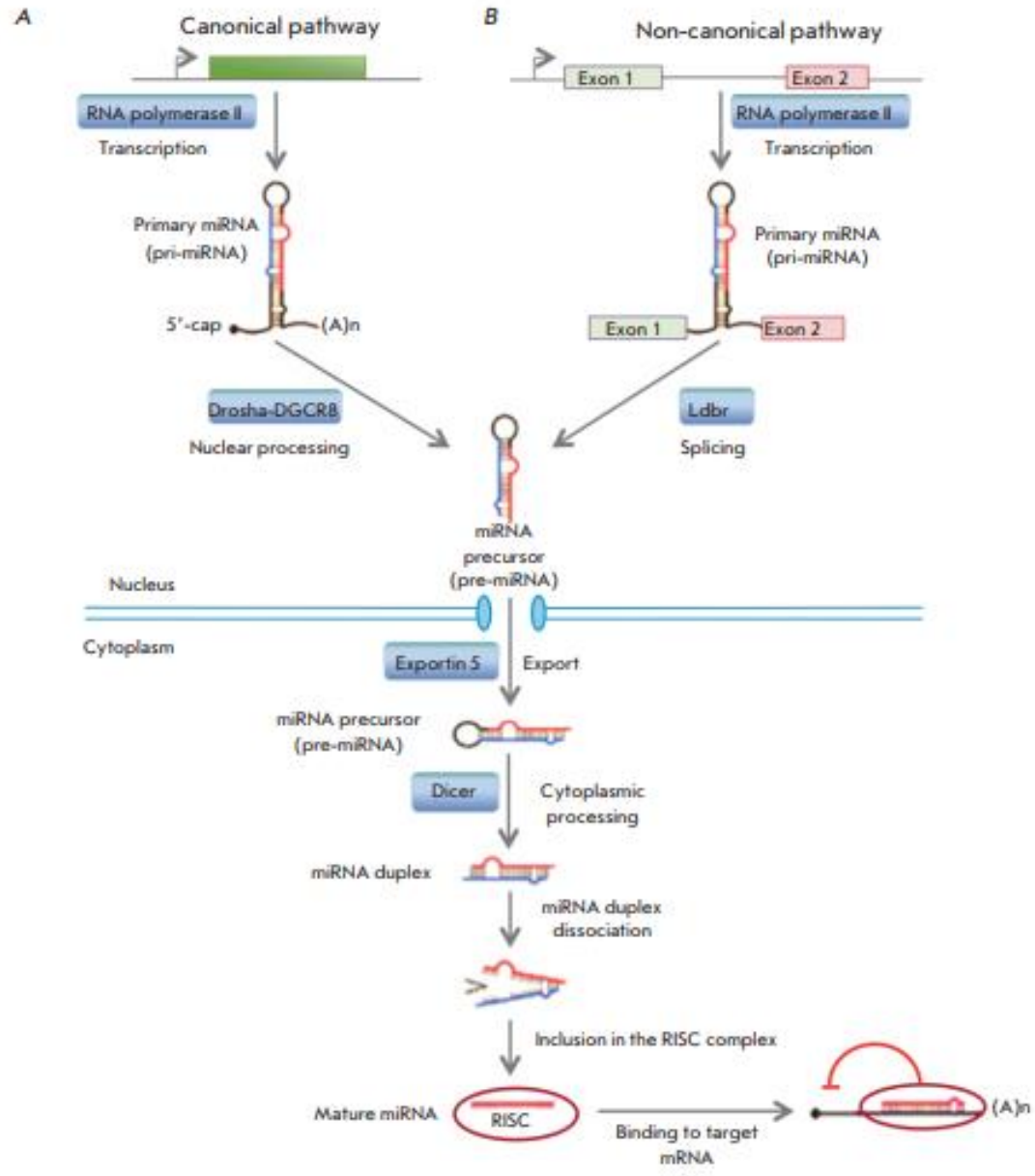

Figure 1-4 miRNA biogenesis. A.) The canonical pre-miRNA pathway produces pre-miRNAs through cleavage of pri-miRNA transcripts by the Drosha-DGCR8 microprocessor complex. B.) The non-canonical pathway. Mirtrons are spliced and debranched by the Ldbr enzyme, after which they fold into pre-miRNA hairpins. Then, the pathways merge. The green box indicates a miRNA gene; exons 1 and 2 are exons of the host gene encoding intronic miRNA [56]

1.3.2.2 miRNA Naming Convention

Given the large number of miRNAs that have been and continue to be discovered, as well as sequence similarities and phylogenetic conservation, universally accepted nomenclature guidelines were developed [73]. The uniform naming system for miRNA annotation is described in Table 1-2.

Table 1-2 miRNA Nomenclature

Term	Definition	Example
Species identifier	Abbreviated three or four-letter prefixes	hsa-miR-101 (*Homo sapiens*), mus-miR-101 (*Mus musculus*), dme-miR-101 (*Drosophila melanogaster*), cbr-miR-101 (*Caenorhabditis briggsae*)
Mature identifier	Mature sequences processed by dicer are designated with upper case R	hsa-miR-7
Precursor identifier	Precursor hairpins are lower case R	hsa-mir-7
Numerical identifier	Sequential numbers are assigned based on historical precedent (earlier discovered miRNAs have lower numbers and more recently discovered have higher numbers). Orthologs have the same number in different species	mir-1, mir-2, mir-3
Paralog identifier	Paralogs that differ in the mature sequence by 1–2 nt are given lettered suffixes following the numerical identifier	mmu-miR-10a and mmu-miR-10b are mouse paralogs of mir-10
Distinct hairpin precursors, same mature miRNA sequence	Numbered suffixes	dme-mir-281–1 and dme-mir-281–2

Table 1-2 continued

Term	Definition	Example
Major form and minor form	Major more highly expressed form is named as described above, and the minor form with the asterisk "*" or star designation	mmu-miR-124 for the major form and mmumiR-124* as the minor form
5 Prime arm and 3 prime arm	The star/* form has been replaced by a more unambiguous system where the mature miRNA in the 5 prime arms of the precursor is designated 5p and the mature miRNA from the 3 prime arms is designated 3p	miR-124-5p, miR-124-3p
miRNA cluster	Multiple miRNAs transcribed on a single RNA, or multiple miRNA genes located closely on a chromosome	miR-17-92 contains a single transcript from which six miRNA genes and 12 mature miRNAs are processed: miR-17, miR-18a, miR-19a, miR-20a, miR-19b-1,miR-92a-1
miRNA families	Defined by matching seed sequences	miRNA families Defined by matching seed sequences

[Adapted from [55]]

1.3.2.3 Biological (Epigenetic) Function of miRNAs

Mature miRNAs, through their guide strands, associate with an Argonaute protein [74] at the core of the RNA-induced silencing complex (RISC) to perform mRNA regulation. Recognition of target mRNA by miRNA generally depends on complementary base pairing between miRNA seed sequence (nt 2–8 at the 5' end of miRNA) and sequences in the 3'-UTR of the target mRNA [58,59]. However, miRNAs are known to also bind to non-canonical sites on target mRNAs [75]. MicroRNAs are negative regulators of gene transcription (i.e. a reciprocal relationship), partially binding to complementary

sequences in mRNA and resulting in post-transcriptional repression of gene expression, as illustrated in Figure 1-5. This is called RNA interference (RNAi) or gene silencing [76].

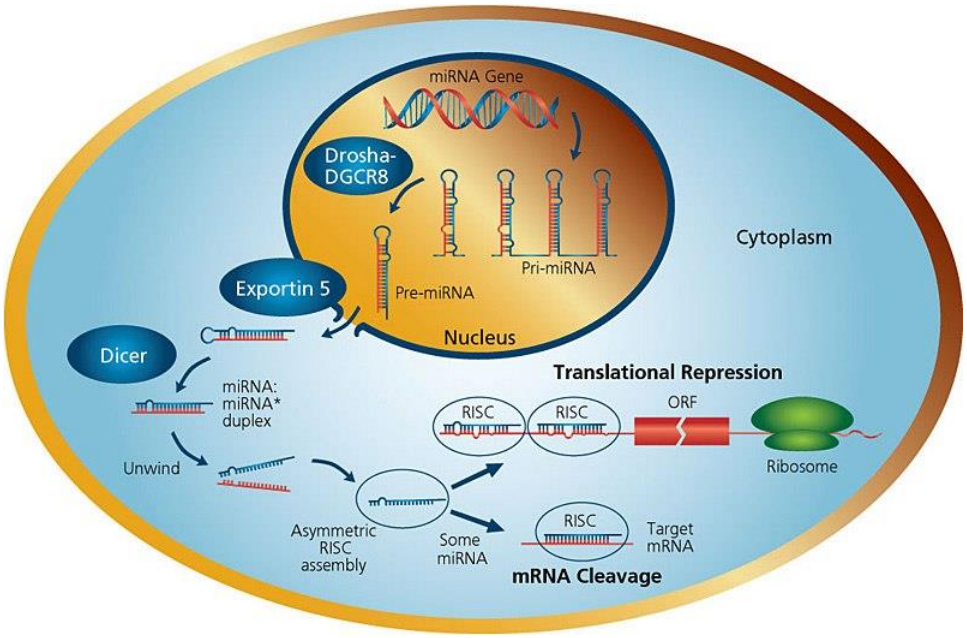

Figure 1-5 A schema portraying miRNA Biogenesis and its Functional Roles in the context of the RNA-Induced Silencing Complex (RISC) [miRNA (microRNA) Introduction (sigmaaldrich.com)]

In this way, protein synthesis/expression is inhibited via one or a combination of these three mechanisms: 1) mRNA endonuclease cleavage: PIWI domain, part of the RISC protein complex, function as an RNAse H and degrades the target mRNA; 2) mRNA degradation: removal of poly-A tail from mRNA and degradation by exonucleases; 3) mRNA translation repression: RISC prevents translation initiation factors or ribosome from binding to the mRNA. The particular mechanism at any time depends on the degree and nature of complementarity sites between miRNA and the mRNA target [77,78]. Moreover, evidence exists to support the proposition that translational inhibition precedes and is necessary for mRNA degradation by miRNAs [79].

1.3.2.4 RNA-Induced Silencing Complex (RISC) Assembly

RISC is a ribonucleoprotein complex containing members of the Argonaute (Ago) family of proteins with an endonuclease activity directed against mRNA strands that are complementary to their bound miRNA fragment (Figure 1-6). The guide miRNA molecule brings the RISC complex close to the target mRNA and recruits enzymes and cofactors that mediate RNA silencing [80]. Dicers are large multicomponent proteins (M.W. = 200 kDa): an ATPase/RNA helicase, a DUF283 (Domain of unknown function) domain, two catalytic RNase III domains (RIIIa and RIIIb), a C-terminal double-stranded RNA-binding domain (dsRBD), and a PAZ (Piwi, Argonaut and Zwille) domain which binds the characteristic two-nucleotide 3' overhangs of miRNA and siRNA. The Dicer enzyme can function as a monomeric unit because its intramolecular RNase III dimer has a single processing center. Each of the RNase III independently cuts one RNA strand of the duplex to generate single miRNA strands with 2-nt 3' overhangs [81].

The guide strand from the Dicer-cleaved pre-miRNA stem-loop is loaded onto the Argonaute protein that is associated with GW182 protein (Glycine-Tryptophan motif of 182 kDa molecular weight, another component of the RISC complex. The presence of other RISC-associated proteins depends on the particular RISC pathway. In the translation repression route, poly-A-binding protein (PABC) interacts with GW182 and proteins of the translational machinery to inhibit translation. On the other hand, the mRNA decay pathway involves GW182-mediated recruitment of CCR4-NOT1 (C-C Chemokine Receptor Type 4- Negative Regulator of Transcription 1) complex, containing at least five CCR or NOT proteins, which acts to deadenylate polyadenylated mRNAs. An mRNA-decapping enzyme 1/2 (DCP1/2) may act afterward to decap m7G mRNAs [82].

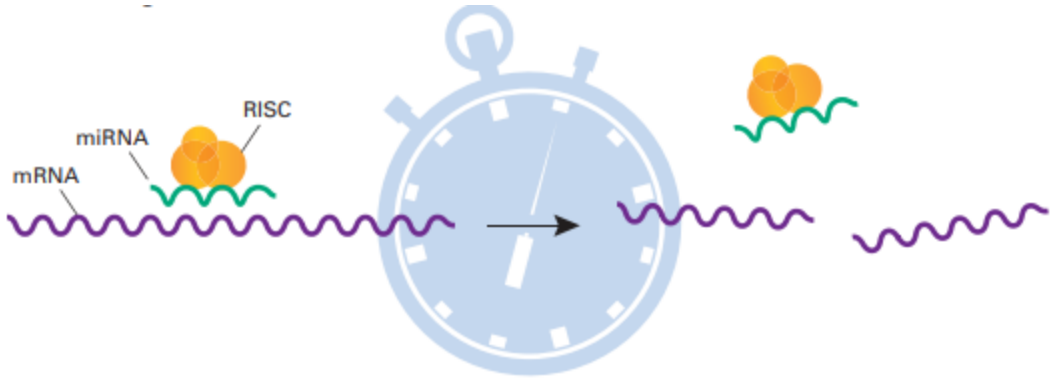

Figure 1-6 Transient interaction of RISC and miRNA/mRNA pair, resulting in miRNA processing [Source: MirTrap Technology: Technical Notes, Clontech 4.14 IN (633655). www.clontech.com]

1.4 DNA Damage Response and Repair (DDR)

Genomes are constantly exposed to DNA damage caused by genotoxic agents of environmental and endogenous origins. Depending on the source of damage, DNA may accumulate a wide variety of lesions including base modification, single-strand breaks (SSBs), or double-strand breaks (DSBs) [83,84]. Damage Repair by the DNA damage response (DDR) pathway comprises three main steps: (i) detection of damage by sensor proteins; (ii) recruitment of repair factors to sites of damage by signal transducers; and (iii) repair by effectors [85]. Specific DNA repair pathways include correction of DNA mismatches (Mismatch Repair, MMR); excision of chemically modified DNA bases (Base excision repair, BER) [86,87]; correction of more complex lesions such as pyrimidine dimers and intra-strand crosslinks (Nucleotide excision repair, NER) [88,89]; single-strand break repair (SSBR) [90]; non-homologous end joining (NHEJ) or homologous recombination (HR) to repair double-strand breaks (DSBs), which are the most toxic and difficult DNA lesions.

The DNA Damage Response loop is a kinase-based signal transduction network that initiates phosphorylation-driven cascades [91]. This DDR group of proteins acts by

transient coordination of DNA repair, replication, cell cycle progression, telomere homeostasis, and the subsequent induction of permanent cell cycle arrest or apoptosis if the damage cannot be repaired [92]. In addition to these normal physiological processes, the DDR loop serves as a molecular defense mechanism against tumorigenesis [93] and virus infection [83].

1.4.1 Base Excision Repair (BER) Pathway/Mechanism

To preserve genomic integrity, eukaryotic cells need a complex but synergistic DNA damage repair and response network of signaling pathways, involving proteins involved in cell cycle arrest, apoptosis, or DNA repair. The functions of the human DNA repair genes are well-established [94,95]. Base excision repair (BER) is the mechanism for the excision and replacement of oxidative DNA damage wherein single nucleotides modified by methylation, alkylation, deamination, or oxidation are removed [96]. Oxidative DNA damage is repaired primarily via the base excision repair (BER) pathway. The base excision repair mechanism had evolved to repair the mutations induced by oxygen radicals. This process is initiated by DNA glycosylases, which remove damaged bases in a substrate-specific manner. Six glycosylases in humans repair oxidized DNA lesions: MutY homolog (MYH), 8-deoxyguanosine DNA glycosylase 1 (OGG1), endonuclease three homolog 1 (NTH1), and Nei endonuclease VIII-like 1, 2, and 3 (NEIL1, NEIL2, and NEIL3). The repair response involves five key enzymatic steps that aim to remove the initial DNA lesion and restore the genetic material to its original state: (i) excision of a damaged base by a DNA glycosylase, (ii) incision of the phosphodiester backbone at the resulting abasic site by an apurinic/apyrimidinic (AP) endonuclease or AP lyase (iii) removal of the remaining sugar fragment by a lyase or phosphodiesterase (iv) gap-filling

to replace the excised nucleotide by DNA polymerase, and (v) sealing of the final, remaining DNA nick by DNA ligase. Defects in base excision repair components lead to reduced cell survival and elevated mutation rates [97].

Figure 1-7 shows the mechanism by which the human 8-deoxyguanosine DNA glycosylase 1 (hOGG1) repairs an oxidized guanine adduct [98]. OGG1, a bi-functional DNA glycosylase that is specific for 8-OHdG, cleaves the N-glycosidic bond of DNA using conserved active site lysine (Lys249) and aspartate (Asp268) residues that initiate a nucleophilic attack on the target nucleotide and forms a covalent protein-DNA intermediate. The subsequent general base-catalyzed abstraction of the C2 hydrogen then promotes β-elimination of the DNA strand 3' to the AP site [99]. By providing the first line of defense against oxidative DNA damage, OGG1 plays an important role in reducing the detrimental effects of DNA oxidative damage [2].

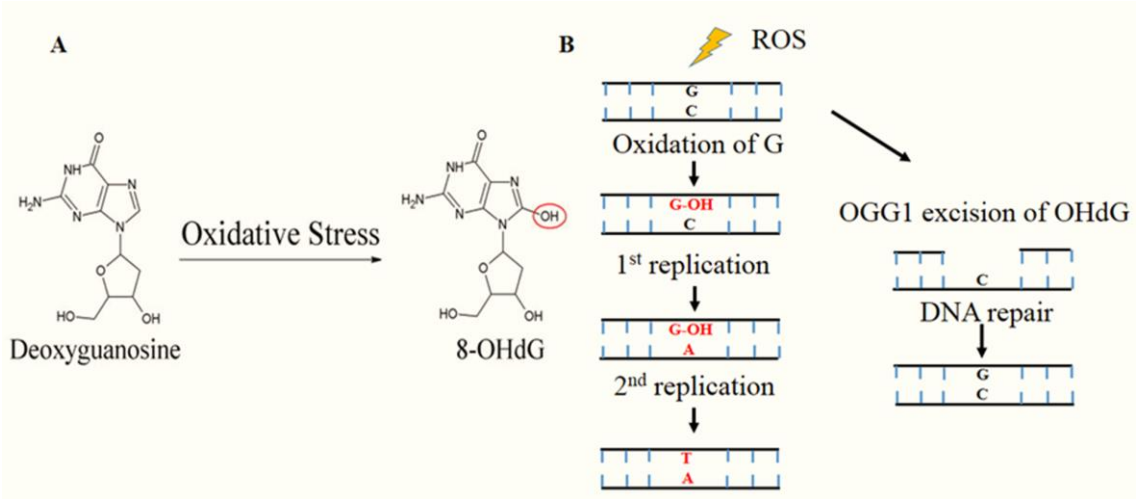

Figure 1-7 Oxidative DNA Damage Response and Repair in Cells. (A) Formation of 8-OHdG by oxidative stress. (B) Mechanism of ROS-induced G: C to A: T DNA mutation and OGG1's substrate-specific excision of the 8-OHdG lesion [98]

1.4.2 The Role of MicroRNAs in DDR Loop Regulation

Gene regulation occurs at the transcriptional and post-transcriptional levels. Recent studies indicated that miRNA plays a significant role in post-transcriptional gene regulation [12] and affect disease development and progression [65]. Changes in miRNA expression play a pivotal role in DNA Damage Response [100]. DDR proteins regulate miRNA expression, while also being influenced by miRNAs. The DNA damage response triggers a complex signaling cascade, which induces the biogenesis of miRNAs at the transcriptional level via the p53 pathway [101]. Conversely, miR-34 has been shown to regulate p53 mRNA expression level [102]. The degree of induction of miRNA expression is predicated on cell type and the nature and severity of DNA damage [64,103]. Changes in transcription and chromatin structure that are an integral part of DDR are also modulated by ncRNAs [104].

A knock-down of key proteins associated with miRNA biogenesis and function, particularly DICER or Ago2, leads to a reduction in survival and checkpoint response after UV damage suggesting that miRNAs play a major role in the cellular response to DNA damage [105]. DNA damage-induced miRNAs have been implicated in the regulation of the cell cycle, apoptosis, and DNA repair, and thus play an integral role in maintaining genome stability [100]. Increased miRNA expression is correlated with decreased mRNA target levels and reduced expression of DNA repair proteins. Key DNA repair proteins such as ATM are regulated by miR-421 and miR-181 [106,107]. MiR-182 expression is inversely correlated with the breast cancer type 1 susceptibility (BRCA1) protein levels in breast cancer cells and impairs homologous recombination-mediated DNA repair pathway [108], while miR-21 targets p53 and TGF-beta in glioblastoma [109].

Gain-of-function studies determined that miR-1255b, miR-148b, and miR-193b suppress the homologous directed (HR) DNA repair pathway [110]. MiR-24 regulates the histone variant H2AX, a protein that has a key role in the double-stranded break DNA repair [111]. MiR-203 inhibits DNA damage repair via the PI3K/AKT and JAK/STAT3 pathways and contributes to the modulation of radiation sensitivity in human malignant glioma cells [112]. Overexpression of miR-92 is associated with an increased accumulation of oxidative DNA damage and immortalization in hepatocellular carcinoma [113]. Astrocytes-derived miR-181, miR-29, and miR-146a enhance neuron survival after cerebral ischemia [114].

Bioinformatics analysis identified miRNA binding sites in the 3'-UTRs of DSBs repair proteins such as RAD51 recombinase [115][116]. While some predictions have been confirmed, a lot of these predictions have not yet been validated experimentally [117][118].

1.5 Methods and Techniques Employed in MicroRNA Target Analysis

The human genome encodes over 2000 miRNAs that are estimated to bind to the 3'UTR region and target 60% of mRNA [58,59]. One miRNA can regulate multiple genes and a single gene can be targeted by multiple miRNAs. Therefore, the identification of these interactions is important for the development of miRNA-based therapeutics. Mature miRNAs recognize their target mRNAs by base-pairing between its seed sequence (usually between nucleotide position 2 – 8) and complementary nucleotides in the 3'-untranslated region (3'-UTR) of mRNAs (gene coding sequence), thereby leading to translational repression and mRNA cleavage [119,120]. However, perfect seed pairing does not necessarily give a reliable prediction for miRNA interactions [121]. New microRNAs'

target genes are identified via a combination of computational 3'UTR target prediction and experimental validation. Several experimental approaches are developed to identify miRNA's gene targets and to confirm their biological function as summarized in the 4-step scheme in Figure 1-8 [122].

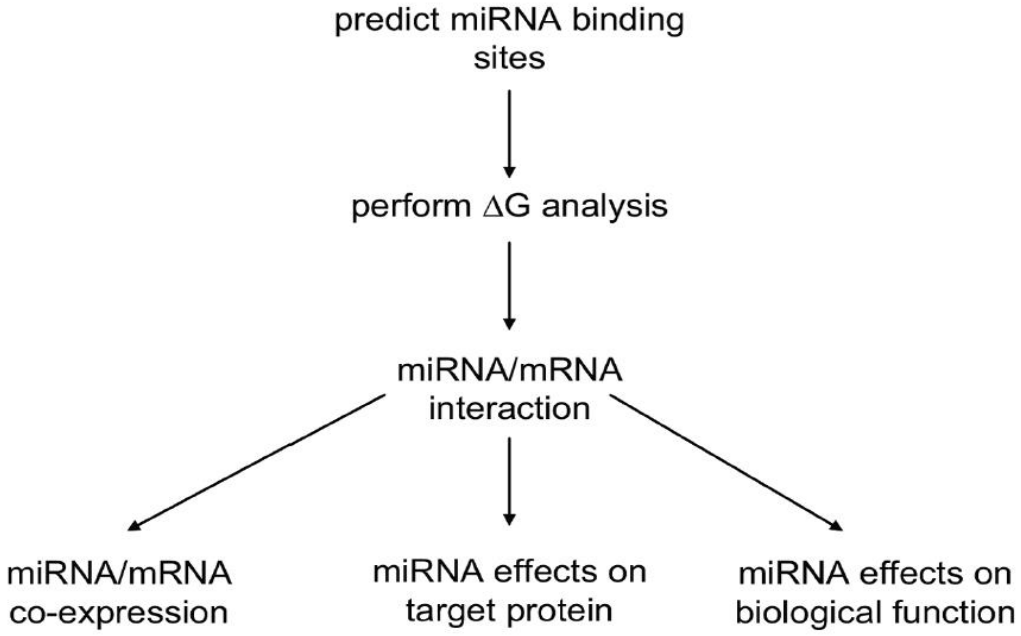

Figure 1-8 Proposed Scheme for miRNA target validation. Prediction methods and validation techniques of both microRNAs and their targets are co-dependent [122]

1.5.1 *In silico* Prediction of miRNA Targets

Computational analyses based on machine learning techniques are used to predict miRNA species that selectively hybridize to the 3' UTR of mRNA transcripts. The *in silico* analysis enables researchers to narrow down their miRNA candidates for experimental validation. There have been cases of failed validation tests despite seed sequence matching predictions [121], suggesting that some contextual features may also be integral to miRNA:mRNA interactions. RNA accessibility was shown to be a function of favorable thermodynamics, which tilts more towards 3'-UTR sites that are devoid of complex secondary structures. That is, the higher the free energy change (ΔG), the more accessible

the mRNA. The free energy change (ΔG) of the 70 nucleotides flanking the 5' and 3' sides of the predicted 3'UTR regions are used to identify prospective miRNA:mRNA pairwise binding.

1.5.2 Experimental Validation of miRNA-Target mRNA Interactions

1.5.2.1 Chimeric Reporter Gene Assay

The experimental approach is based on cloning of the 3'-UTR of the predicted target gene immediately downstream of the luciferase or green fluorescent protein (GFP) open reading frame in a reporter plasmid [123]. The recombinant plasmid and a miRNA of interest are then transiently co-transfected into a host cell and luciferase activity and fluorescence are measured 24 – 48 hours after transfection. It is expected that the binding of a given miRNA to its specific mRNA target site will repress the production of the reporter protein thereby decreasing its expression/activity which can be measured and compared to a control reporter plasmid. The disadvantage of this technique includes an increased number of false-positive and false-negative results due to non-physiologic interactions [124].

1.5.2.2 Immunoprecipitation Technique

Immunoprecipitation permits the identification of functional miRNA:mRNA relationship based on their physical interactions using an antibody-mediated "pull-down" strategy of the complex [124,125]. The Argonaute (Ago) protein family binds to miRNAs and partially to the complementary sequences in the 3'-UTR of their target mRNAs. Antibodies against Ago can be used for co-immunoprecipitation of the Ago-bound mRNAs. A novel and robust immunoprecipitation technique, MirTrap System (Clontech® Laboratories, Cat # 632017), has been developed for this purpose. The MirTrap technology

is a powerful discovery tool that helps identify and enrich microRNA targets in mammalian cells. It is based on the principle of sequence complementarity that allows actual physical interaction between miRNAs and mRNA transcripts [80]. The system allows the expression of a dominant-negative subunit of RISC protein that enables a miRNA of interest to bind to its target mRNA but restricts further processing of the transcript. The negative subunit is integrated into the endogenous Ago/RISC complex and "locks" a miRNA-target mRNA in the complex. The flag epitope tag (DYKDDDDK) is linked to the subunit and allows capture and isolation of the entire Ago/RISC complex, together with the microRNA/target mRNA pair of interest. Thus, the microRNA and its target can be effectively immunoprecipitated (enriched) and subsequently identified by next-generation sequencing or validated by quantitative PCR (qPCR).

1.5.3 Indirect Experimental Validation of miRNA-Target mRNA Interactions

Indirect validation can be conducted at three levels: transcriptomics, proteomics, and metabolomics.

1.5.3.1 Transcriptomics: miRNA and Target mRNA Inverse Transcription

For the target mRNA to be modulated, it must have an inverse expression level with its homologous miRNA. An older approach is *in situ* hybridization, which leveraged the enhanced efficiency, stability, and discriminatory power of digoxigenin (DIG)-labeled "locked nucleic acid" (LNA) antisense miRNA-specific probes. Hybridization is performed utilizing fixed and mounted tissues at 37^0C overnight, followed by a low stringency wash [126]. The probe-target complex is visualized by utilizing a digoxigenin antibody conjugated to alkaline phosphatase acting on the chromogen nitroblue tetrazidium and bromochloroindolyl phosphate. However, data interpretation can be erratic because of

the relatively narrow window between signal and background; so it is advisable to be used as an adjunctive technique. Northern blot analysis using LNA-modified oligonucleotide probes has also been employed [127]. Real-time quantitative PCR (RT-qPCR) is considered the gold standard for validation of the expression level of the predicted miRNA:mRNA complex [128].

1.5.3.2 Gain of Function and Inhibition: Proteomics and Metabolomics Analyses

A typical approach to validate the functional relationship of a miRNA/mRNA target pair is a transient over-expression ("gain-of-function") of a given miRNA mimic (a synthetic double-stranded version of an endogenously expressed mature miRNA) in a cell type known to express the putative target protein, and subsequently quantifying differences in mRNA and protein expression using RT-qPCR and Western blot, respectively [129]. Gain of function studies is likely to have "off-target" effects, as aberrant expression of miRNAs could target genes that would otherwise not be affected under physiological conditions. Therefore, a two-way experimental validation is often employed (Figure 1-9). This includes over-expression (using miRNA mimics) and inhibition (using "loss-of-function" studies in which a specific endogenous mature miRNA function can be inhibited using antisense oligoribonucleotides). These single-stranded RNAs are chemically modified (i.e. 2′-O′-methoxyethyl phosphorothioate or LNA) to improve stability and potency.

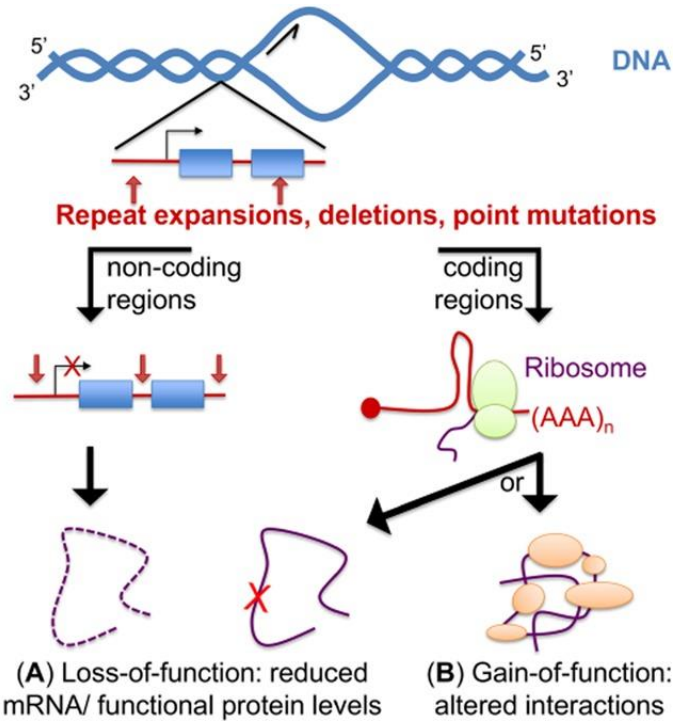

Figure 1-9 Mechanisms conferring protein loss and toxic gain-of-function effects. The diagram illustrates pathogenic mutations (repeat expansions, deletions, point mutations) that may occur either in noncoding or coding regions of the genome (left and right sides, respectively). (A) Protein loss-of-function. Haploinsufficiency can occur when the level of a particular mRNA is down-regulated due to mutations in noncoding regions of genes such as in promoters/introns, or if the promoter is subjected to histone/DNA modifications (transcriptional repression), but also if mutations in 5′ or 3′ untranslated regions (UTRs) decrease mRNA stability. Protein loss-of-function can also occur when mutations in coding regions alter directly the activity of the mutated protein (misfolding, alteration of the active site). (B) Protein toxic gain-of-functions are caused by mutations in coding regions that either promote abnormal interactions, increase the interaction of the mutated protein with its natural binders and/or promote misfolding/aggregation [Adopted from [130]]

The choice of cells utilized for performing gain-of-function and loss-of-function studies is important as each cell line has varying levels of endogenous miRNA and target gene expression [131–133]. Since miRNAs modulate gene expression by both translational repression and mRNA cleavage, the effect of a miRNA mimic can be assayed at the protein and metabolic levels. If a given mRNA is the correct biological target of a specific miRNA, it stands to reason that fluctuations in the miRNA level should give rise to an inversely

corresponding change in the protein encoded by the target mRNA, and invariably, its phenotypic expression. Once the impact of miRNA on the gene and protein level of the target mRNA has been confirmed, the impact on the relevant cellular processes is investigated.

Depending on the protein target of interest, biological assays could investigate different signaling pathways, cell proliferation [134], cell differentiation [135], apoptosis [136]. However, since this is an indirect measure of miRNA's effect on protein levels, the phenotypic assay must be preceded or accompanied by a direct protein assay. Moreover, to further identify whether a miRNA species modulate the protein expression of its target mRNA, a “rescue assay” can be carried out whereby the effect of a given miRNA can be rescued by overexpression of that protein [122]. Conversely, a knock-out (gene silencing) study can be carried out by the use of small interfering RNAs (siRNAs) targeted at complementary regions on the mRNA transcript. The binding of siRNA effectively silences the expression of the gene, and thus, the protein, so that with inhibition of the miRNA, and the consequent under-expression of the target gene and its encoded protein, the amount of protein produced should be higher than without the inhibition.

1.6 Cellular Oxidative Stress

Oxidative stress is generally defined as an imbalance in oxidative metabolism whereby the scavenging capacity of the cell’s antioxidant system can not keep up with the rate of reactive oxygen species (ROS) production in high oxygen-demanding organelles like the mitochondria, peroxisomes, endoplasmic reticulum, and during inflammatory processes, mainly in macrophages [137],. Nucleic acids are susceptible to oxidation by environmental and endogenous factors, and several types of ROS, such as singlet oxygen

(O^{2-}) and hydroxyl radicals (OH^{-}), generated as byproducts of normal oxidative metabolism, especially in the mitochondria [138]**,** or by ionizing radiation exposure (*e.g.* X-rays and γ-rays), can induce oxidative modification of the DNA bases, producing lesions including the ring-opened formamido-pyrimidine derivatives of guanine and adenine, 8-hydroxy-2'-deoxyguanosine (8-OHdG), formyluracil, dihydroxyuracil, and thymine glycol [139]. Despite the body's antioxidant enzymes mitigating the cell's hyper-oxidative state to preserve the cell's functionality, an imbalance between the production of ROS and the biological repair of the oxidative damage can result, and thereby causes mutations to DNA which plays a pivotal role in cancer development and progression, as well as aging and age-related neurological disorders [140].

1.6.1 8-OHdG as an Oxidative Stress Biomarker

Among the five nucleobases, guanine is the most susceptible to oxidation because of its high electron density. The most common biomarker of ROS-induced DNA damage is the mutagenic base byproduct, 8-OHdG, an oxidized derivative of deoxyguanosine [141]. Thus, the concentration of 8-OHdG within a cell is a well-established marker of nucleic acid oxidative damage and an indicator of oxidative stress [142]. Elevated levels of 8-OHdG have been reported in leukemia [143], breast cancer [144], colorectal cancer [145], lung cancer [146], Parkinson disease [147], and Alzheimer's disease [148].

8-OHdG is highly mutagenic, causing DNA mutations by incorporation of adenine instead of cytosine during DNA replication that leads to C: G to A: T substitutions in the nucleic acid sequence. The human 8-deoxyguanosine DNA glycosylase 1 (hOGG1) is a bi-functional 8-OHdG-specific glycosylase that plays an important role in nicking off 8-OHdG mutations (Figure 1-7). Thus OGG1's expression level in cells is equally a gauge

of the DNA repair capability of cells [2]. Decreased expression levels of OGG1 correlate with a high frequency of 8-OHdG adducts and DNA mutations [149]. A single nucleotide polymorphism caused by oxidation of the cysteine residue-326 [Cys-326] has been linked to deficient OGG1 activity, and thus, has been used as a marker of individual susceptibility to oxidative DNA damage [150]. However, the focus of these published studies was on the genetic changes that influence OGG1 activity in cells and didn't consider non-coding RNA regulation.

1.6.2 The Brain's Susceptibility to Oxidative Stress

The brain is a prime target of reactive oxygen species, and so of the resulting oxidative stress, because of its heavy oxygen dependence, high energy requirements (high glucose metabolism), extensive lipid composition, and more importantly, its relatively weak antioxidant system, in comparison to other tissues [3]. The relatively slower rate of 8-OHdG clearance from brain tissues makes it even more vulnerable to oxidative stress [151]. Neural cells are continuously challenged by ROS, and effective repair of ROS-induced 8-OHdG accumulation is critical to maintaining brain function and reducing the rate of C: G to A: T transversion mutation (Refer to Figure 1-7). The base excision repair is one of the mechanisms that protect the brain cells from oxidative lesions by preventing both nuclear and mitochondrial mutations [2]. The reduced cellular capacity of DNA damage repair is implicated in the process of neurodegeneration [152].

1.6.2.1 Astrocyte as a CNS Model for Oxidative Stress

Astrocytes are the most abundant glial cells in the central nervous system. They maintain electrolyte-water balance, energy metabolism and homeostasis, defense, synaptic transmissions, and regeneration of the CNS [4,5]. Therefore, human astrocytes are an ideal

biological model to investigate the relationship between oxidative stress, DNA damage and repair, miRNA and OGG1 mRNA, and protein expression levels. Understanding the epigenetic regulation of astrocyte DNA repair mechanisms could lead to the identification of novel targets for the treatment of CNS disorders. Considering the important role in maintaining brain activity, astrocytes can be regarded as a potential target for therapies aimed at the prevention and cure of age-related neurodegenerative diseases [97].

1.6.3 Crosstalk Between ROS and MicroRNAs

Changes in microRNA expression profile and ROS signaling have been associated with tumor development, progression, metastasis, and therapeutic response, prompting investigations into possible crosstalk between ROS and microRNAs. Emerging evidence suggests a reciprocal connection between ROS signaling and the miRNA pathway whereby ROS induces epigenetic alterations of miRNA genes [153]. It has been proposed that ROS are involved in various steps of miRNA biogenesis via several mechanisms which include: inhibition and enhancement of the expression of certain miRNA genes through the epigenetic regulatory enzymes, DNMT1 and HDACs; the regulatory activation of stress-related transcription factors such as p53, nuclear factor (NF)-κB to induce miRNA expression [13,14]; and the recruitment of the miRNA processing machinery, Drosha and Dicer, which can be directly or indirectly regulated by ROS [15].

Figure 1-10 elucidates the proposed mechanism to explain this complicated and poorly understood mechanism underlying ROS-regulated microRNA expression.

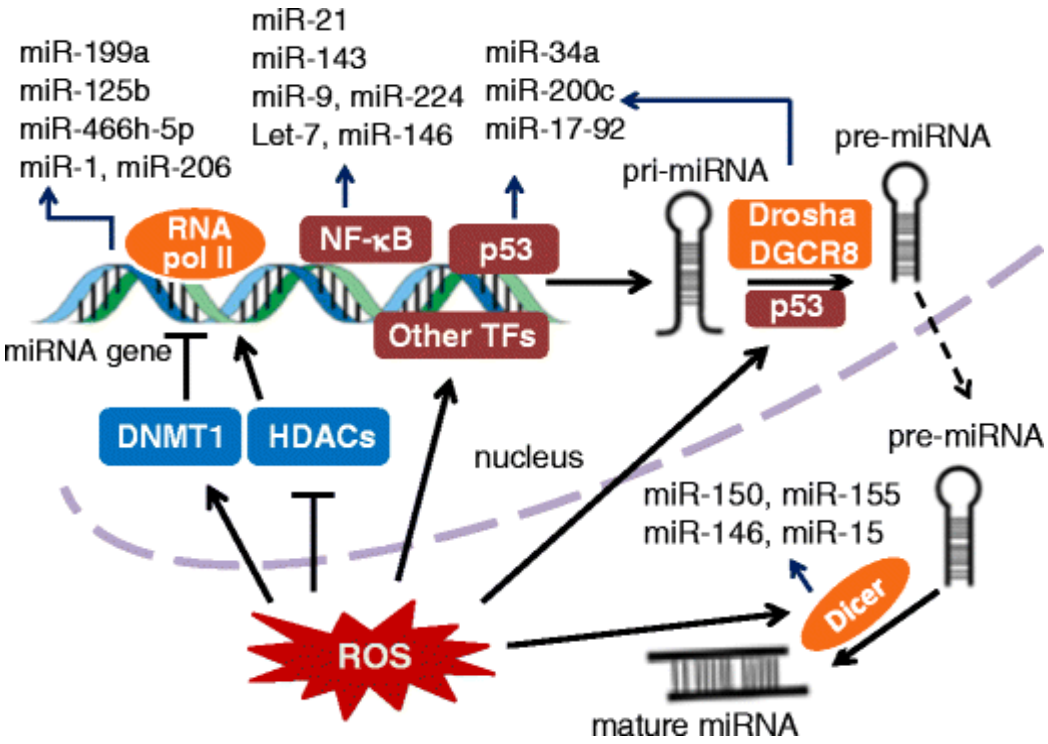

Figure 1-10 Schematic model showing mechanisms in which ROS regulate microRNA expression. ROS are involved in every step of miRNA biogenesis. ROS can induce epigenetic alterations of miRNA genes. For example, ROS inhibit and enhance the expression of certain miRNA genes through DNMT1 and HDACs, respectively. ROS can also activate transcription factors to induce miRNA expression. Moreover, Drosha and Dicer, which are two essential enzymes for miRNA biogenesis, can be directly or indirectly regulated by ROS [15]

1.6.4 Chromium Toxicity

The industrial use of heavy metals and mainly chromium-based products in the world is increasing rapidly. This poses a risk of oxidative damage in brain cells that is correlated with the development of neurological disorders [154]. Chromium has been the subject of multiple toxicological investigations following the increase in an occupational exposure and the release of the chemical into the environment [155]. While the biological effects of chromium have been extensively studied both *in vitro* and in animal models, including spermatotoxicity [156], hepatotoxicity and neurotoxicity [157], the genetic and

epigenetic response of the cells of the central nervous system have not been sufficiently characterized.

Among heavy metals, chromium poses a particularly serious threat due to its high oxidation resistance. In combination with iron and oxygen, chromium is deposited as ferrochrome ore, ranking as the sixth most abundant element in the earth's crust. Its ubiquity and persistence in the environment increase the risk of chromium exposure and toxicity in the general population [158]. According to a Toxics Release Inventory of 3,391 large processing facilities in the United States, chromium accounted for 94.1% of total environmental release into the soil (30,862,235 pounds) and 0.3% into water (111,384 pounds). The survey reported a 0.4 – 8.0 µg L^{-1} concentration of chromium in tap water in U.S. households [159]. Other environmental sources of chromium are buildings plastered with chromium-containing cement, asbestos roofing, emissions from chromium-based automotive catalytic converters, and tobacco smoke [160]. In nature, chromium is present in its stable trivalent form (Cr^{+3}). Hexavalent chromium (Cr^{+6}) is considered the most toxic form, because it has a high oxidation potential, high solubility, and can easily cross the cell membrane [161]. Cr^{+6} in the environment is almost totally derived from anthropogenic sources [162,163]. Absorbed chromium is carried in the bloodstream, eventually being distributed to all tissues. The dual factors that determine the toxicity and biodistribution of chromium compounds are oxidation state and solubility [164].

The mechanism of chromium (VI)-induced enhanced production of reactive oxygen species, as well as the resulting oxidative tissue and DNA damage are well documented [154,165]**.** Several types of chromium-induced structural DNA damages have been reported including DNA strand breaks [166,167], DNA-protein crosslinks [168,169],

and the formation of chromium-DNA adducts, which lead to repair errors [170]. The genotoxic effects of chromium are mediated by the formation of intermediates during the reduction of Cr^{+6} to Cr^{+3}. The free radical species produced during the process attack and cause oxidation of macromolecules such as DNA and lipids, with negative consequences for human health, including neurotoxicity, hepatotoxicity, nephrotoxicity, genotoxicity, carcinogenicity, and immunotoxicity [171,172].

1.6.4.1 Sodium Dichromate

Sodium dichromate (Chromic acid or Disodium salt) is an odorless, red or orange-red crystalline inorganic compound, with a molecular weight of 261.97 g/mol in its anhydrous form ($Na_2Cr_2O_7$, CAS No. 10588-01-9), and 298.00 g/mol in its dihydrate form ($Na_2Cr_2O_7 \cdot 2H_2O$, CAS No. 7789-12-0). Its structural formula is represented in Figure 1-11. Owing to its oxidizing potential, sodium dichromate is used as a corrosion inhibitor and to make virtually all chromium-based compounds and materials [173,174], and are thus, widely employed in various industrial processes including electroplating operations, leather tanning, textile manufacturing, stainless steel welding, wood treatment, and in paint pigment production [175].

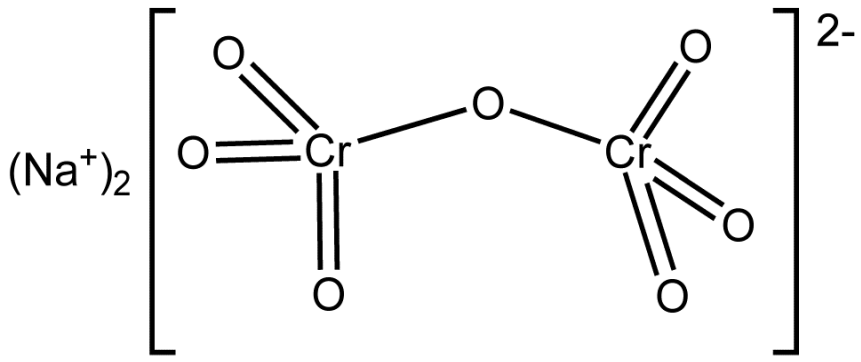

Figure 1-11 The structural formula of sodium dichromate [https://commons.wikimedia.org/wiki/File:Na2Cr2O7.png]

Hexavalent chromium, as typified by sodium dichromate, has been classified as a Group 1 human carcinogen [176]. Sodium dichromate is associated with oxidative DNA damage in human lymphocytes [177], and induced OGG1 downregulation in human A549 lung carcinoma cells [178]. As shown in previous studies, Cr^{+6} can lead to increased lipid peroxidation in the brain [179,180], and hence, neurotoxicity [181–183]. Since the central nervous system is a target for exposure to chromium or its compounds, it is necessary to assess its toxicity response for human safety assessment near hazardous waste sites.

1.6.5 Radiation Toxicity

Reactive oxygen species (ROS) produced as a result of radiation exposure lead to DNA mutations including oxidized nucleobases, as well as single-strand and double-strand breaks in normal cells. If these lesions remain unrepaired, the cell will either enter apoptosis or the resulting DNA mutations will be passed on to progeny cells, leading to deleterious changes in the phenotype [184]. Mitochondria, double-membrane organelles that provide cellular adenosine triphosphate (ATP), are proposed to play a key role in radiation-induced genomic instability. Accumulating evidence suggests that radiation-induced mitochondrial damage is more extensive than radiation-induced nuclear damage [185,186]. Previous studies have indicated that exposure of neurons to radio-frequency radiation resulted in an increased production of reactive oxygen species causing mtDNA damage as quantified by a decrease in DNA copy number [187]. There are approximately 2 – 10 copies of the mitochondrial genome per mitochondrion and tens to hundreds of mitochondria per cell, such that one cell may contain up to several thousand mitochondrial genomes. Mitochondrial DNA (mtDNA) is believed to be more susceptible to ROS damage

because of the lack of protective proteins and histones leading to the accumulation of more oxidative mtDNA damage relative to nuclear DNA [188].

1.6.5.1 Radiation Therapy: Risks and Benefits

Proton radiotherapy differs from photon radiotherapy in the use of charged particles, with a finite, energy-dependent range that can be adjusted to match the depth of the target, allowing for better targeting of diseased tissue and avoidance of healthy tissue. Clinically, this leads to reduced damage to non-target tissues and better clinical outcomes [189]. Due to its off-target effect, radiation therapy can cause disruption of the hypothalamic-pituitary axis and an increased risk of secondary malignancy. However, proton therapy is reportedly associated with improved outcomes in patients with gliomas and is associated with a decreased risk of late effects from treatment, including neurocognitive decline, endocrinopathy, and secondary malignancies in pediatric brain tumor patients [190,191]. High-throughput transcriptome analysis indicated that treatment with 2 Gy X-ray radiation causes alteration of several key pathways involved in cancer development and radiation resistance that include P53, TGF-β, VEGF, Hippo, and serotonergic synapse pathways [192]. Another study confirmed that the suppression of mitochondrial function is associated with the acquisition of radioresistance in glioma cells [193]. The radiation-induced bystander effect is associated with the increased rate of ROS production mitochondrial impairment, and DNA damage [194]. Additionally, radiotherapy has been implicated in the development of secondary brain tumors under a wide range of doses and treatment conditions [195]. The dose/fractionation of radiotherapy for the treatment of glial tumors is constantly evolving as a result of advances in imaging methods

and personalized medicine. While standard therapy includes a total dose of 60 Gy, daily radiation treatments can vary between 1.8 Gy–3.5 Gy [196].

1.7 Extracellular Vesicles (EVs)

Extracellular vesicles were erroneously thought to be storage compartments for cellular waste material, until their recently discovered role in cell-to-cell communication [16,18,197]. The term is used to broadly describe a heterogeneous population of cell-derived vesicular bodies, whose origin is either from endosomal compartments (exosomes, size range ~ 30 to 150 nm) or plasma membrane shedding (ectosomes, size range ~ 50 nm to 1 μm). The latter constitute microvesicles, oncosomes, and apoptotic bodies [198]. Considering their biological roles in cell-cell communication, the clinical applications of extracellular vesicles for biomarkers assessment and drug delivery are being explored [19].

1.7.1 Exosomes: Biogenesis and Mechanisms of Action

Exosomes are the smallest category of extracellular vesicles (30 – 150 nm diameter) that originate from the endocytic pathway of their host cells as intraluminal vesicles (ILVs), formed by inward budding of maturing early endosomes (EEs) or late endosomes (LEs) to yield multivesicular bodies (MVBs) (Figure 1-12). Cargoes are sorted into the ILVs by mechanisms mediated by the endosomal sorting complex required for transport (ESCRT) and other associated proteins, or by ESCRT-independent (lipid-driven) mechanisms. While some of the MVBs get fused and degraded by lysosomes, some fuse with the plasma membrane from where they are released as exosomes [199].

In the extracellular space, the secreted exosomes can influence the physiological response of the nearby recipient cell (paracrine signaling) or circulate in the extracellular fluid to remote sites in the body. Interaction with recipient cells is by one of three ways

[200]: 1) receptor-mediated exchange whereby exosomes bind and activate surface receptors on the recipient cell; 2) membrane fusion via a connexin-dependent mechanism that transfers exosomal cargoes to recipient cells, or 3) endocytosis/micropinocytosis which involves internalization of exosomes and their subsequent fusion with endosomal compartments to transfer their cargo. Endocytosis is usually the preferred route for those cells that do not possess antigen-presenting capacity, like some microglial cells [201].

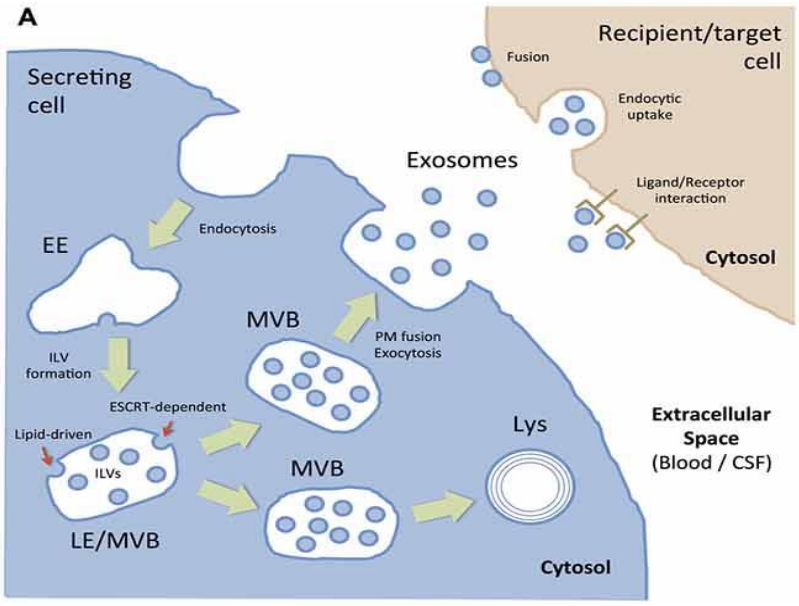

Figure 1-12 Biogenesis, targeting, and composition of exosomes [200]

The ease of access to exosomes from virtually any biological fluid forms the rationale for the use of exosomes as non-invasive biomarkers for assessment of disease status and toxicity [21,29]. Exosomes are released by the cells into a wide variety of body fluids, including ascites, breast milk, amniotic fluid, tears, synovial fluid [202,203], blood [204], semen [205], urine [206], saliva [207], and cerebrospinal fluid [208].

1.7.2 Exosomal Cargoes

Exosomes encapsulate nucleic acids (DNA, mRNA, and miRNA), proteins, and lipids, and other metabolites, depending on the cell type, location, and physiological or pathological state of the cell. Generally, exosomes are enriched in cytosolic proteins involved in MVB formation, membrane trafficking and fusion, and tetraspanins (CD9, CD,63, CD81) [30]. Several comprehensive databases that are annotated with the International Society for Extracellular Vesicles' (ISEV) minimal experimental requirements for the definition of extracellular vesicles are available for exosome researchers to validate or update the proteomic and genomic contents of exosomes released from different cell types and experimental conditions. Exocarta [209] and Vesiclepedia [210] are manually curated web-based compendium of exosomal cargoes (RNA, proteins, and lipids) that also catalog the mode of purification and characterization of the exosomes. Additionally, ExoCarta (http://www.exocarta.org) features dynamic protein-protein interaction networks and biological pathways of exosomal proteins. These databases are especially useful for comparing obtained data and assessing the purity of an exosomal preparation [211]. For instance, the simultaneous presence of canonical, endosome-specific proteins like Rab5 and the exosomal tetraspanins in exosomes from a particular cell or tissue sample, can be used to exclude the presence of membrane vesicles derived from membrane shedding (ectosomes) and disruption (necrosis and apoptosis) [212].

1.7.3 Biomedical Applications of Exosomes

Exosomes are released under normal physiological conditions, but their number is often increased upon cellular activation or neoplastic transformation [27]. Clinical investigators have demonstrated that during viral infections, the number of extracellular

vesicles secreted by infected cells increases and that the EVs are used as delivery vectors of viral materials [213]**.** Because exosomes reflect the state of their originating cells, their contents may potentially be useful as cell-type-specific biomarkers for various diseases. Exosomal miRNAs can be measured using RT-qPCR, microarrays, or small RNA sequencing and serve as biomarkers for the development and progression of pathological conditions [214]. Therefore, exosome-based diagnostics could become an integral part of a personalized and precise medical approach.

The diagnostic utility and therapeutics delivery potential of exosomes have been investigated in medical and clinical settings. These studies include investigations into sperm maturation along the male reproductive tract [215], HIV-1 inhibition [205], immune response stimulation for cancer immunotherapy [216], mediation of inter-organ cross-talk in metabolic diseases like obesity and diabetes [217], propagation of pathogenicity by brain exosomes via enrichment in neurotoxic proteins which contributes to neurodegeneration [218], detection of exosomes in the tumor microenvironment where they regulate angiogenesis, immunity, and metastasis in cancer [219], exosomal evasion mechanisms driving chemotherapeutic resistance in aggressive B-cell lymphoma [220]. The heterogeneity, endogenous origin, and ubiquitous distribution of exosomes in all biological fluids make them an accessible source of biomarkers for disease diagnosis [221,222].

The area of miRNA therapeutics is rapidly developing and offers novel strategies to modulate genetic instability by delivering synthetic miRNA mimics to correct abnormal miRNA expression [223,224]. MiRNAs represent attractive therapeutic targets since they can be easily synthesized both in their sense and antisense (inhibitory) orientation, and delivered by biocompatible nano-vehicles. In addition to its immense potential in the areas

of liquid biopsy, exosomes have also found application in targeted therapeutics delivery due to their ability to protect nucleic acid and proteins from degradation. Relative to other lipid-based drug excipients such as liposomes, exosomes have a more efficient cellular uptake [225,226] and payload delivery [227], and are generally well tolerated by cells, with minimal immune clearance [228].

1.8 Purification of Extracellular Vesicles (EVs)

1.8.1 The Need for Pure Exosome Populations

The analysis of exosome-specific transcriptomes and proteomes is critical for obtaining accurate clinical data. Inefficient purification techniques lead to the extraction of both exosomes and other extracellular vesicles that have different sizes and cellular origins. The most commonly used procedures involve multiple series of high-speed ultracentrifugation steps to remove cellular debris and separate and pellet the exosomes. The disadvantage of this technique is that it does not separate the exosomes from other vesicular structures and larger protein aggregates due to overlapping biophysical properties [229].

Antigen-specific isolation and genetic analysis of disease-responsive exosome subpopulations that express the same surface protein markers are essential to evaluate their clinical relevance [33]. Exosomes are released in normal physiological conditions, but their number is often increased upon cellular activation or neoplastic transformation [27]. CD63-positive exosomes are present at a higher level in prostate cancer cells compared to normal prostate cells [230], and their selective isolation would be of paramount importance in tissues that are not accessible to direct examination, such as the central nervous system. Particular cell lineages of the CNS, for instance, neurons, secrete exosomes in the

cerebrospinal fluid which carry specific markers such as the L1 cell adhesion molecule, the GPI-anchored prion protein, and the glutamate receptor, GluR2/3 [231]. Selective purification of this subpopulation will enable researchers to look into the (patho)physiological response of neurons in neurodegenerative disorders. In early Alzheimer's disease, increased levels of phosphorylated tau protein are detected in the exosome fraction of the cerebrospinal fluid [26]. This is a very promising finding and points to the possibility for an early diagnosis of Alzheimer's disease through analysis of the pure exosomal content of biological fluids.

The development of a technology for the isolation of a pure population of exosomes will facilitate the studies of their function in the development and progression of biological disorders. A rapid, and antigen-selective technology that provides high purity devoid of remnant matrices from current column chromatographic methods [232], will lead to more accurate data. Such an innovation would be a versatile platform with applications in disease diagnostics and monitoring of treatment response.

1.8.2 Existing Purification Methods: Advantages and Disadvantages

The most widely used methods for exosome purification include ultracentrifugation, size-exclusion techniques, polymer precipitation, immunoaffinity separation, and microfluidics [233].

Considered the gold standard in exosome isolation, high-speed ultracentrifugation (differential and density-gradient) gained widespread usage due to its operational simplicity. The main disadvantages of this technique are its high-cost equipment, lengthy run-time, and low yield. Moreover, co-isolation of non-exosomal vesicles and proteins is a common issue, since vesicle subpopulations are not thoroughly defined due to overlapping

biophysical properties [229,234–236]. The polymer precipitation technique, on the other hand, doesn't require a sophisticated setup and provides a relatively high total product yield. This method, however, has a low sample to reagent volume and produces exosomal samples with low purity [237].

Solid-phase exosome purification (SPEP) is the most promising alternative technology that could help to address the present technical challenges encountered in traditional liquid-phase separation techniques. Some solid-phase methods have made interesting attempts that scratched the surface of these challenges but fell short of holistically tackling all identified challenges. Although size-exclusion chromatography [238] has a simpler protocol that involves more readily available equipment as well as yields a purer exosome subpopulation compared to ultracentrifugation, it still has a low total yield and is a non-specific capture method [239].

Immuno-affinity techniques are quite labor-intensive and involve the use of antibody-coated fixed-phases like nanocubes [240], the surface of plastic plates [241] or magnetic beads [242], which are target-specific and can be used for almost any biological media. This method, typified by the well-known Dynabeads® magnetic separation technology, is highly specific and has a highly concentrated yield and purity at the time of capture, in addition to ensuring the integrity of isolated exosomes [243]. However, the pH and ionic concentrations of the reagents required to elute the exosomes from the stationary phases for downstream analysis can easily alter the properties of most of the exosome products, rendering them inadequate as best-practice models for exosome utilization [244]. The greatest limitation to widespread adoption of the immunoaffinity-based method is its high reagents cost that limits the sample volume being analyzed.

Microfluidics strategies for exosome isolation [245] integrate already established purification methods on a lab-on-a-chip platform. Some reported microfluidics systems are based on the applications of immunomagnetic beads [20], nanoporous membranes [246], and size-dependent displacement of extracellular vesicles [247,248]. This method, however, has no standardized protocol and yields a variety of experimental results. Thus, the challenge to develop a purification technique that can selectively isolate exosomes rapidly, reproducibly, efficiently, and in a clinically advantageous manner has been recognized as a perennial problem [249].

To overcome the identified technical challenges, traditional exosome purification technologies are sometimes used in combination in an attempt to provide a simple, fast, efficient, and affordable technique to isolate exosomes in a solid phase [250]. A novel ultrafast-isolation system called EXODUS, consisting of a low-cost disposable module and an automated workstation, employs a nanoporous membrane to rapidly isolate and concentrate exosomes from biofluids via acoustofluidic streaming [251]. Despite advantages over existing methods, the negative oscillatory pressure applied to the sample could lead to reduced integrity of the exosomes in the sample. Also, the cost and technical barriers associated with this method can be limiting factors to their extensive application.

To date, no one has successfully developed a microprobe-based, antigen-specific technology for single-step and high-throughput purification of intact exosomes that is also cost-friendly.

1.9 Layer-by-Layer (LbL) Assembly

Layer-by-layer self-assembly is an iterative thin film fabrication technique that is based on electrostatic adsorption of alternating layers of oppositely charged

polyelectrolytes (Figure 1-13) to form a substrate architecture for a variety of biosensing applications [252]. Electrostatic attraction and molecular interactions have been attributed as the driving force for the precisely controlled multilayer buildup with a nanometer resolution. Alternate adsorption cycles do not occur between polyelectrolytes of identical charges but rather with oppositely charged polyions, leading to a repeatable increment in the film's thickness at each step.

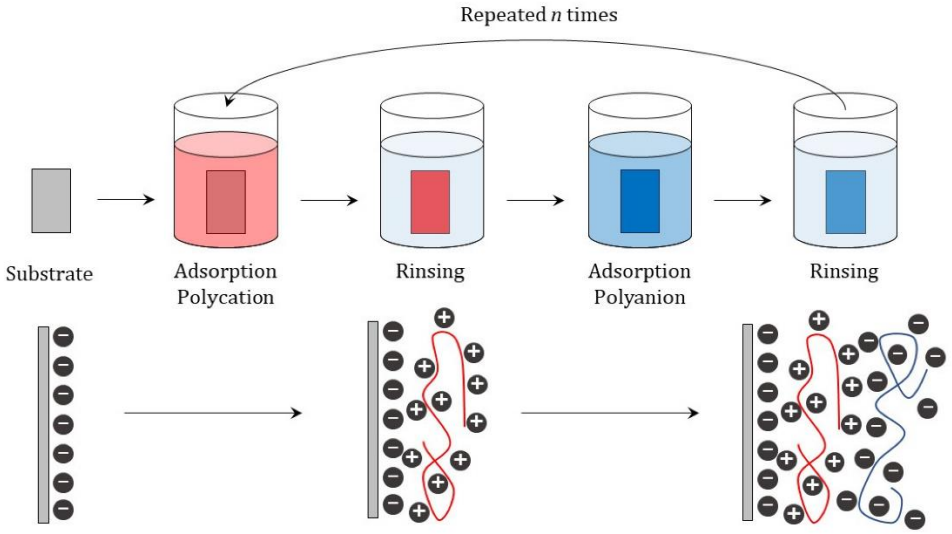

Figure 1-13 Schematic of the Layer-by-Layer Assembly Process [252]

According to pioneer work in this field [253], linear growth regime is reproducible up to 25 molecular layers, after which long-range dimensional instability might set in. Although films with high numbers of bilayers have been shown to exhibit good stability, it is not necessarily the case in all situations [254]. As such, modulating and optimizing the number of layers in a thin film becomes germane in any LBL procedure. Non-linear film growth has been widely reported at the first two to three layers before saturation kinetics comes into play to ensure uniform deposition [255,256]. Previous studies indicate that a minimum of four bilayers is required for uniform substrate coverage and that polyion films

are thermostable at up to 200 ^{0}C temperature and are insoluble in water and many organic solvents [257,258].

Thin-film deposition over surfaces via LBL assembly provides a multilayer architecture that has been applied in diverse biomaterials encompassing biosensors, biocatalysts, tissue scaffolds, and microporous capsules which presents the prospects of controlled drug delivery in the presence of appropriate stimuli like pH change or irradiation [259]. In this study, the LBL protocol will be used to immobilize biotin on the surface of stainless-steel microneedles for subsequent covalent attachment of streptavidin-conjugated anti-CD63 antibodies.

CHAPTER 2

IMPACT OF PHOTON AND PROTON IRRADIATION ON MITOCHONDRIAL FUNCTION AND 8-OHDG BASE-EXCISION REPAIR MECHANISM IN HUMAN ASTROCYTES

2.1 Motivation

Previous studies have indicated that 8-OHdG mutations increase in cancer patients exposed to radiation therapies [260]; however, how the rate of DNA damage accumulation corresponds to the source of radiation treatments has not yet been established. Since proton and photon radiations are two of the most common treatments for cancer patients [261], these radiotherapies will be investigated in this study. Comparative information regarding low-dose proton and photon radiation treatment on mitochondrial biogenesis and base-excision DNA repair capabilities of human astrocytes is lacking. Understanding the cellular response and exploring the underlying mechanism for radiotherapy-induced cytotoxicity of healthy astrocytes will contribute to the development of optimized treatment.

2.2 Specific Objectives

This study aims to assess and compare the effects of proton and photon radiation on the changes in mitochondrial mass and oxidative activity, as well as gene expression

levels of the base-excision repair protein, 8-oxoguanine DNA glycosylase (hOGG1) in healthy human astrocytes.

Radiation-induced changes in mitochondrial mass and oxidative activity will be assessed using MitoTracker™ Green FM and MitoTracker™ Orange CM-H_2TMRos dyes, respectively. MitoTracker™ Green FM is non-fluorescent in aqueous solutions and becomes fluorescent only when it accumulates in the mitochondrial lipid environment. MitoTracker™ Orange CM-H_2TMRos is oxidized by molecular oxygen in actively respiring cells and allows assessment of *in vitro* oxidative activity of mitochondria. RT-qPCR will be employed to quantify OGG1 expression as an assessment of the DNA-repair status of the irradiated cells.

2.3 Materials and Methods

2.3.1 Proton and Photon Irradiation of Cultured Astrocytes

Human primary astrocytes (Sciencell, Carlsbad, CA) were cultured at 37°C, 95% humidity, and 5% CO_2/air in Astrocyte Medium (Sciencell, #1801), supplemented with 1% penicillin/streptomycin solution (Sciencell, #0503), 2% Fetal Bovine Serum (Sciencell), and 1% astrocyte growth supplement (Sciencell #1852). When cells reached 80% confluence, they were transported to Willis Knighton Cancer Center in Shreveport, Louisiana, USA for radiation treatment with 0.5 Gy and 3 Gy proton and photon radiation. Cells were transported and irradiated in standard T-25 cell culture flasks filled with 35 mL cell media. Before irradiation of actual cell cultures, a “blank” T-25 flask filled with 35 mL of water was provided to WKCC so that appropriate irradiation parameters could be established. The blank flask underwent a workflow similar to that of a cancer patient, including 1) computed tomography (CT) scans (CT Big Bore, Philips, Amsterdam) using

straightforward, reproducible setup geometries tailored to proton and photon irradiations and 2) development of several “treatment plans” within the WKCC treatment planning system (Raystation™, Raysearch Laboratories, Stockholm) to achieve the desired dose levels. All the treatment plans utilized a single anterior-posterior treatment field, i.e. the radiation was directed downward toward the flask as it lay flat on the treatment couch. All treatment plans were also generated in a manner that allowed for approximately 5 mm in setup uncertainty during the actual irradiation scenarios. X-ray photon doses were delivered with a 6X energy beam using a VersaHD™ clinical linear accelerator (Elekta, Stockholm). Proton doses were delivered with energies ranging from 87 MeV to 111 MeV using a ProteusONE™ clinical proton therapy gantry (Ion Beam Applications, Louvain-la-Neuve).

2.3.2 Cell Viability Assays

Cell viability was quantitated by assessing the number of cells containing nuclear changes indicative of apoptosis (chromatin condensation and nuclear fragmentation) after staining with DAPI (ThermoFisher Scientific, cat.#62248). Human astrocytes were seeded in 6-well plates at a density of 300,000 cells per well. After treatment with 3 Gy Proton and photon radiation, DAPI was then added to each well at a final concentration of 1 μg ml^{-1} . After a 10-min incubation in the dark at 20 ˚C, cells were washed with PBS and examined by fluorescence microscopy (EVOS FL, ThermoFisher Scientific) using DAPI EVOS™ Light Cube settings. Three biological replicates were included in each treatment group and six high power fields from each well were averaged for each replicate.

The percentage of senescent cells in untreated and radiation-treated cells was assessed using Cell Event™ Senescence Green Detection Kit (ThermoFisher Scientific,

cat.# C10850) according to the vendor's guidelines. The cells were seeded on a 6-well plate at a density of 300,000 cells per well and incubated overnight. The wells were washed with PBS and fixed with 1 mL per well of 2% paraformaldehyde solution for 10 min at room temperature. The cells were washed, with 1 mL 1% BSA in PBS, followed by adding 1 mL working solution (1:1000 dilution, 25 μM). The plate was incubated for 2 h at 37 ˚C without CO_2, protected from light. The fluorescein-based probe containing two galactoside moieties serve as a target for β-galactosidase, a common biomarker for senescent cells. The enzymatically cleaved product would be retained within the cell due to the covalent binding of intracellular proteins and emit a fluorescent signal with absorption/emission maxima of 490/514 nm. After incubation, the cells were washed 3 times with PBS to remove the working solution, and then subsequently stained with DAPI (1 μg mL^{-1}) for 5 min at room temperature to label the nucleated cells for accurate counting. The cells were washed thoroughly with PBS to remove excess DAPI, and Fluorobrite DMEM media was added before imaging. The percentage of senescent cells in each treatment group was determined as a ratio of the DAPI-stained green-labeled (senescent) to DAPI-stained unlabeled cells. Three biological replicates were analyzed and averaged for each treatment group. The images were acquired using the EVOS FL imaging system equipped with GFP EVOS™ Light Cube.

2.3.3 Determination of Mitochondrial Mass

Mito Tracker™ Green FM (Thermo Fisher Scientific, cat. #M7514) which localizes in the mitochondria regardless of membrane potential was used to monitor the mitochondrial mass. Control and 3 Gy proton treated cells were incubated for 45 min with 200 nM MitoTracker™ Green FM in a CO_2 incubator followed by fixation with 2%

paraformaldehyde and 5 min incubation with 1 μg mL^{-1} of DAPI. The cells were imaged in FluoroBrite DMEM Media using an EVOS FL imaging system using DAPI and GFP EVOS™ Light Cubes. Using ImageJ (v1.52a, NIH), an outline was drawn around each cell and circularity, area, mean fluorescence measured, along with several adjacent background readings. The total corrected cellular fluorescence (TCCF) = integrated density – (area of selected cell × mean fluorescence of background readings), was calculated.

2.3.4 Assessment of Oxidative Capacity of Mitochondria

The mitochondrial oxidative activity was assessed using the reduced MitoTracker™ Orange CM-H_2TMRos fluorescent probe (Thermo Fisher Scientific, cat. # M7511). The probes were dissolved in dimethylsulfoxide (DMSO; Sigma Aldrich) to a 1 mM stock solution before use. Control and 3 Gy treated cells were seeded in a 6-well culture plate and stained with 200 nM MitoTracker™ Orange CM-H_2TMRos for 30 min in a CO_2 incubator followed by fixation with 2% paraformaldehyde and 5 min incubation with 1 μg mL^{-1} of DAPI (ThermoFisher Scientific, cat. #62248). After staining, the dye solution was replaced with 1 mL FluoroBrite DMEM Media (Thermo Fisher Scientific, cat. # A1896701). Images were obtained using using an EVOS FL imaging system using DAPI and RFP EVOS™ Light Cubes. To confirm that the accumulation of the dye in the cells was associated with the accumulation of ROS, the cells were incubated with 50 μM carbonyl cyanide p-trifluoromethoxyphenylhydrazone (FCCP; Sigma Aldrich). FCCP enhances the potential for auto-oxidation, increases the production of ROS, and reduces the mitochondrial membrane potential [262]. ImageJ analysis was conducted as already described above.

2.3.5 Gene Expression Analysis

RNA from radiation-treated and control cells was extracted using a Qiagen RNeasy kit (Cat. #74104). The primers for one-step reverse transcription PCR were purchased from Integrated DNA Technologies, Coralville, IA. Amplification of the OGG1 gene was performed using primer sequences:5′ - ACT CCC ACT TCC AAG AGG T-3′ and 5′ -GAG GAA CAG ATA AAA GAG AAA AGG C-3′ . The housekeeping gene glyceraldehyde 3-phosphate dehydrogenase (GAPDH) was amplified using the following sequences for forward and reverse primers: 5′ -ACA TCG CTC AGA CAC CAT G-3′ and 5′ -TGT AGT TGA GGT CAA TGA AGG G-3′ . The one-step reverse-transcription PCR reaction was performed using the Luna Universal RT-qPCR kit (New England Biolabs, cat. # E3005S). Twenty nanograms of total RNA were reverse-transcribed for 10 min at 55 ˚C followed by inactivation for 10 s at 95 ˚C. The amplification segment consisted of 40 cycles of 30 s at 60 ˚C and 10 s at 95 ˚C at a ramp heating rate of 0.2 ˚C/second. The relative quantification of OGG1 was normalized to the gene expression levels of GAPDH using the $2^{-\Delta\Delta CT}$ method.

2.3.6 Statistical Analysis

Data are expressed as mean ± SEM with n denoting the number of experiments. Statistical significance between sham-control, proton, ad photon irradiated groups was tested using one-way ANOVA with Tukey's posthoc analysis, and *p* values less than 0.05 were considered as statistically significant.

2.4 Results

2.4.1 Irradiation Induces Moderate Cellular Senescence and Apoptosis in Human Astrocytes

The percentage of senescent cells was assessed in the sham-control and radiation-treated groups before MitoTracker straining to assess the effect of radiation treatment on the percentage of senescent cells in the population. It was estimated that the average percentage (n = 3) of senescent cells was 6.5 %, 12.5 %, and 11.6 % in the control-, 3 Gy photon-, and 3 Gy proton-treated cell lines. Due to their limited replicative cycles, normal cells can become senescent and enter cell cycle arrest. But they remain metabolically active without undergoing apoptosis or mitosis, adopting a unique phenotype that includes the appearance of multinucleated cells, increased vacuolization, expression of pH-dependent β-galactosidase, and morphological changes where cells become unusually enlarged and extended [263].

Cell viability, as measured by the capacity of the cells to maintain membrane integrity and exclude DAPI, was estimated in all treatment groups. The percentage of apoptotic cells in the sham-control, 3 Gy photon, and 3 Gy proton irradiated cells was 12%, 37%, and 29% respectively. These data suggest that moderate doses of X-rays and proton reduce cell viability *in vitro* in human astrocytes as the impact is more pronounced after photon treatment.

2.4.2 Low-dose Irradiation is Associated with an Increase in Mitochonrial Mass

To assess mitochondrial function, the mitochondrial mass of the astrocytes was assessed using MitoTracker™ Green FM staining. The total cell fluorescence of the 3 Gy photon radiation-treated cells was more significantly increased when compared to the 3

Gy proton and control groups (Figure 2-1). These results indicate that the oxidative stress induced by the ionizing radiation leads to an increase of the mass of the mitochondria, most likely related to the stimulation of biogenesis as a protective mechanism to maintain cellular energy status.

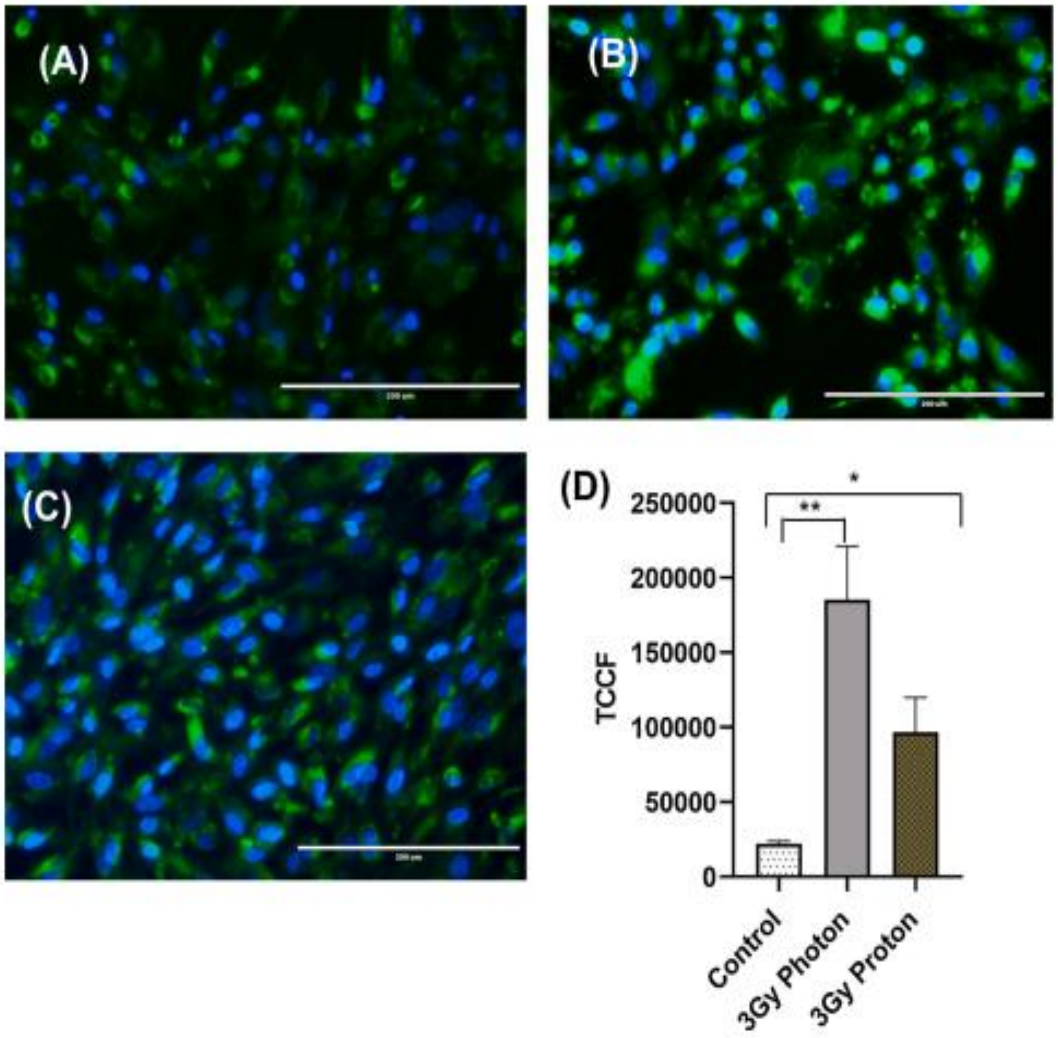

Figure 2-1 Florescence intensity and distribution of MitoTracker Green FM dye in (A) sham-control cells, (B) 3 Gy photon treated cells, and (C) 3 Gy proton treated. (D) The total corrected cell fluorescence (TCCF) indicates that mitochondrial mass is significantly increased in irradiated cells. Bar, 200 μm. Data represent means+/- SEM for each group (n = 8), *p < 0.05, **p < 0.01, ANOVA statistical analysis, Tukey's Honest Significant Difference test [11]

2.4.3 Mitochondrial Oxidative Activity Increases with Photon and Proton Radiation

The real-time changes in oxidative activity in the mitochondria of human astrocytes were investigated using a MitoTracker™ Orange CM-H_2TMRos, a reduced version of MitoTracker™ Orange that fluoresces upon oxidation. The dye is oxidized by intracellular ROS into fluorescent MitoTracker™ CMTMRos, which is sequestered in mitochondria by thiol reactivity of its chloromethyl moiety. Measurements of MitoTracker™ Orange fluorescence revealed a significant increase in the oxidative activity in the mitochondria of the 3 Gy proton and photon-treated cells in comparison to the sham-control. FCCP, an uncoupler of mitochondrial oxidative phosphorylation, causes a marked increase in intracellular ROS and apoptosis [262]. Therefore, it was selected as a positive control to confirm that the staining protocol reflects ROS levels in the mitochondria. Sham-control cells were treated with 50 μM FCCP just before the staining. This caused an increase in the fluorescence intensity due to the increase in the oxidative burden caused by FCCP (Figure 2-2).

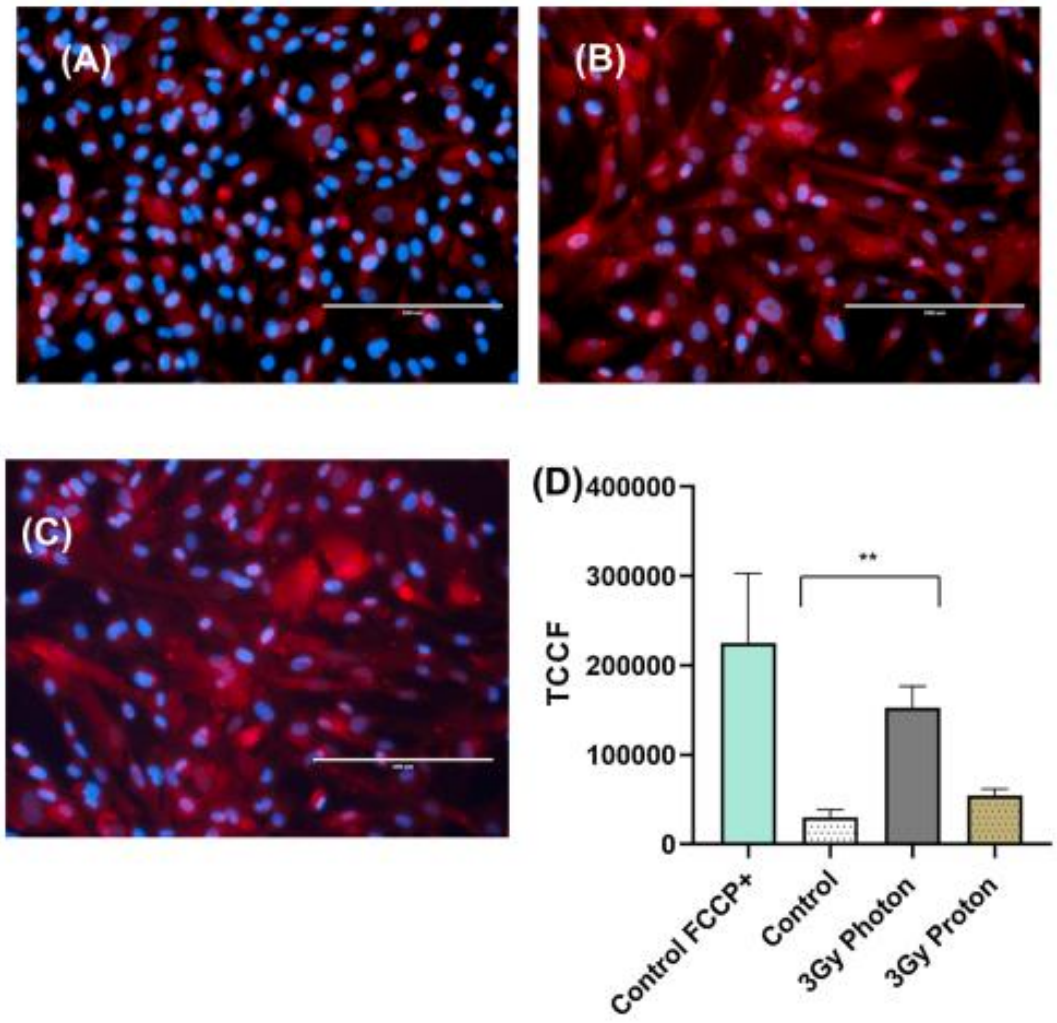

Figure 2-2 Fluorescent microscope images (20×objective lens) of human astrocytes stained with MitoTracker™OrangeCM-H2TMRos. The nucleus of the cells was stained with DAPI. (A) Sham-control cells. (B) 3 Gy photon treated cells. (C) 3 Gy proton treated. (D) The total corrected cell fluorescence (TCCF) indicates that mitochondrial oxidative activity is significantly increased in irradiated cells and the fluorescence is increased after treatment with the positive control 50 μM FCCP. Bar, 200 μm. Data represent means+/- SEM for each group (n = 8), **p < 0.01, ANOVA statistical analysis, Tukey's Honest Significant Difference test [11]

2.4.4 Proton and Photon Irradiation Downregulates OGG1 Gene Expression

To investigate whether high energy radiation affects the base-excision repair capabilities of human astrocytes, mRNA expression levels of OGG1 were examined via real-time RT-qPCR. As shown in Figure 2-3, a significant downregulation of OGG1 was

observed after treatment with 3 Gy of proton and x-ray photon radiation. Lower proton radiation dosage did not significantly decrease OGG1 expression; however, 0.5 Gy of photon treatment caused a significant decrease in OGG1 expression. These results suggest that both proton and photon radiation interfere with the base-excision repair capabilities of healthy, human glial cells in a dose-dependent manner. The detrimental effects are more pronounced after exposure to x-ray photons than with the proton beam.

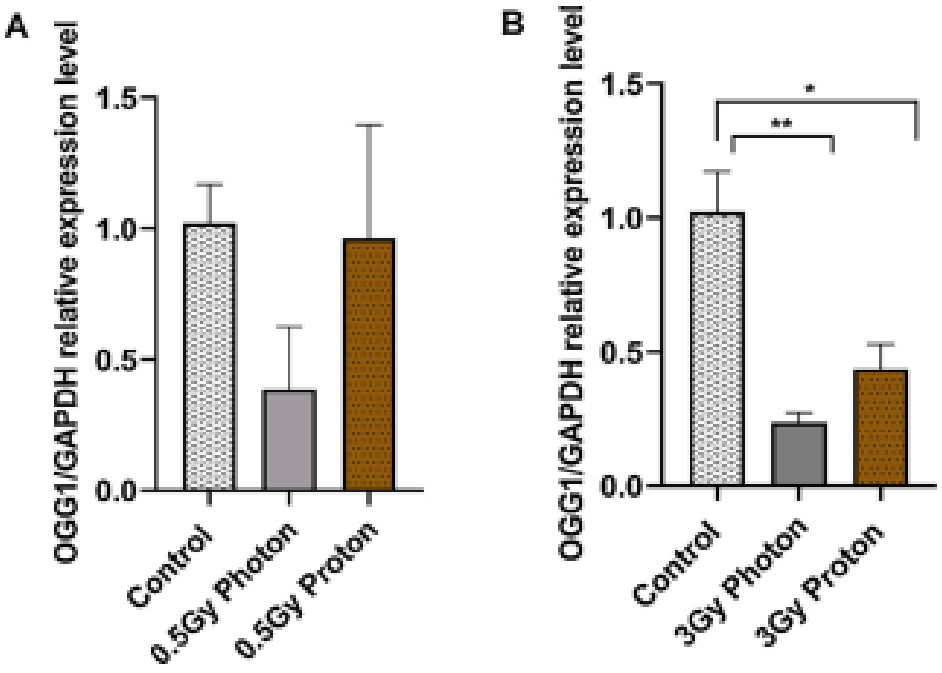

Figure 2-3 Effect of proton and photon radiation treatment on OGG1 mRNA expression in human astrocytes. Compared with the controls, the expression level of OGG1 was downregulated after treatment with 0.5 Gy (A) and 3 Gy (B) photon and proton radiation. Data represent means +/-SEM for each group (n = 5).*p < 0.05, **p < 0.01, ANOVA statistical analysis, Tukey's Honest Significant Difference test [11]

2.5 Discussion

The present study aimed to assess the changes in the mitochondrial mass, ROS levels, and DNA base-excision repair capabilities of human astrocytes treated with proton and photon radiation. Prior studies support proton radiation therapy as a more targeted,

viable approach to cancer treatment [189]. Several studies associate proton treatment with reduced tumor recurrence and neurocognitive late effects as a result of reduced damage to surrounding tissues [190,191]. Radiation treatment was associated with an increased level of mitochondrial ROS production and larger mitochondrial mass, parameters that are indicative of elevated mitochondrial stress.

Reactive oxygen species produced in radiotherapy induces a variety of DNA lesions, including oxidized base damage, single-strand breaks, and double-strand breaks in normal cells. If these lesions remain unrepaired, it may result in cell death through mitotic catastrophe and apoptosis. A high percentage of oxidative DNA damage induced by radiation is repaired by the base-excision repair pathway [264]. The results from this study indicate that both types of radiation caused impairment of the base-excision repair capabilities of the glial cells (Figure 2-3), but the detrimental effects were less pronounced after proton treatment. Inhibition of OGG1 post-irradiation can result in suppression of the other genes (APEX 1, XRCC1) involved in this DNA repair pathway and lead to the accumulation of unrepaired adducts. Multiple studies indicate that this leads to an increase in DNA mutations in both nuclear and mitochondrial genomes that result in carcinogenesis and mitochondrial impairment [265]. Genomic 8-OHdG accumulation increases after treatment with UV radiation [266], X-rays [267], and γ-radiation [268]. Previous studies have indicated that epigenetic mechanisms are involved in regulating the activity and the expression levels of OGG1. Histone deacetylases class I (HDACI) interacts with and deacetylates OGG1, enhancing its cleavage activity [269]. Impairment of oxidative DNA repair mechanisms is regulated by miR-200 via suppression of OGG1 expression levels [270].

Oxidative stress is generally defined as an imbalance that favors the production of ROS over antioxidant defenses. The results of this study indicated that ROS levels significantly increased after photon irradiation. Treatment with the FCCP, an ionophore and uncoupling agent, leads to increased production of cellular reactive oxygen and a pronounced rise n fluorescence in both treated and control cells (Figure 2-2). Ionizing radiation alters the atomic structure of the cellular macromolecules either through direct interactions or via products of water radiolysis. To cope with the induced stress and the changes in the redox environment, the cells respond at the molecular levels to counteract the toxic effects of radiation. These include changes in mitochondrial membrane potential, mitochondrial respiration, and mitochondrial ATP production, which indicate radiation-induced upregulation of the mitochondrial electron transport chain [271]. While the majority of ROS are produced during normal mitochondrial respiration, the mitochondria are the primary source of radiation-induced oxidative burden and the main target for its damaging effects. This leads to changes in mitochondrial biogenesis, mtDNA mutation, diminished ATP production, and impaired function [272].

The observed increase in the mass of mitochondria is probably a cellular response mechanism to counteract oxidative stress and the loss of mitochondrial function, and to recover ATP synthesis capacity. The data from this study indicate a statistically significant increase in mitochondrial mass after treatment with 3 Gy dosage of both photon and proton sources relative to the control (Figure 2-1). Other studies have demonstrated that mitochondrial mass is increased in cells both directly treated with gamma radiation source or exposed to the bystander effect [273]. Mitochondrial mass is increased under oxidative stress suggesting that this cellular response results from an increase in ROS production.

The change in mitochondrial size is dependent on both de novo synthesis of nuclear DNA encoded proteins and their import into mitochondria that is dictated by the membrane potential of mitochondria. The increase in the mitochondrial mass of cells under oxidative stress is not dependent on the presence or function of mtDNA [274].

Our senescence-associated data, measured in response to both proton and photon radiation treatments, is likely associated with impaired mitochondrial dysfunction and oxidative stress. The photon treatment had a greater overall effect on mitochondrial function than the proton irradiation. These results are not attributable to the defects of mitochondrial biogenesis, because MitoTracker Green FM staining showed that the mass of mitochondria increased, not decreased. An increase in mitochondrial mass does not necessarily correlate with an increase in mtDNA content. Previous work indicates that mitochondrial DNA replication is independent of and uncouples from mitochondrial fission [275]. Because mitochondria contain proteins synthesized by both nuclear and mitochondrial DNA, the nuclear proteins can still be produced even though the mitochondrial DNA is defective. In response to mitochondrial dysfunction, there may be a disproportional synthesis of nuclear-encoded proteins that may contribute to the increase in mitochondrial mass, even when the mitochondria may lack mitochondrial DNA due to replication impairment [186,276]. Therefore, the number of mitochondrial genomes per mitochondria must be even lower when compared to the sham-control cells.

CHAPTER 3

IDENTIFICATION OF MIRNA-MRNA REGULATORY NETWORK ASSOCIATED WITH OXIDATIVE DNA DAMAGE IN HUMAN ASTROCYTES

3.1 Knowledge Gap

While the role of miRNAs in carcinogenesis and neurological disorders is a relatively new area of research, due to its therapeutic potential, the field is rapidly growing and numerous miRNAs that modulate disease-related physiological processes have been identified [65,66]. Thus, understanding the epigenetic regulation of astrocyte DNA repair mechanisms could lead to the identification of novel targets for the treatment of neurological and neurodegenerative diseases. Although much progress has been made in elucidating the function of various miRNAs, there is a paucity of scientific data regarding the specific miRNAs that regulate the proteins involved in the base excision repair pathway.

3.2 Hypotheses and Specific Objectives

DNA damage regulates the biogenesis of miRNA expression at the transcriptional level via the p53 pathway [101]. With the cross-talk between ROS and miRNA-processing enzymes [15], there is a very high possibility that closely related miRNAs and their target

genes would be involved in mediating the oxidative stress-induced cellular response. Therefore, it is hypothesized that ROS-induced DNA damage will alter the epigenomic (miRNA expression) patterns of affected cells and modulate functionally related DDR-associated genes. This study, therefore, aims to perform high throughput small RNA sequencing and functional analysis to identify novel ROS-induced differentially expressed miRNAs that modulate the expression of genes that are associated with the DNA repair mechanism in human astrocytes.

It is also hypothesized that increased accumulation of nuclear 8-OHdG adducts in the astrocytes will correspond with sodium dichromate treatment. This scientific hypothesis will be tested by quantifying genomic 8-OHdG accumulation as a function of ROS-induced DNA damage.

3.3 Materials and Methods

3.3.1 Cell Culture

Human primary astrocytes (Sciencell, Carlsbad, CA) were cultured in T-25 flasks containing 5 mL of Astrocyte Medium (Sciencell, #1801), supplemented with 1% penicillin/streptomycin solution (Sciencell, #0503), 2% Fetal Bovine Serum (Sciencell), and 1% astrocyte growth supplement (Sciencell #1852). The cells were grown at 37°C, 95% humidity, and 5.0% CO_2/air until they reached 80% confluence. Uniform seeding density of 2.1×10^6 cells per flask was maintained during subculture using Countess II FL Automated Cell Counter **(**ThermoFisher Scientific**,** Waltham, MA).

3.3.2 Sodium Dichromate Treatments

Depending on the specific experiments, cells were treated with various concentrations of sodium dichromate (10 µM, 10 mM, and 100 mM), and incubated for 16 h before being harvested for analysis. Non-treated cells were maintained in parallel and used as control.

3.3.3 Cytomorphological Evaluation

Before cell harvest, images of control (non-treated) and 10 µM $Na_2Cr_2O_7$- treated cells were captured using an inverted phase-contrast light microscope, to evaluate the changes in cell morphology following the treatment.

3.3.4 Comet Assay

Human astrocytes were grown in T-25 flasks to 80% confluency and treated with 10 µM sodium dichromate for 16 h. Trypsin was added to both the control (non-treated) and treated cells for 5 min at 37°C to detach the cells. 15,000 cells were then collected and centrifuged for 5 minutes at 4°C. The cell pellets were suspended in 200 µL of 6% low-melting-point agarose (pre-warmed to 37°C). The agarose cell suspension (60 µL) was pipetted onto an agarose-coated coverslip and placed over a slide. The coverslip was removed after 10 min and the samples were placed in lysis buffer (100 mM EDTA, 2.5 M NaCl, 10 mM Tris-HCl, 1% Triton-X, pH 10) at 4°C overnight. The slides were placed in chilled ddH_2O for 5 min, rinsed one more time with chilled ddH_2O for 10 min, and washed with enzyme reaction buffer (40 mM HEPES, 0.1 M KCL, 0.6 mM EDTA, 0.2 mg mL^{-1} BSA, pH 8). Formamidopyrimidine [fapy]-DNA glycosylase (FPG, New England Biolabs) was diluted in the enzyme reaction buffer to a final concentration of 8 U mL^{-1}. Both treated and control samples were incubated with either enzyme reaction buffer or FPG for 30 min

at 37°C. The slides were placed in the electrophoresis buffer for 20 min to allow equilibration and gel electrophoresis was performed for 20 min at 30 V and 300 mA. The slides were placed in a neutralization buffer (0.4M Tris-HCL, pH 7.5) for 20 min, rinsed with ddH_2O for 10 min, and allowed to dry overnight at 37°C. The samples were rehydrated in water the next day and stained with 2.5mg mL^{-1} propidium iodide (ThermoFisher Scientific, cat. #P1304MP). After 20 min of incubation with the dye, the slides were rinsed with ddH_2O for 10 min and dried overnight at 37°C. Comets were visualized using a Nikon Eclipse Ti microscope at 150X magnification. The OpenComet plugin for Image J was used to quantify the tail moment from the tail length and staining intensity of the head and tail [277,278]. At least 70 cells were analyzed for each condition.

3.3.5 High-Throughput Small RNA Sequencing and Analysis

3.3.5.1 Library Preparation and Ion Torrent™ Sequencing

The human astrocytes (Non-treated, 10 µM, and 10 mM Sodium Dichromate-treated) were lysed and the small RNA fractions were enriched using mirPremier® MicroRNA Isolation Kit (Sigma-Aldrich, Cat. # SNC10). Six samples were processed for Small RNA sequencing analysis that includes 3 biological replicates in the treatment and control. The concentration of small RNA fraction was determined using a Qubit RNA HS Assay Kit (ThermoFisher Scientific, Cat. # Q32852) using Qubit 4 Fluorometer (ThermoFisher Scientific, cat. #Q33238). Next-generation sequencing (NGS) small RNA libraries were size-selected to enrich for constructs containing mature miRNAs. The sequencing was performed on Ion Torrent™ next-generation sequencing systems **(**ThermoFisher Scientific**,** Waltham, MA**)**.

3.3.5.2 MicroRNA-Seq and QA/QC Analyses

Computational analysis of FASTQ data files that include the raw data was performed using the microRNA-Seq algorithms of the *Partek® Flow®* software, v10.0 (Partek Inc., 2020), an intuitive visual interface that allows the queuing and execution of a string of pipeline commands. Quality control parameters were checked to obtain the average base quality score per reading (Phred quality score), distribution of the raw read lengths to assess enrichment in microRNAs; base trimming and coverage breakdown were also carried out to confirm that the reads mapped reasonably within a microRNA.

3.3.5.3 Differential miRNA Analysis and Visualization

The reads were aligned using the Bowtie algorithm that allows for 1 mismatch and processed via Partek's default MicroRNA-Seq pipeline that mapped the reads to a reference genome (*Homo sapiens*, hg38) indexed to miRBase Mature Micro*RNA* (version 21). The differential gene expression analysis was performed using Partek's Gene Specific Analysis (GSA) algorithm, which applies multiple statistical models to each gene to account for each gene's varying response to different experimental factors (in this case, sodium dichromate treatment), and differing data distributions. The miRNA gene list obtained was further filtered such that only miRNAs that meet the set threshold ($\geq$ 2-fold, FDR$<$ 0.01, p-value $<$ 0.05) were selected.

Hierarchical clustering and visualization plots were generated on the platform to aid visualization and interpretation of the data: a principal component analysis (PCA) plot was generated to identify outliers between the Non-treated and 10 µM Sodium Dichromate-treated groups; a Volcano plot was plotted to show the distribution of upregulated and

downregulated miRNA genes; while a heatmap diagram was generated to visualize sample clustering among the differentially expressed miRNAs.

3.3.5.4 miRNA Functional Enrichment Analysis

The biological processes and genes targeted by the differentially expressed miRNAs were identified using miRNet 2.0 [280].

3.4 Results

3.4.1 Sodium Dichromate Induces Oxidative DNA Damage in Astrocytes

Sodium dichromate treatment was associated with reduced growth and distinct morphological changes in human astrocytes (Figure 3-1). Phase-contrast microscope images obtained after 16 hours of 10 µM sodium dichromate treatment (Figure 3-1B) shows cytomorphological changes, cytoplasmic granulation, and reduced proliferative density, indicative of stressor effects – unlike the normal spindle-like astrocytes which displayed a typical cellular structure (Figure 3-1A).

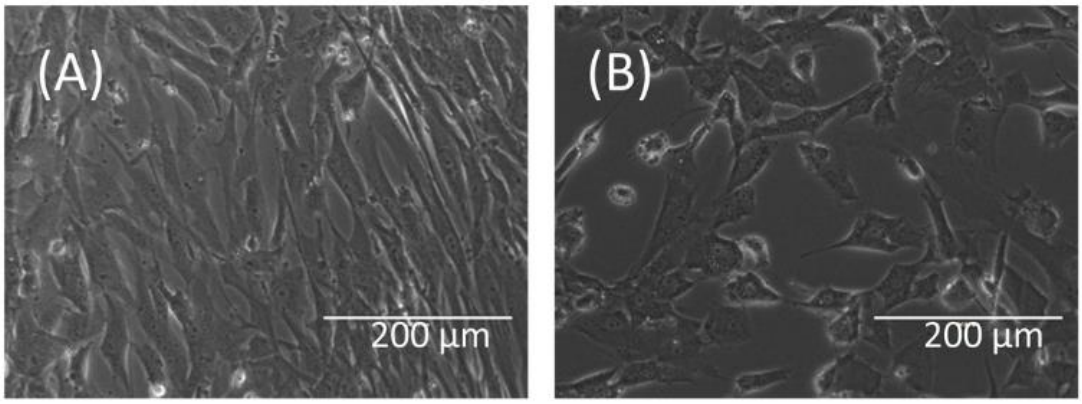

Figure 3-1 Bright-field image of human astrocytes, 10x magnification (A) control, and (B) treated with 10µM sodium dichromate

A formamidopyrimidine-DNA glycosylase (FPG) modified comet assay was performed to assess the sodium dichromate-induced oxidative DNA damage. The comet

assay detects DNA strand breaks by measuring the migration of DNA from individual nuclei in an alkaline environment, and can also detect oxidative DNA damage when the nuclei are treated with a DNA glycosylase enzyme (Amanda J. Lee et al., 2004). The average tail moment was used as a measurement of the magnitude of strand breakage (-FPG) or oxidative DNA damage (+FPG). The sodium dichromate-treated cells displayed longer tail lengths and tail moments in comparison to the control samples (Figure 3-2). Elongated tails and larger tail moments are consistent with the fragmentation of nuclei due to strand breakage or recognition and removal of damaged bases by FPG that recognizes 7, 8-dihydro-8-oxoguanine (8-oxoguanine), 8-oxoadenine, fapy-guanine, methy-fapy-guanine, fapy-adenine, 5-hydroxy-cytosine, and 5-hydroxy-uracil [281].

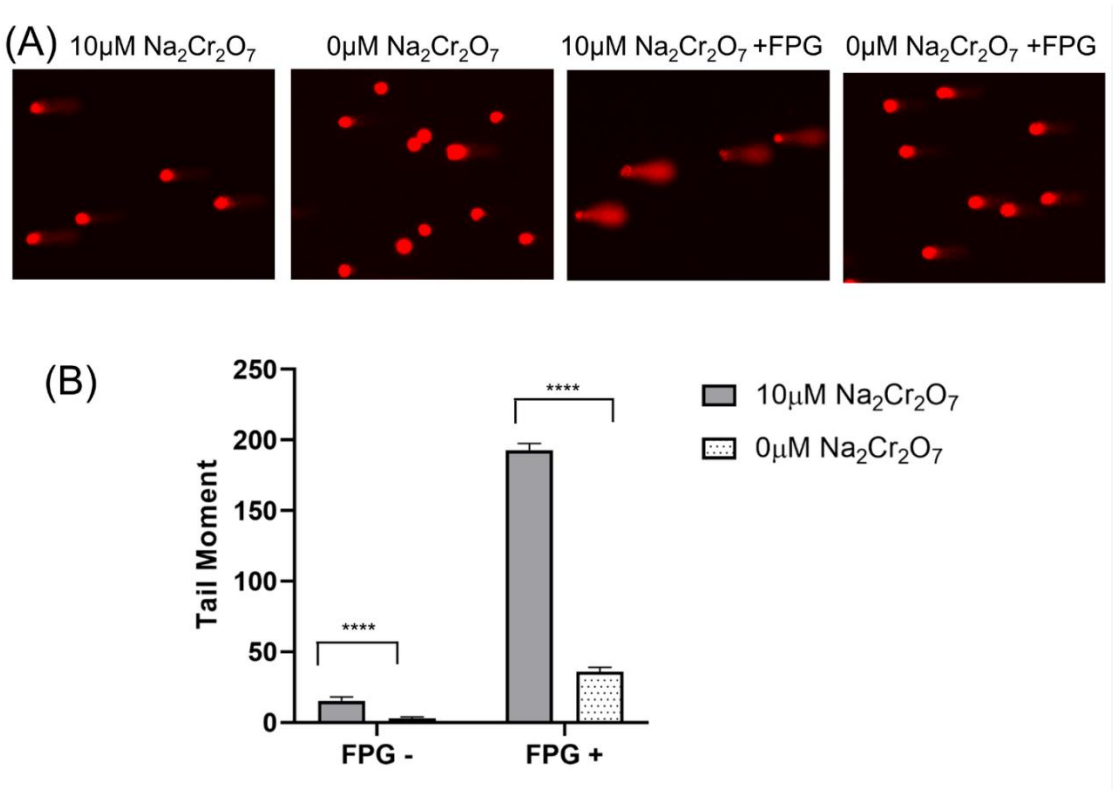

Figure 3-2 Sodium dichromate increases oxidative DNA base damage. The alkaline comet assay with FPG treatment was used to detect oxidative base damage following 10 μM Na2Cr2O7 treatment for 16 h (A) and the tail moment was measured using OpenComet (B). Analysis was performed on one experiment with at least 70 cells in each experimental group. Error bars represent SD and **** represents $P < 0.0001$ using a Student's t-test

3.4.2 Pre-Alignment QA/QC Charts

In all 6 samples (3 replicates each of 10 μM-treated and Non-treated), the average Phred quality score ranged from 28% to 31% (Figure 3-3). Fragments with a Phred score of 20% signifies that the specific base call is 99% accurate, while 30% means it is 99.9% accurate, so the raw data is well within acceptable limits. The distribution of the raw read lengths showed that they are relatively short, with greater enrichment for microRNAs (Figure 3-4). Using a quality score cut-off of 28 and a minimum read length set at 15, the quality of the reads was improved by base trimming from both ends (Figure 3-5). To assess the improved read quality, a coverage breakdown for each sample confirmed that a good

portion of the reads mapped fully or partly within a microRNA (20% on the average), while a sizeable portion did not map within a microRNA (Figure 3-6). This is not unexpected, especially for the human genome that includes large segments of intronic regions interspersing the gene-coding sequences [282].

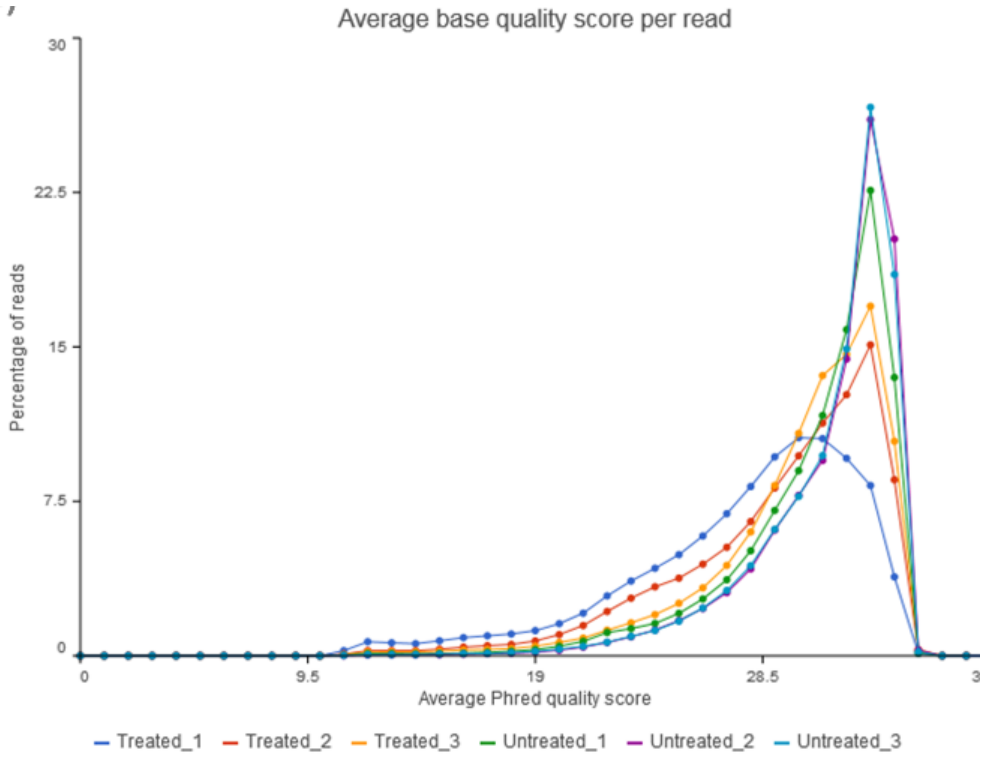

Figure 3-3 Pre-alignment QA/QC showing average base quality score per reading. The Phred quality scores of the analyzed samples ranged from 28% to 31%

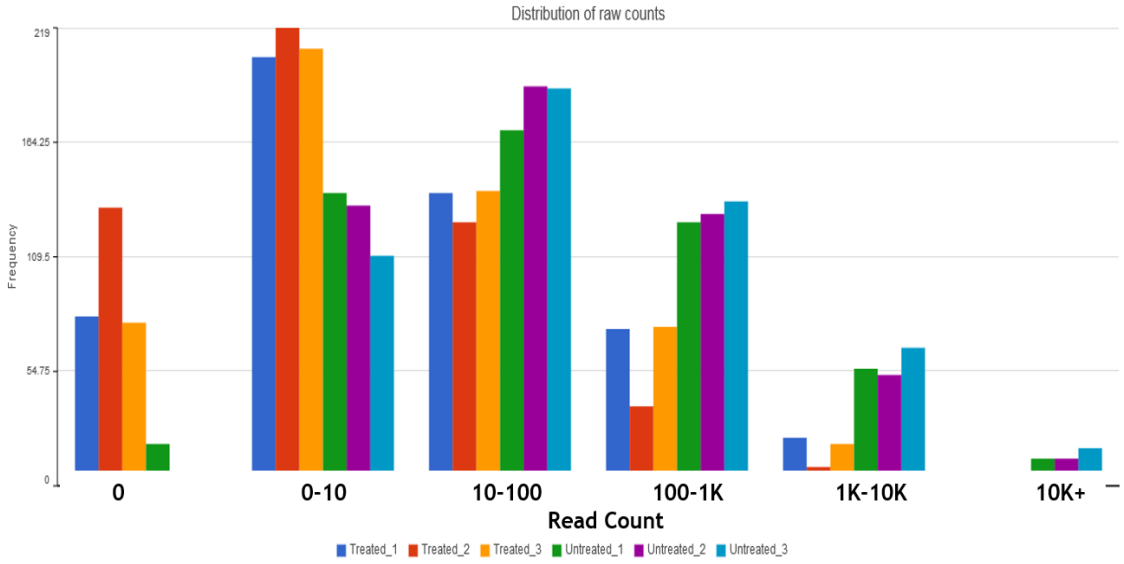

Figure 3-4 Size distribution of raw counts of transcripts

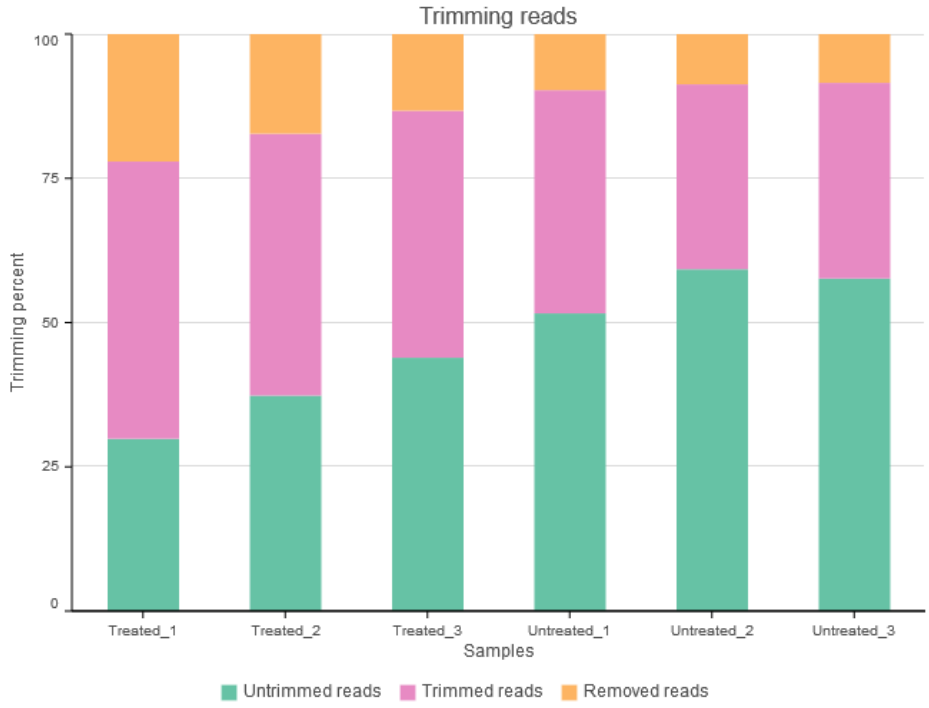

Figure 3-5 Percentage representation of trimmed bases (quality score cut-off = 28; minimum read length = 15

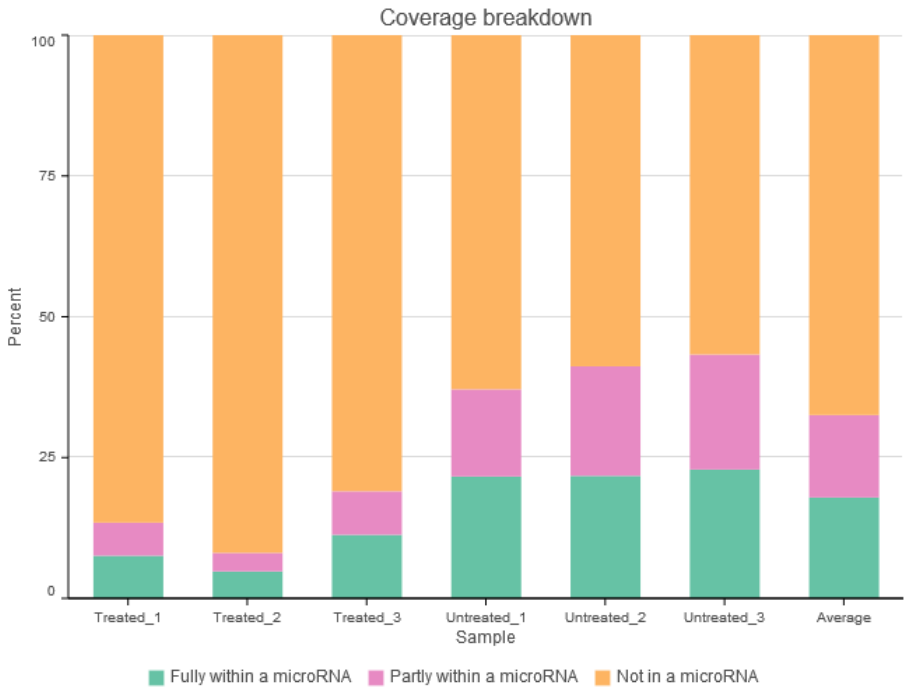

Figure 3-6 Coverage breakdown of raw reads post-trimming

3.4.3 Small RNA Sequencing Identifies a Large Number of Differentially Downregulated MicroRNAs

The differential gene expression analysis identified a list of significantly differentially expressed miRNAs (≥ 2-fold, FDR< 0.01, p-value < 0.05) following 10 µM sodium dichromate treatment: 231 miRNAs were found to be downregulated, while only 2 were upregulated (Appendix C.1).

The MicroRNA-Seq data analysis for the 10 mM sodium dichromate-treated cells vis-à-vis non-treated cells yielded 56 downregulated miRNAs (which include miR-7, miR-17, miR-103a, miR-155, miR-182, miR-let-7d, miR-let-7e, etc.) and 6 upregulated miRNAs (miR-25, miR-30c, miR-153, miR-204, and miR-365a) (Appendix C.2).

3.4.4 Hierarchical Clustering Plots

A principal component analysis (PCA) plot was generated to identify outliers among the two treatment groups (Figure 3-7), while a Volcano plot delineated the distribution of upregulated and downregulated miRNA genes (Figure 3-8). Hierarchical sample clustering via heatmap diagram was generated to visualize the sample clustering of the differentially expressed miRNAs (Figure 3-9). Essentially, PCA compresses the expression data from thousands of genes to represent the overall variation in expression as a single dot on a graph – one dot per sample being analyzed. Each dot represents the number of reads multiplied by the influence of each corresponding gene on the overall variation in expression, in terms of the two most important dimensions of variation (the two axes), called principal components. Genes with the largest variation between samples will have the most influence on the principal components. That is, genes that are much more highly expressed in one group than in another group will have a high degree of influence on the principal components. Samples with similar noncoding RNA expressions that correlate with the treatment conditions cluster together in a PCA plot and heat map, as shown in Figures 3-7 and 3-8.

Other PCA plots for specific miRNAs known to be involved in oxidative DNA damage, miR-21 [283] and miR-335 [284], also showed delineated clustering (Appendices C.6 and C.7).

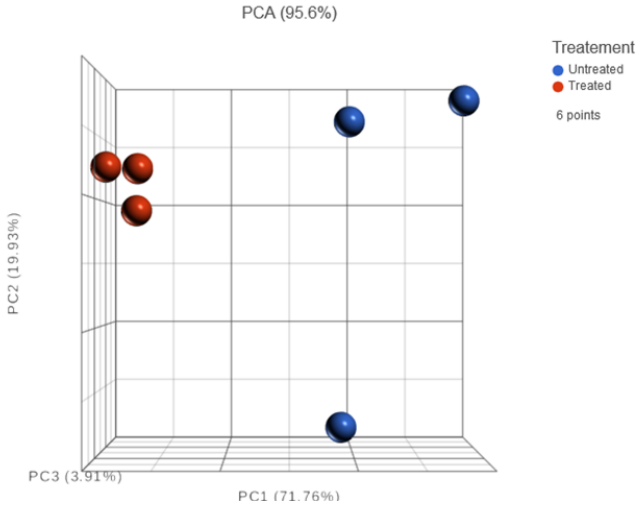

Figure 3-7 Principal Component Analysis (PCA) plot showing clustering of the treated and control samples. The two most informative components were plotted by the Partek® Flow® software

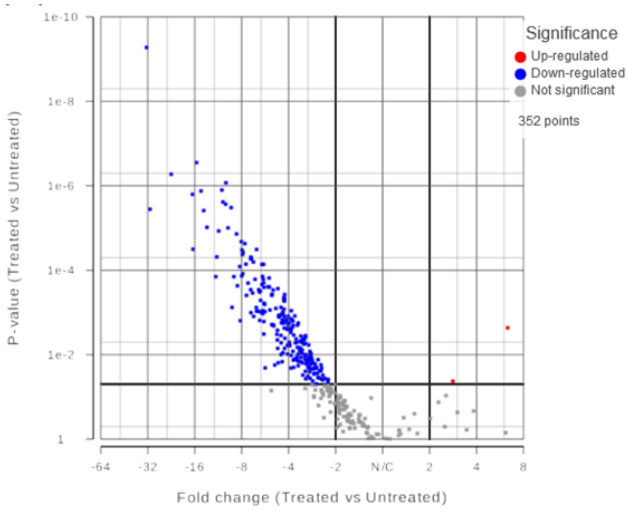

Figure 3-8 Volcano plot depicting the distribution of upregulated and downregulated miRNA genes in treated samples relative to controls

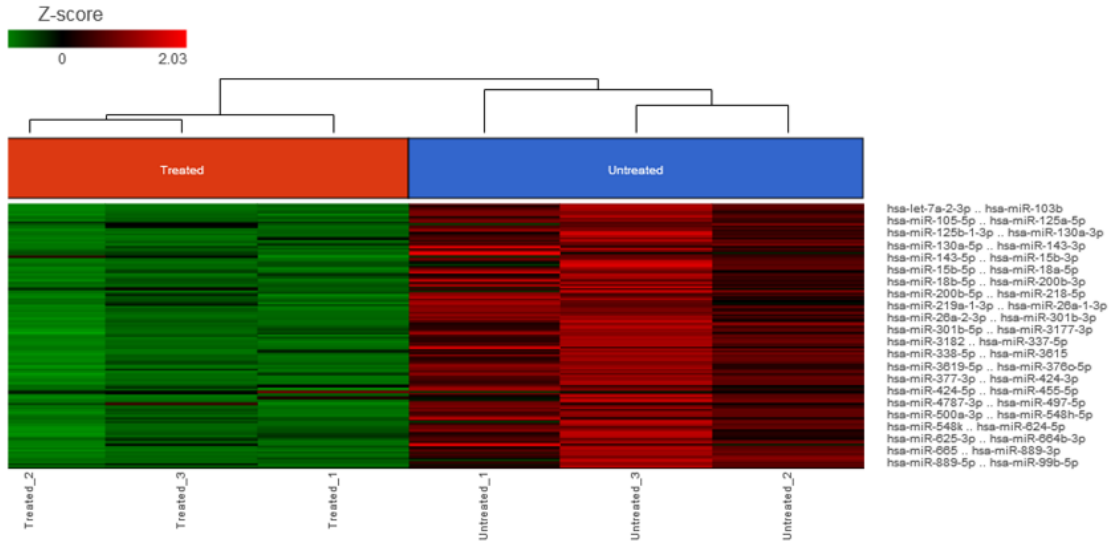

Figure 3-9 Unsupervised hierarchical clustering using the differentially expressed miRNAs between treated and control samples represented as a heat map. The heat map colors correspond to microRNA expression as indicated in the color key: Red (up-regulated) and Green (down-regulated)

3.4.5 Gene Ontology Analysis Identifies Biologically Significant miRNAs

The annotation feedback came from three combined databases (miRTarBase v8.0, TarBase v8.0, and miRecords) hosted on miRNet 2.0, and used the Kyoto Encyclopedia of Genes and Genomes (KEGG) database option, with an "all genes" hypergeometric test setting.

3.4.5.1 miRNA-Gene/Pathway Analyses

The search results returned 49 miRNAs and 13,585 target genes involved in molecular pathways associated with signaling, cell cycle control, and DNA damage and repair, etc. (Appendices C.1 and C.3). The most statistically significant pathways include cancerogenesis and cell cycle control (Table 3-1).

Table 3-1 Top pathways enriched in putative miRNA-targeted genes

Biological Process/Pathway	**Adj. p-Value**	**Genes**
Pathways in cancer	2.11E-16	285
Cell cycle	2.79E-11	120
Neurotrophin signaling pathway	3.24E-07	114
Wnt signaling pathway	3.19E-06	129
ErbB signaling pathway	8.73E-06	81
RNA transport	1.15E-05	113
Glioma	1.29E-05	62
Axon guidance	1.71E-05	106
p53 signaling pathway	3.11E-05	64
Jak-STAT signaling pathway	0.000241	88
MAPK signaling pathway	0.000362	218
mTOR signaling pathway	0.001303	42
Pyrimidine metabolism	0.001896	87
RNA degradation	0.001896	54
Ribosome biogenesis in eukaryotes	0.004891	49
Purine metabolism	0.004891	134
Apoptosis	0.006644	71
Alzheimer's disease	0.015065	43
Prion diseases	0.016875	20
mRNA surveillance pathway	0.027838	68
Huntington's disease	0.03759	25
VEGF signaling pathway	0.05427	62

Among the differentially expressed microRNAs (Appendix C.1), 10 downregulated miRNAs were identified to target DNA repair proteins, according to miRNet 2.0's curated database of proven interactions. These include miR-15a-5p, miR-16-5p, miR-17-5p, miR-93-5p, miR-125a-5p, miR-125b-5p, miR-128-3p, miR-155-5p, miR-335-5p, let-7b-5p (Figure 3-10, Table 3-2). The annotations for two upregulated miRNAs, miR-1248 and miR-4284, were discovered on miRDB [285].

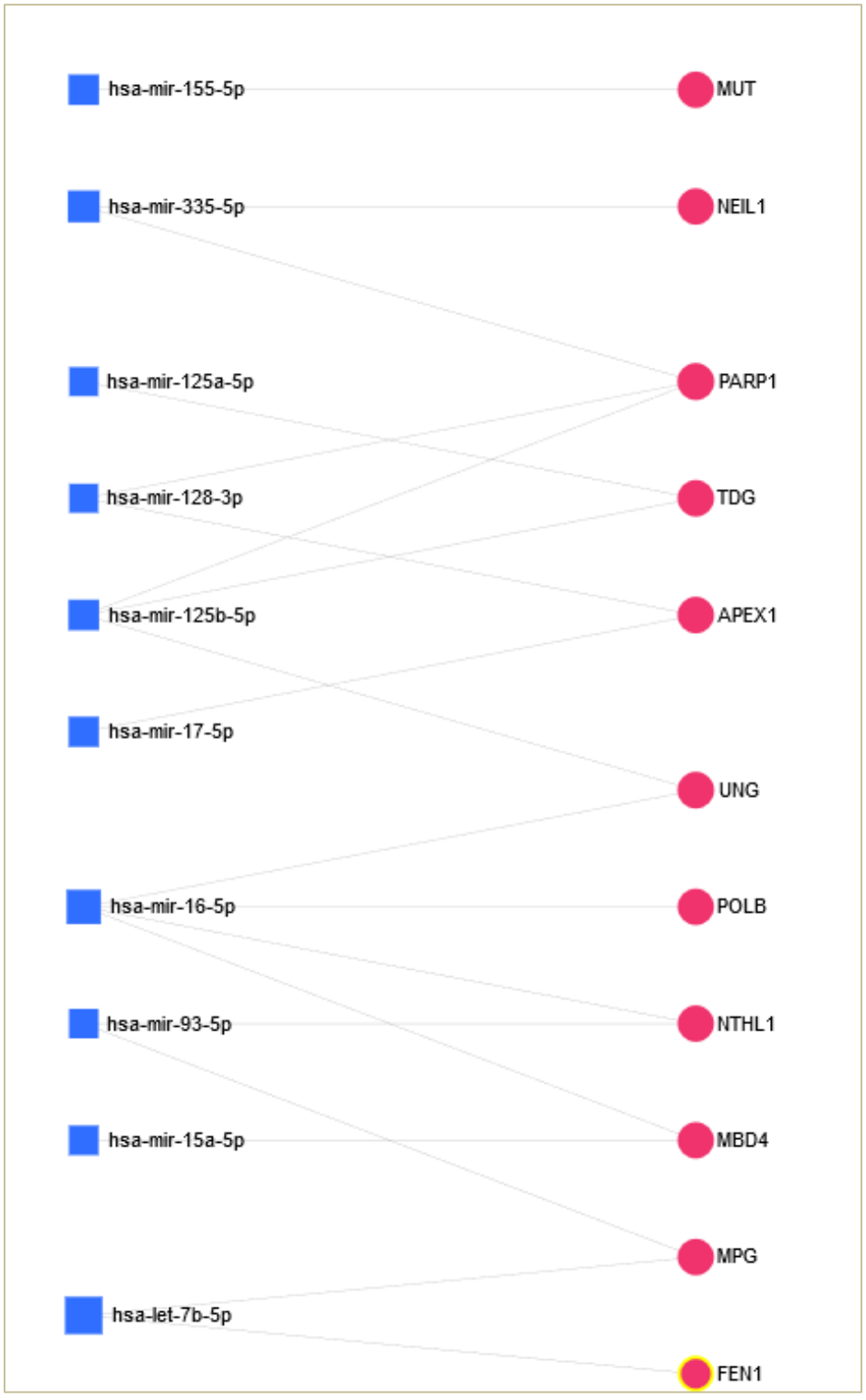

Figure 3-10 A coherent group of miRNAs target DNA repair proteins. Network constructed on miRNet 2.0

Table 3-2 List of differentially expressed BER-associated MicroRNAs ($p < 0.05$)

Post-Treatment Regulation	miRNA ID	Fold Change	Experimentally validated DNA repair gene targets
Downregulated	hsa-miR-16-5p	10.1	UNG/UDG, MBD4, NTHL1
	hsa-miR-128-3p	8.05	APEX1
	hsa-miR-17-5p	7.97	APEX1
	hsa-miR-93-5p	5.89	NTHL1, MPG
	hsa-miR-125b-5p	5.78	UNG/UDG, TDG
	hsa-miR-125a-5p	4.29	TDG
	hsa-miR-15a-5p	4.28	MBD4
	hsa-miR-155-5p	3.19	MUT
	hsa-miR-335-5p	2.81	PARP1
	hsa-let-7b-5p	2.48	MPG, FEN1
Upregulated	hsa-miR-4284 [3]	6.33	No Hit
	hsa-miR-1248 [3]	2.82	OGG1 [3]

3.4.5.2 miRNA-Disease Associations

Further analysis of the miRNA-disease associations identified 21 mRNAs that were experimentally validated to be linked to 143 pathologies (Appendix C.4). miR-107, with a betweenness value of 9972.589 and 102 degrees, was linked to more brain-linked pathologies than all of the other miRNAs (Figure 3-11), followed by miR-9-5p, miR-128-3p, miR-125b-5p, miR-181b-5p, and miR-139-5p.

[3] No hits were found on the miRNet-hosted databases as the miRNAs have not been annotated. Both miRNAs had several hits on miRDB. Only miR-1248 had a BER target protein, OGG1.

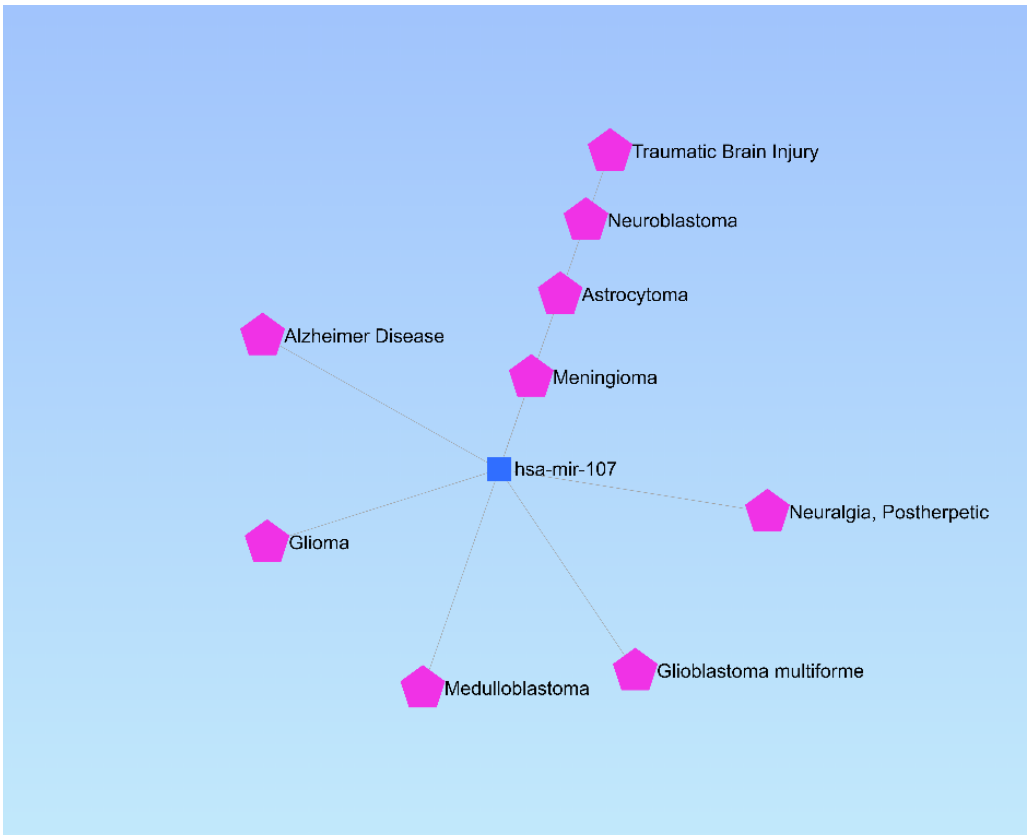

Figure 3-11 CNS-associated pathologies mediated by hsa-miR-107. The network was constructed on MiRNet 2.0

3.4.5.3 Protein-Protein Interaction (PPIs)

Empirically proven protein-protein interactions (PPIs) were also investigated on miRNet-hosted STRING Interactome, v11 [286], set at a confidence score cutoff of 500. A list of 18,553 proteins interacting with one another was generated (Appendix C.5).

3.5 Discussion

The brain is intrinsically vulnerable to ROS-induced oxidative stress. Cell shrinkage, cytoplasmic granulation, nuclear fragmentations, and cell lysis are the major visible hallmarks of apoptosis [287]. This study indicated that that sodium dichromate-induced oxidative DNA damage resulted in varying degrees of cell shrinkage and changes

in cell morphology in the human astrocytes. Incorporation of mismatched base pairs occurs frequently during DNA replication while a cascade of self-destructing cellular events is initiated to prevent the replication and transfer of damaged DNA to daughter cells. Therefore, oxidative stress-induced ROS activates the proapoptotic cellular machinery [288]. Previous work confirmed the relationship between the TNF-related apoptosis-inducing ligand (TRAIL) expression in human astroglial cells and immune cell effector functions [289]. Other members of the death ligand/receptor pairs like the Fas/Faslg pair are also recruited following oxidative stress, and this is supported by our PPI data (Appendix C.5). The apoptotic mechanisms are synergistic and act either through sensitivity priming [290] or through bystander cytotoxicity [291].

Our findings indicate that there is a trend towards a decrease in miRNA expression in treated cells, suggesting an underlying upregulation in the transcription of multiple genes. Logically, at the center of this phenomenon could be the involvement of ROS in the pathways of microRNA biogenesis, especially at the transcription level via p53's regulatory effect on the Drosha enzyme, as have been variously reported [15,101]. Since the p53 signaling pathway is among the top pathways highlighted by our Gene Ontology analysis (Table 3-1), p53 could be responsible for the global downregulation of miRNAs through a negative feedback loop mechanism. In a previous study, exogenous H_2O_2 exposure has been shown to cause a significant decrease of Dicer expression resulting in the downregulation of 89% of microRNAs that are normally expressed in cerebromicrovascular endothelial cells [292].

Functional enrichment analysis identified physiological and pathological processes that are regulated by differentially expressed miRNAs. The biological processes that are

highly regulated by the miRNA network include genes regulating cell cycle control, protein processing in the endoplasmic reticulum, axon guidance, and neurotrophin signaling which promotes survival, growth, and differentiation of neurons and neurites (Table 3-1). In addition to supporting neuronal growth, neurotrophins play an important role in the pathophysiology of many neurodegenerative and psychiatric disorders [293]. This indicates that genes involved in the cell cycle and CNS response may be regulated by stress-induced miRNAs. Pathways in cancer accounted for the highest hits (285 genes), supporting the correlation between oxidative stress and cancer that has been established by multiple groups [14].

Non-coding RNA-mediated expression of the genes associated with apoptosis that include the Caspase protein family, TP53, BAX, BCL2, FADD, ATM, FAS, FASLG, corresponded with the decrease in cell density and cytoskeleton architectural changes in treated cells (Figure 3-1). Genes involved in RNA metabolism and transport were also deregulated. These included UPF1, the gene that codes for RNA helicase and translocase enzyme that is essential for nonsense-mediated decay, mediating both mRNA nuclear export and mRNA surveillance through ribonucleoprotein (RNP) remodeling [294]. Post-transcriptional regulation of gene expression in response to cellular stress occurs on RNP granules [295]. This could be used for the development of stress-adaptive miRNA-based therapeutics by recreating the concentration- and phase-dependent assembly of these membranous compartments in cells of interest.

This study identified numerous, and often, overlapping targets for the dysregulated miRNAs (Table 3-1). It is a well-established fact that miRNAs are pleiotropic and redundant regulators, and therefore one miRNA can target multiple genes, as well as

multiple miRNAs can target a single gene [56]. MicroRNAs that target genes within the DNA damage repair (DDR) loop were mostly downregulated, indicating an activation of the DDR transcriptome. Functional enrichment analysis showed that the majority of the targeted genes are associated with signaling, cell cycle control, and maintenance of DNA integrity. This supports our hypothesis that oxidative stress alters the miRNA expression signature to reflect bloc activation of coherent, functionally related pathways. Members of the DDR loop, a kinase-based functional network that initiates phosphorylation-driven cascades [91], were over-represented in the analyzed data sets. Key players within the DDR loop that were captured in our data set include PI3K, ATM, ATR, which are essential in maintaining genome stability and reducing pathological processes [92,296,297]. This presents a veritable lead for the investigation and development of molecular mechanistic models for DDR loop activation. DNA-damage response RNAs (DDRNAs) have been proposed as a requirement to fully activate the DDR response [298,299]. These DDRNAs, like miRNAs, are generated by Drosha and Dicer processing, and they have the same sequence as their cognate damaged DNA. Thus, this sequence specificity may help them to act as guides for the localization and activation of DDR proteins.

Because of its therapeutic target potential, microRNAs are actively being explored for the management and treatment of major neurodegenerative disorders. Specifically, miR-155 upregulation has been implicated in amyotrophic lateral sclerosis (ALS), and its inhibition slowed down disease progression in pre-clinical models [300]. Downregulated, as per our results, tinkering with safe serum or CSF-infused chromium levels may be a viable supplemental strategy to inhibit miR-155 in the therapeutic regimen for ALS patients and may be potentially applied to other neurological disorders where miR-155 is

increased, including multiple sclerosis [301] and glioblastoma [302]**.** One way to achieve this may be via the manipulation of chromium bioavailability, as have been done in a sorption study that demonstrated the reduced bioavailability of chromium by binding to iron particles in an acidic medium [303]. However, variability in individual responses to sodium dichromate has been observed [304]**,** which may need to be factored into such clinical approaches.

Most drinking water supplies in the United States contain < 5 µg/L of chromium since hexavalent chromium is a common disinfection by-product, raising safety concerns. Cr(III) is oxidized to Cr(VI) by added oxidants (such as potassium permanganate) and disinfectants (chlorine, chloramine) used in water treatment plants [305,306]. Chromium (III) ion is classified as an essential nutrient that is normally present in blood and urine in trace amounts and required for normal energy metabolism. Moreover, the Institute of Medicine of the National Academy of Sciences recommended an adequate intake of chromium(III) of 20 – 45 µg/day for adolescents and adults [307]. Therefore, the findings from this study can be used by environmental and health agencies to make informed safety and dietary recommendations.

CHAPTER 4

MICRORNAS AND DNA REPAIR GENES: TARGET PREDICTION AND VALIDATION

4.1 Overview and Hypotheses

The results from the next-generation small RNA sequencing experiments indicate that sodium dichromate-induced oxidative stress is associated with differential expression of multiple miRNAs.

Base excision repair (BER) is one of the mechanisms that protects the brain cells from oxidative stress by preventing both nuclear and mitochondrial mutations. The human 8-deoxyguanosine DNA glycosylase 1 (hOGG1) is an 8-OHdG-specific BER enzyme that plays an integral part in reducing the rate of mutations. By being in the frontlines of mitigating the effects of reactive oxygen species, OGG1 contributes to decreasing the detrimental effects of oxidative DNA damage [2]. Therefore, identifying a subset of potential miRNAs that control the post-transcriptional expression of OGG1 will provide an assessment of the epigenetic regulation of the OGG1-mediated DNA repair mechanism in response to ROS-induced oxidative damage.

A common feature of most validated targets is that their cognate miRNAs preferentially bind to the 3′ untranslated regions (3’-UTR) sites that do not have complex secondary structures and are located in the accessible regions of the RNA based on

favorable thermodynamics [122]. Based on the small RNA sequencing and Comet assay data, we hypothesize that some of the miRNA species that exhibited differential expression following oxidative stress will bind within the 3'UTR region of the OGG1 transcript.

The expression levels of the miRNA candidates and their target mRNAs will be initially verified using RT-qPCR. Since miRNA expression level is inversely related to the expression level of its target mRNAs, it is expected to see a reciprocal mRNA and protein expression pattern from the ensuing RT-qPCR and Western analyses. The interaction between the putative miRNA/mRNA pairs will be further validated via miRNA transfection (mimic or inhibitor) and/or immunoprecipitation assays (MirTrap System) coupled with reverse transcription qPCR (RT-qPCR) technique [308]. The MirTrap technology facilitates the discovery and detection of low abundance mRNA targets that can be lost during traditional, less sensitive immunoprecipitation methods. We hypothesize that if the transfected miRNA binds to the 3'UTR region of mRNA transcripts of interest, the mRNA target will co-immunoprecipitate with the RISC complex.

4.2 Research Methodology

4.2.1 *In Silico* Prediction of OGG1-targeting MicroRNA Candidates

Multiple bioinformatics databases – mirWalk 2.0 [309], MiRDB [310], and TargetScan [311] – were utilized to predict the probability of functional miRNA binding sites within the 3'UTR of all eight splice variants of OGG1 mRNA (OGG1-1a, −1b, −1c, −2a, −2b, −2c, −2d and −2e) that are registered in the NCBI gene and nucleotide database. OGG1-1a is the only OGG1 present in the nucleus, the other seven isoforms excise 8-OHdG from the mitochondrial genome [312]. The selection criterion was based on a miRNA candidate getting a hit in at least two of the prediction algorithm tools which factor

in seed-site pairing, site context, free-energy, and target conservation across multiple vertebrates [313,314]. The computational analysis was focused on miRNA targets conserved across mammals as these are more likely to be of functional significance [315].

4.2.2 Validation of miRNA-mRNA Interactions

Selected miRNA-mRNA target pairs were further analyzed to validate the predicted regulatory network. Given the negative regulatory effect of miRNAs on their mRNA targets, emphasis was placed on upregulated miRNAs and their impact on the expression levels of OGG1, a canonical BER enzyme that is directly involved in base excision repair. In addition to RT-qPCR, the pairwise binding between the selected miRNAs and the 3'UTR region of the OGG1 mRNA was confirmed via a combination of miRNA mimic or inhibitor transfection and/or immunoprecipitation of tagged RNA-induced silencing complex (RISC) that include miRNA/mRNA OGG1 pair.

Poly-(ADP-Ribose) polymerase 1 (PARP-1), an auxiliary DNA damage repair protein [316] and miR-335, one of its cognate miRNAs identified earlier (Figure 3-10; Table 3-2), were also analyzed via reverse-transcription qPCR (RT-qPCR). Interestingly, OGG1 binding to PARP-1 stimulates its poly(ADP-ribosyl)ation activity which is essential in the repair of oxidative DNA damage [317].

4.2.2.1 Reverse Transcription Quantitative PCR (RT-qPCR)

RT-qPCR was performed to validate the changes in the expression levels of the selected, biologically relevant miRNAs and their mRNA targets before and after 10 µM sodium dichromate treatment. The MicroRNAs, hsa-miR-335-5p (Sigma Aldrich, cat. #MIRAP00323) and hsa-miR-1248 (Sigma Aldrich, cat. # MIRAP00761), were validated using the MystiCq® MicroRNA Quantitation System (Sigma-Aldrich, St. Louis, MO).

Briefly, cDNA was synthesized from treated and control small RNA samples using MystiCq™ microRNA cDNA Synthesis Mix Kit according to the manufacturer's instructions. The cDNA concentration was measured using a Qubit 4 Fluorometer (Thermo Fisher Scientific, cat. #Q32854). Equal amounts of each cDNA (2ng), mixed with 10 µM of each MystiCq microRNA qPCR Assay Primer and 10 µM of MystiCq Universal PCR Primer plus MystiCq microRNA SYBR Green qPCR Ready-mix, were amplified as recommended by the manufacturer on a LightScanner 32 real-time PCR instrument. Relative quantification of miRNA expression was determined by using the Livak-Schmidt ($2^{-\Delta\Delta CT}$) method and normalized against SNORD 44 provided with the MicroRNA Quantitation System [318,319]. The results are represented as mean ± standard error calculated from three biological replicates.

The mRNA targets OGG1 and PARP1 were reverse-transcribed separately using the TaqMan™ RNA-to-CT™ 1-Step Kit (ThermoFisher Scientific, cat. # 4392653) and LUNA One-step RT-qPCR kit (New England BioLabs Inc., cat. #E3005S) respectively, on a QuantStudio™ 3 Real-time PCR system (Applied Biosystems, Cat. # A28567). Total RNA was harvested individually from treated and control cells with an RNA Miniprep Kit (Zymo Research, cat. #R1054), while the quantity and quality of the extracted RNA were determined by the Nanodrop 2000 system **(**Thermo Fisher Scientific, Waltham, MA**)**. Equal amounts of RNA (6 ng) were mixed with 10 µM forward and reverse primers (PARP 1 and GAPDH) to 0.5 µM final concentration, and reverse-transcribed for 10 min at 55°C, followed by inactivation of reverse transcriptase and cDNA denaturation at 95°C for 1 min. The subsequent amplification followed the vendor-recommended 40-cycle program of 10 seconds at 95°C, 30 s at 60°C, and 10 s at 95°C per cycle at a ramp heating/cooling rate of

20°C sec^{-1}. The GAPDH and PARP1 gene primer sequences (Integrated DNA Technologies, Coralville, ID) are shown in Appendix D.1. OGG1 mRNA expression level was analyzed using OGG1 and GAPDH TaqMan™ Gene Expression Assay (FAM) (ThermoFisher Scientific cat. # 4453320, 4448892), with an initial reverse transcription of 6 ng RNA at 48^0C for 15 min, followed by AmpliTaq Gold® DNA polymerase activation at 95^0C for 10 min, and a final 40-cyle amplification of 95^0C for 15 s and 60^0C for 1 min. Data were normalized to the C_T values of the internal control gene GAPDH, and analyzed using the $2^{-\Delta\Delta CT}$ method [320].

To further probe sensitivity to exposure, changes in OGG1 mRNA expression at higher concentrations of sodium dichromate (10 mM and 100 mM) were assessed via RT-qPCR, using the same parameters as above.

4.2.2.2 Capillary Western Analyses

Automated Western blotting was performed for quantification of the relative amount of OGG1 to the housekeeping protein, GAPDH using the ProteinSimple Wes® System. Human astrocytes were grown till they reached 80% confluence and treated with 10 µM $Na_2Cr_2O_7$ for 16 h. Both control and treated cells were trypsinized, washed with PBS, and lysed with M-PER™ Mammalian Protein Extraction Reagent (ThermoFisher, cat. #78501) and protease inhibitor to extract total protein. The protein concentration was determined using Pierce™ BCA Protein Assay Kit (ThermoFisher Scientific, cat. # 23227) and 1µg of protein was loaded per lane. The capillary western blot analysis was performed according to the vendor's instructions. The protein lysates were mixed with a 5 × Master Mix. The samples and the protein ladder (12 kDa, 40 kDa, 66 kDa, 116 kDa, 180 kDa, and 230 kDa) that provided the molecular markers for the assay were added to the wells in the

plate. Both the control and treated samples were probed with anti-GAPDH and anti-OGG1 polyclonal antibody (ABclonal Science Inc., cat. #A1384) diluted 1:50 with antibody diluent. HRP-conjugated anti-rabbit secondary antibodies and chemiluminescent substrate were used for the detection step. The separation electrophoresis and the detection step were performed with the Wes Protein Simple capillary system. The areas under the peak correlate with the intensity of the bands and were calculated by the Compass Software (ProteinSimple). The ratio between the area under the peak of OGG1 and GAPDH was used as an assessment of the relative signal intensity of the immuno-detected protein.

4.2.2.3 Exogenous miR-103a Expression: Co-immunoprecipitation with OGG1 mRNA

The pairwise binding between miR-103a (identified as differentially downregulated in 10 mM sodium dichromate-treated samples) and OGG1 mRNA target (verified by RT-qPCR to be upregulated in 10 mM sodium dichromate-treated samples), was validated via immunoprecipitation of RISC using the cutting-edge miRNA discovery technology developed by Clontech (Mountain View, CA) – the MirTrap System (Cat. # 632017).

4.2.2.3.1 MirTrap System: Working Principle

The MirTrap System entails transfection of double-stranded miRNA mimics, followed by immunoprecipitation of tagged RNA-induced silencing complex (RISC) that includes miRNA/mRNA OGG1 pair. The guide strand of the mimic is designed to have the same sequence as the endogenous miRNA, while the passenger stand has a complementary sequence. Both oligonucleotides contain 3’ overhangs and are phosphorylated at 5’ends. Since transfected miRNA “mimics” the endogenous miRNA of interest and recognizes the mRNA target, the RISC becomes flooded with microRNA

mimic/target RNA complexes which outcompete the endogenous microRNA/target RNA. The MirTrap Vector introduces the expression of a dominant-negative subunit of RISC protein that traps the miRNA/mRNA pair into the RISC and limits further processing. The protein subunit is integrated into the endogenous Argonaut (Ago)/RISC complex and tagged with a FLAG-epitope that has a DYKDDDDK sequence motif, thereby allowing the immunocapture and isolation of the entire Ago/RISC/miRNA/mRNA complex, and thus, selective purification of the target mRNA that undergoes direct regulation by the transfected miRNA of interest. The presence or absence of the precipitated target mRNA sequence is subsequently validated via sequencing or reverse-transcription qPCR (RT-qPCR) analysis.

4.2.2.3.2 MirTrap System Protocol

According to the vendor's protocol (Figure 4-1), the miR-103a mimic (Dharmacon^{TM} miRIDIAN Mimic, Cat. # C-300522-03-0002) was co-transfected with the pMirTrap vector that encodes the FLAG-tagged dominant-negative GW182 protein subunit of the Ago/RISC complex (Appendix D.2.1) in the human astrocyte cell line. Control miRNA (miR-132) together with the pMirTrap Control Vector and pMirTrap vector were transfected in parallel with the main pMirTrap vector and miRNA mimic to evaluate the transfection efficiency. The control vector encodes the gene for green fluorescent protein (AcGFP1) which is a target for the control miR-132, as well as the DsRed Express protein that is unaffected by miR-132 (Appendix D.2.2). Thus, a good expression of DsRed Express (assessed via fluorescence microscopy) indicates successful transfection of the pMirTrap Control plasmid, and if it is accompanied by a low AcGFP1 expression, it is indicative of successful miR-132 transfection.

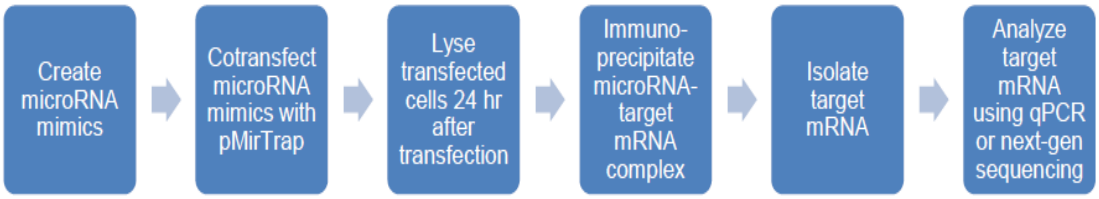

Figure 4-1 The MirTrap System: Protocol Overview

Following transfection, the astrocytes were lysed, and a portion of the lysate was used to isolate total RNA (Before Immunoprecipitation, BIP). The RISC complex was immunoprecipitated from the remaining lysate using anti-DYKDDDDK (FLAG-tag) beads, and the bead-bound target mRNA was isolated (After Immunoprecipitation, AIP). Both "BIP" and "AIP" RNA isolates were analyzed via RT-qPCR (One-Step SYBR® PrimeScriptTM RT-PCR Kit II, Takara Bio, Cat. # RR086A), using the 3 sets of primers included in the MirTrap Control Kit (positive control AcGFP1; negative control hPlod3; internal control hGAPDH) to assess the efficiency of the transfection, and using primers specific for the experimental miRNA target, OGG1 to calculate its fold enrichment in the "AIP" samples relative to the "BIP" samples. A minimum of 2.5-fold enrichment of triplicate experiments was considered a threshold for a miRNA:mRNA binding.

4.2.2.4 miR-1248 and miR-103a Inhibition: Assessment of miRNA:OGG1 Functional Relationship

4.2.2.4.1 miRNA Inhibitor Transfection Protocol

Human astrocytes were seeded at a uniform density of 3 x 10^5 cells per well in 6-well plates and incubated for 72 h. At 80% confluency, the cells were transfected separately in triplicates with *mir*Vana® hsa-miR-1248 and hsa-miR-103a inhibitors (ThermoFisher Scientific, Cat. # 4464084), and with *mir*Vana® negative control #1 (ThermoFisher Scientific, Cat. # 4464076), according to manufacturer's protocol. Briefly, the miR-1248

inhibitor and the negative control #1 were reconstituted to 10 µM stock concentrations with nuclease-free water, and then 3 µL of each was diluted in 150 µL Opti-MEM™ I Reduced Serum Medium (ThermoFisher Scientific, Cat. # 31985062) to obtain 30 pmol per well. 9 µL Lipofectamine™ RNAiMAX Transfection Reagent (ThermoFisher Scientific, Cat. # 13778100) was diluted in 150 µL Opti-MEM™ I Reduced Serum Medium. Both diluted reagents were mixed at a 1:1 ratio and the resulting miRNA-lipid complex was incubated for 5 min at room temperature. The transfection reagent mix was added to cells at 250 µL per well, so that the final amount of miRNA inhibitor or negative control used per well is 25 pmol, while the final amount of Lipofectamine™ RNAiMAX Transfection Reagent per well was 7.5 µL. The transfected cells were incubated at 37^0C for 48 h. Control experiments of non-transfected cells were also maintained in triplicate.

The efficacy of the transfection protocol was confirmed by assessing the expression levels of miR-1248 post-inhibition, using an hsa-miR-1248 primer (Sigma Aldrich, cat. # MIRAP00761) and the MystiCq® MicroRNA Quantitation System (Sigma-Aldrich, St. Louis, MO) on a QuantStudio™ 3 Real-time PCR system (Applied Biosystems, Cat. # A28567), as earlier described (See section 3.2.2.1: Reverse Transcription Quantitative PCR (RT-qPCR)).

4.2.2.4.2 Relative Quantification of OGG1 mRNA via RT-qPCR

To assess the expression levels of the OGG1 mRNA after inhibitions of miR-1248 and miR-103a, total RNA was extracted from the transfected and non-transfected cells using the Quick-RNA™ Miniprep Kit (Zymo Research, Cat. # R1054), and quantified with the Quibit™ RNA HS Assay Kit (ThermoFisher Scientific, Cat. # Q32852), used with the Quibit™ 4 Fluorometer (ThermoFisher Scientific, Cat. # Q33238). RT-qPCR was

performed with a TaqMan™ RNA-to-CT™ 1-Step Kit (ThermoFisher Scientific, cat. # 4392653) to analyze the gene expression level of OGG1 using GAPDH as an internal control (ThermoFisher Scientific cat. # 4453320, 4448892).

4.3 Statistical Analysis

Statistical analyses were performed using GraphPad 6.0.1 software **(**GraphPad Software Inc., San Diego, CA, USA**)**. A p-value less than 0.05 was considered significant and the results are expressed as mean ± SEM.

4.4 Experimental Outcomes

4.4.1 Computationally Predicted miRNA/OGG1 mRNA Interactions

Bioinformatics analysis for differentially expressed (DE) miRNA species that selectively hybridize to the 3' UTR of OGG1 mRNA predicted two miRNAs that satisfied the criterion of a hit in at least two of the used miRNA-mRNA interaction databases. The search on miRDB (Appendix D.3.1), filtered by a target prediction score of ≥75 and excluding miRNAs with more than 2000 predicted targets in the human genome, returned 32 positive results which included two of the differentially expressed miRNAs in our data set: miR-1248 (ranked 10^{th} with a score of 88) and miR-103a (ranked 11^{th} and 12^{th} with a score of 87). miR-1248 got a second positive call on miRWalk (Appendix D.3.2), while miR-103a was corroborated on TargetScan (Appendix D.3.3). As obtained from the RNA-Seq data analysis, miR-103a was significantly downregulated in both 10 µM (~ 3 fold; $p < 0.05$) and 10 mM (~ 2.5 fold; $p < 0.05$) samples (Appendices C.1 and C.2). Because of its very high significance in the 10 mM sample (p=1.13141E-77) and the upregulation of OGG1 following 10 mM treatment (Figure 4-7), miR-103a was selected as a likely candidate of OGG1 targeting for further validation. On the other hand, miR-1248 was

upregulated (~ 2.8 fold; $p < 0.05$) in the 10 µM samples only, and so was selected for its possible negative regulation of OGG1.

4.4.2 RT-qPCR Confirms miR-335 and PARP-1 Interaction

PARP-1 was significantly upregulated and miR-335 downregulated in 10 µM-treated astrocytes compared to the non-treated samples. Hence, PARP-1 is a target of miR-335 (Figure 3-10, Table 3-2) and the PCR results (Figure 4-2) validate the trend obtained from the small RNA-seq analysis. Moreover, the relationship between miR-335 and PARP-1 has been previously experimentally validated [321].

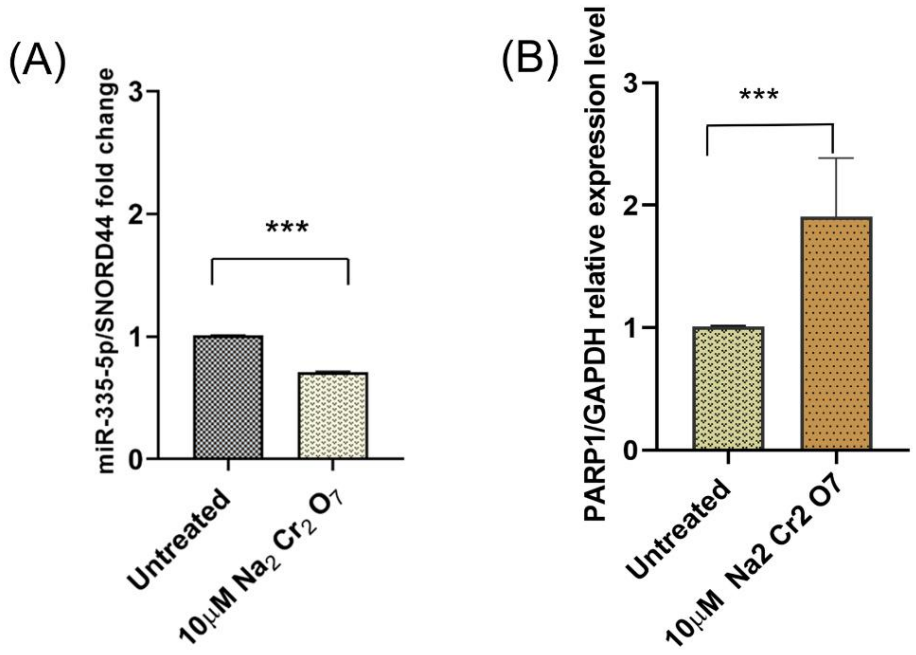

Figure 4-2 RT-qPCR confirmed (A) downregulation of miR-335, and (B) upregulation of its target mRNA, PARP-1 ($p<<0.001$), n=3

4.4.3 Validation of Novel miRNA-Target mRNA Interactions

Assessment of the expression levels of the selected miRNAs (miR-1248 and miR-103a) and the OGG1 target corroborate the opposite expression pattern that is consistent

with the negative regulatory effect of miRNAs on their mRNA targets, as shown in the following sections.

4.4.3.1 OGG1 is a Validated Target of miR-1248

PCR analysis indicates that miR-1248 is upregulated while its computationally predicted target mRNA, OGG1 is downregulated (Figure 4-3). These findings are in agreement with the established inverse expression relationship between miRNAs and their target mRNAs. Furthermore, OGG1 protein expression was reduced after sodium dichromate treatment (Figure 4-3C). In the treated sample, the OGG1 band was less intense when compared to the control sample, indicating a decreased expression.

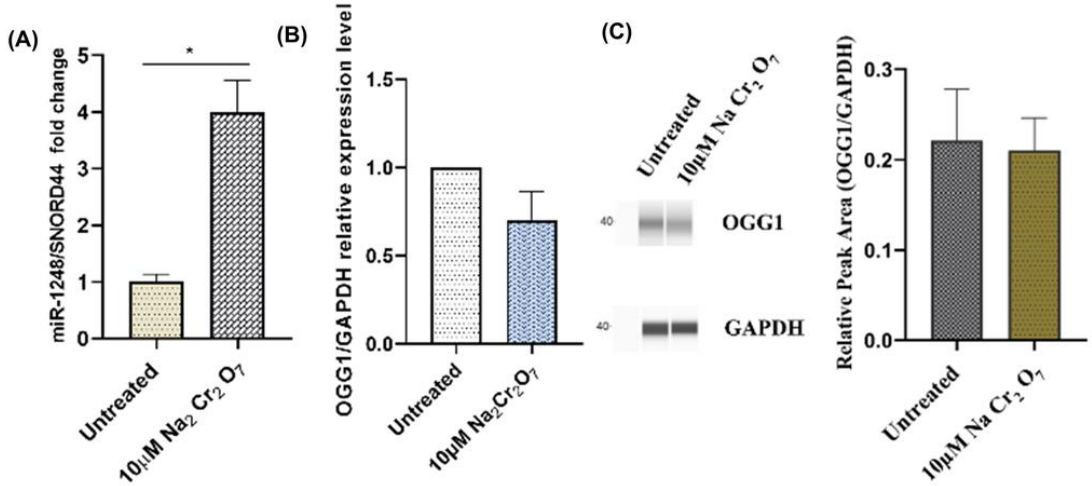

Figure 4-3 Effect of sodium dichromate treatment (10µM, 16 hours) on (A) miR-1248, P<0.05, (B) OGG1 mRNA expression level (C) OGG1 protein expression estimated using Protein Simple Wes® system Capillary western blot results were shown as gel-like images of OGG1 (37kDa) and GAPDH (37kDa) for control and treated samples. The relative area under the curve, error bars represent standard deviation, 1µg of protein lysate was loaded per lane, (n=3)

The knockdown experiment showed that the inhibition of miR-1248 via transfection of human astrocytes is associated with an upregulation of OGG1 mRNA expression relative to the negative control-transfected and non-transfected controls (Figure

4-4A). Experiments were performed to assess the expression level of miR-1248 after the transfection to validate the successful inhibition of the targeted miRNA. As shown in Figure 4-4B, the expression of miR-1248 was downregulated after transfection with the inhibitor.

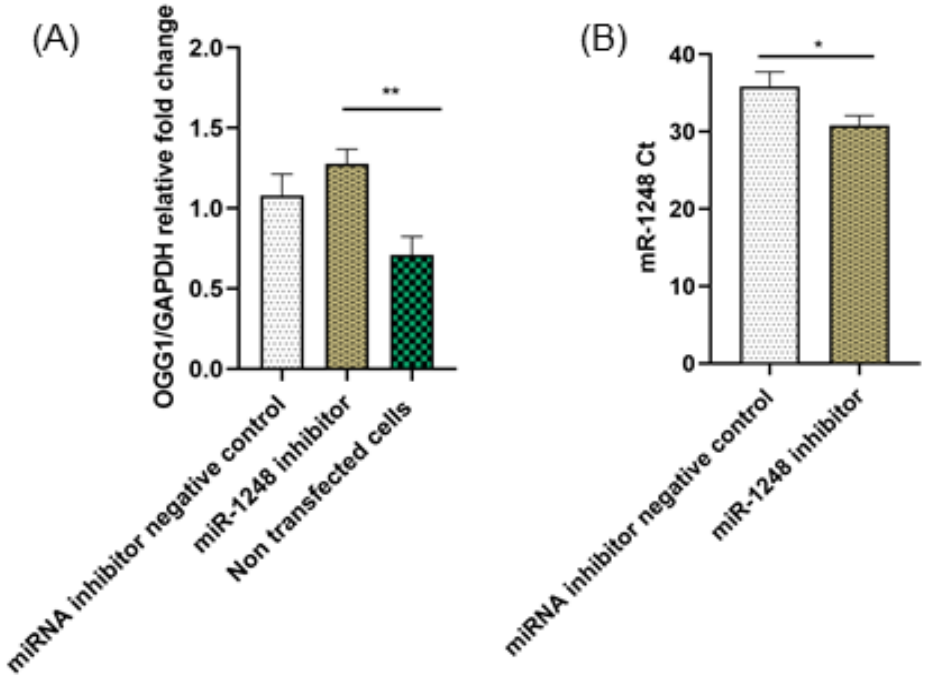

Figure 4-4 OGG1 and miR-1248 expression analysis after inhibition experiments. (A) OGG1 upregulation ($p<0.01$), and (B) miR-1248 downregulation ($p<0.05$), after inhibition of miR-1248 in human astrocytes ($n = 3$)

4.4.3.2 miR-103a is a Possible Regulator of OGG1

The transfection was considered effective based on the fluorescent imaging results (Appendix D.4.1). The MirTrap control transfection experiments showed high expression of DsRed Express (red fluorescence) with almost undetectable AcGFP1 expression (green fluorescence). The RT-qPCR analysis to assess the fold enrichment of both positive (AcGFP1) and negative (hPlod3) controls (Appendix D.4.2) corroborated the imaging results. An 8-fold enrichment was observed for AcGFP1 (which contains miR-132

recognition elements in its 3'-UTR and so is expectedly enriched after immunoprecipitation). Conversely, hPlod3 (which is not a miR-132 target and serves as a negative control) had no significant enrichment (1.77 fold) (Figure 4-5).

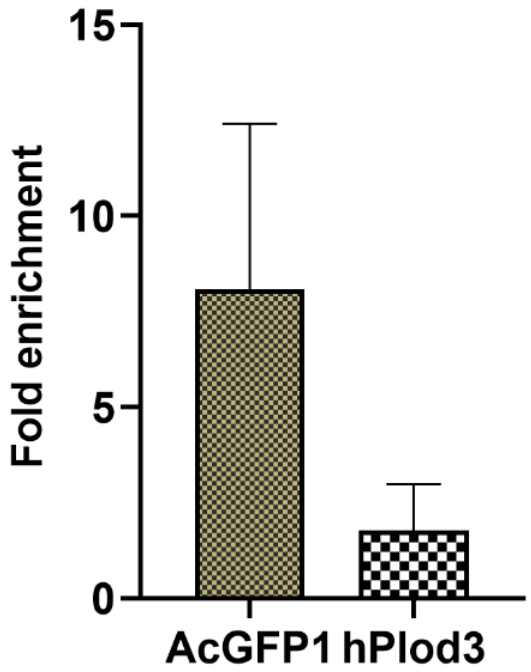

Figure 4-5 RT-qPCR analysis showing fold enrichment of positive control (AcGFP1) and negative control (hPlod3) genes after co-transfection of MirTrap Control vector and miR-132

The co-transfection of astrocytes with miR-103a mimic and the pMirTrap vector (containing tagged RISC) resulted in co-immunoprecipitation of the miR-103a-OGG1 complex which was validated by RT-qPCR, with an average OGG1 mRNA fold enrichment of up to 7 (Table 4-1).

Table 4-1 Average fold enrichment for miR-103a/OGG1 mRNA target via immunoprecipitation analysis

	Ct OGG1	Ct GAPDH	ΔCt	2-ΔCt	Fold Enrichment
Before IP Sample 1	27.35	19.29	8.06	0.003747125	
After IP Sample 1	32.06	25.79	6.27	0.012958118	3.458148925
Before IP Sample 2	28.06	20.01	8.05	0.003773189	
After IP Sample 2	34.9	29.06	5.84	0.017457612	4.626752736
Before IP Sample 3	28.84	19.12	9.72	0.001185737	
After IP Sample 3	34.79	28.92	5.87	0.017098339	14.4200074
Average enrichment					**7.501636354**

Inhibition of miR-103a via transfection experiments resulted in the upregulation of OGG1 when compared to the negative control-transfected cells and the non-transfected cells (Figure 4-6), adding another layer of confidence to the validated miR-103a:OGG1 interaction.

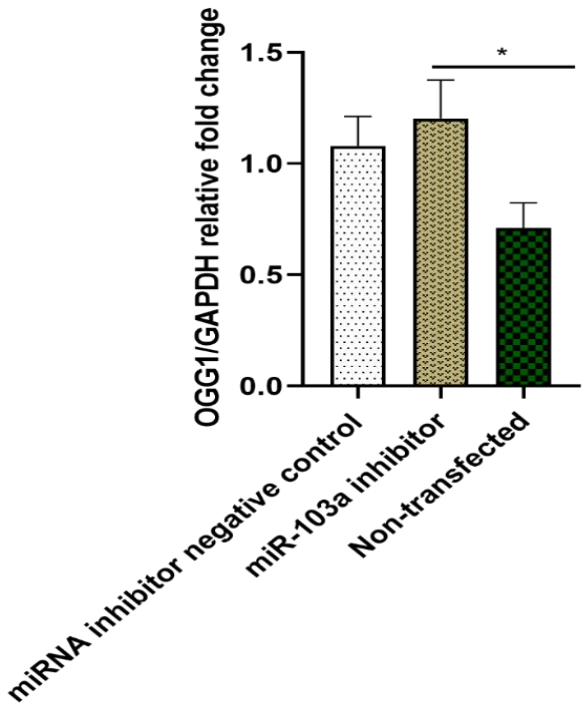

Figure 4-6 OGG1 upregulation ($p<0.01$) after inhibition of miR-103a in human astrocytes ($n = 3$)

4.4.4 Sodium Dichromate Exerts Dose-dependent Effect on OGG1 Expression

Having confirmed the downregulatory impact of 10 µM sodium dichromate on human OGG1, the study sought to investigate the outcomes of exposure to higher doses (10 mM and 100 mM). The RT-qPCR analysis confirmed a proportional dose-dependent increase in OGG1 mRNA expression with increasing $Na_2Cr_2O_7$ concentrations (Figure 4-7).

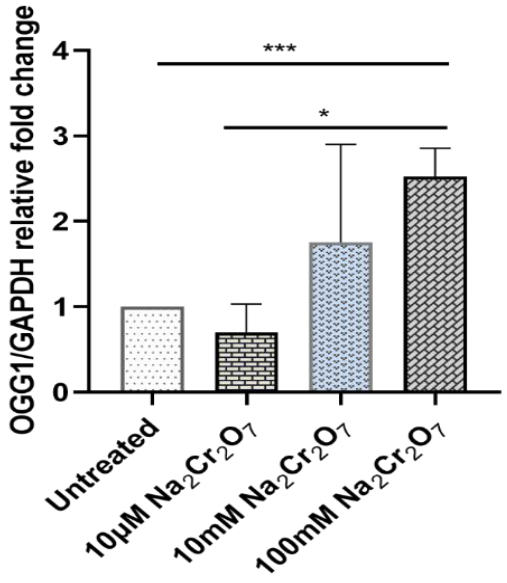

Figure 4-7 Dose-dependent increase in OGG1 expression with increasing Na2Cr2O7 concentrations

4.5 Discussion

Most degenerative diseases have underlying genetic etiologies linked to oxidative stress and resultant chronic inflammation. Both are closely related pathophysiological processes, one of which can be easily induced by the other [322–325]. Oxidative stress is associated with mitochondrial dysfunction [326], progressive neurodegeneration, and neuronal death [327]. Emerging evidence continue to support a strong relationship between microRNAs and oxidative stress – and the associated DNA damage response pathways

[91,270,328,329]. Base excision repair (BER) is the major pathway for the repair of oxidative DNA damage. It acts by the removal and replacement of nucleotides modified by methylation, alkylation, deamination, or oxidation [96].

The small RNA sequencing results indicate that a significant number of miRNAs are downregulated (231) following sodium dichromate treatment (Appendices C.1 and C.2). miR-1248 and miR-4284 expressions were upregulated (> 2.0-fold) due to cellular stress. Complementary sequence matching predicted that miR-1248 binds to the 3'-UTR of OGG1, a DNA glycosylase that is involved directly in the BER pathway (Table 3-2). The fact that all the miRNAs participating in the BER network (Figure 3-10) are downregulated suggests that their target DNA repair enzymes are upregulated. However, the mRNA expression level of OGG1 is decreased (Figure 4-3), because its predicted regulator, miR-1248 is appropriately upregulated.

OGG1 as an experimentally validated target of miR-1248 has no backing in literature, and that prompted us to follow that lead to successfully establish a novel miR-1248:OGG1 interaction via miR-1248 inhibitor transfection experiments (Figure 4-4). Based on our experimental results, miR-1248 was upregulated after sodium dichromate-induced oxidative stress that leads to reduced expression of OGG1 and increased accumulation of 8-OHdG in the DNA (Figure 3-2). Normally, the glycosylase would excise the oxidized adduct to reduce cellular damage. Interestingly, OGG1 deficiency has also been associated with a protective role against inflammatory lesions and mutagenic effects associated with *Helicobacter pylori* infection in a mouse model [330]. Since age-associated cellular inflammation contributes to neurodegeneration, understanding the epigenetic mechanisms by which oxidative stress triggers chronic inflammation can lead

to the development of therapeutics for dementia and associated diseases. The scores of protein-protein interactions (Appendix C.5) that involve the amyloid precursor protein (APP), a synaptic protein driving sporadic and familial Alzheimer's disease [331,332], lends credence to that possibility.

The induced expression of a relatively large number of pro-inflammatory proteins in our PPI data set (Appendix C.5) may reflect a requirement for the activation of astrocytes by cytokines produced from other immune cells during oxidative stress, possibly brain microglia. miR-1248 is pro-inflammatory, regulating the expression of mRNAs involved in chronic inflammatory reactions in an age-dependent fashion [333]. The inverse relationship between miR-1248 and OGG1 (Figure 4-3) and the upregulation of the mRNA target (OGG1) after miR-1248 inhibition (Figure 4-4) validates the computationally predicted regulatory relationship between the miRNA/mRNA pair. miR-1248 was previously reported to be involved in post-transcriptional regulation of IL-5 inflammatory response [334], activation of IFN production with modulation of calcium signaling [335], and TRIM24-mediated proliferation, and invasion of non-small cell lung cancer cells [336].

Our results (Figure 4-2) support a previous finding [321] that oxidative stress caused the downregulation of miR-335, leading to increased expression of PARP-1. PARP-1 modulates transcriptional responses by remodeling chromatin structure [337]. Interestingly, OGG1 binding to PARP-1 has been shown to play a functional role in the recognition and repair of oxidative DNA damage by stimulating its poly(ADP-ribosyl)ation activity [317]. Our results suggest that the astrocytes may sense DNA damage via PARP-1, but there may not be sufficient OGG1 levels to repair the damage. Conversely, and very importantly, activated PARP-1 has been reported to exert inhibitory effects on the

activity of OGG1 [338]. This negative feedback loop could well contribute to the impaired 8-OHdG excision capacity of OGG1 in the cells undergoing oxidative stress, as observed in the Comet assay. The PARP-1-DNA trapping ability of certain PARP-1 inhibitors has been employed successfully in cancer therapy. There is an ongoing debate on their appropriateness and safety in neurodegenerative disorders due to the cytotoxic effects on astrocytes [339]. In addition to blocking enzymatic activity, some of these inhibitors alter the way PARP-1 interacts mechanistically with DNA – and this could be deleterious if this interaction involves OGG1. Therefore, the selective use of PARP inhibitors to treat neurodegenerative disorders should be investigated further, keeping in mind the polypharmacological properties of PARP-1 inhibitors and the proposed reciprocal interaction with OGG1.

Immunoprecipitation experiments that involve actual physical binding of miRNA/mRNA pairs confirmed that OGG1 mRNA is also a target of miR-103a (Figure 4-5). To the best of our knowledge, this is the first documented evidence of miR-103a-OGG1 interaction, apart from bioinformatics prediction on miRDB and TargetScan. Other established targets of miR-103a are PARP-1, CDK5R1, and RUNX2. Poly-(ADP-Ribose) polymerase 1 (PARP-1) is a DNA damage sensor protein involved in DNA repair as well as tumor transformation. miR-103a modulates oxidative stress in hypertension through PARP-1 regulation [75]. It was also reported to play a role in the regulation of osteoblast differentiation by directly targeting the 3'-UTR of RUNX2 mRNA to inhibit matrix mineralization and bone formation [340,341]. CDK5R1 encodes p35, a specific activator of the serine/threonine kinase CDK5, which plays a crucial role in central nervous system

development and maintenance. So miR-103a affects neuronal migration by modulating CDK5R1 expression [342].

The corresponding dose-dependent increase in OGG1 mRNA expression with increasing $Na_2Cr_2O_7$ concentrations negates the inverse relationship earlier established with 10 μM treatment, and therefore points to the activation of an alternative stress response mechanism that does not involve, or perhaps overrides, the miRNA-mediated regulatory pathway. Other biological mechanisms can play a role in the restoration of cellular homeostasis after increased potency of a stressor, including senescence [343] and impaired mitochondrial dysfunction [11,271]. Also, histone deacetylase class I (HDACI) has been reported to epigenetically interact with and enhance the cleavage activity of OGG1 [269]. These alternative response mechanisms deserve further investigation.

CHAPTER 5

EXOPRIME TECHNOLOGY: 'SMART' MICROPROBE IMBUED WITH BIOSENSING ELEMENTS FOR SOLID-PHASE IMMUNOISOLATION AND OMICS ANALYSIS OF SURFACE-MARKER-SPECIFIC EXOSOMAL SUBPOPULATIONS

5.1 Rationale

The need for technology that can isolate pure exosomes rapidly, reproducibly, and efficiently, has been recognized in the scientific community [249]. Multiple technologies that improve exosomal isolation have been developed by exploiting the biochemical properties of exosomes, and the process has rapidly evolved in recent years. While these techniques have advantages and disadvantages, the most important drawback is that they purify a heterogeneous population of exosomes that express different surface markers, which is clinically disadvantageous.

Despite the efforts to develop systems for exosomes purification, little has been reported on the development of solid-phase platforms for selective capture of extracellular vesicles that express the same surface marker. A rapid, antigen-selective technology that provides high-purity exosomal preparations will accelerate extracellular vesicles research and the development of exosome-based products and applications.

5.2 Aim and Hypothesis

Selective isolation of surface-protein marker-specific exosomal subpopulations for subsequent genetic analysis is critical in studies to evaluate their clinical relevance because they carry unique cargo that accurately represents the state of the cell [33]. A study has shown the enrichment of CD63-positive exosomes in prostate cancer cells relative to normal prostate cells [230]. The overexpression of the Epithelial Cell Adhesion Molecule (EpCAM) in multiple types of cancers is linked to increased proliferation of epithelial cells, as is seen in the development of tumors [344,345]. Given that EpCAM expression is confined to epithelial tissues, its detection in mesenchyme-derived organs like the blood or lymph nodes has been attributed to tumor-derived exosomes, making it a useful diagnostic biomarker in circulating tumor cells (CTCs) in the blood of carcinoma patients. The prognostic potential of EpCAM-1 for the early diagnosis of ovarian cancer has been reported [346].

This study aims to develop a direct, one-step exosome sampling technology – ExoPRIME – for selective capture of CD63+ exosome populations using an immune-affinity protocol. Therefore, we hypothesize that the designed microprobe will specifically capture and enrich exosome subpopulations expressing the CD63 antigen.

5.3 Experimental Workflow

5.3.1 Functionalization of ExoPRIME Microprobe

5.3.1.1 Preparation of Polyelectrolyte Solutions

Three polyelectrolyte solutions were used for this study: PEI, PSS, and PAA. Positively charged poly[ethyleneimine], 3% w/v was prepared from 50% w/v PEI (MP Biomedicals, cat. # 195444) by adding 6 mL PEI to 94 mL deionized water to obtain a

3mg/mL PEI solution, with pH adjusted to 5 using HCl and NaOH. The negatively charged poly[sodium 4-styrenesulfonate], 3 mg/mL PSS solution was prepared by dissolving 300 mg PSS (Sigma-Aldrich, cat. # 243051) in 100 mL deionized water and adjusted to pH 8. Polyacrylic acid, another negatively charged polyelectrolyte, was prepared from a 35% w/v stock by diluting 8.6 mL PAA (Sigma-Aldrich, cat. # 523925) in 91.4 mL deionized water and adjusted to pH 8. To compact the resulting thin film and reduce its thickness, 25 µL 0.5 M NaCl prepared from a 5 M stock (Sigma-Aldrich, cat. # 7647-14-5) was added to all polyelectrolyte adsorption solutions to increase their ionic strength [347].

5.3.1.2 Thin Film Deposition via Layer-by-Layer (LbL) Assembly

Deposition of multilayered polyelectrolyte coating over the Serin™ stainless steel microneedle (300 µm × 30 mm) was performed using LbL thin-film deposition technique [348]. The surface of the microneedle was polished with sandpaper to increase its roughness and surface area. The needles were cleaned, to remove organic contaminants, by a successive ultrasonic wash in acetone (Sigma-Aldrich, cat. # 270725) (5 min), ultrapure water (5 min), hexane (Alfa Aesar, cat. # L13233) (15 min), and with ultrapure water again (15 min, 50℃). The needles were further cleaned ultrasonically in acetone for 5 min and then dipped in warm acetone (50℃) for another 15 min, before chemically etching them with sulfochromic acid (prepared by dissolving 6 g $Na_2Cr_2O_7$ (Ward's science, cat. # 470302-532) in 100 mL H_2SO_4 (Ward's science, cat. # 470302-858)) at 60℃ for 10 min. The etching of the microneedles provides a uniform negative (OH^-) substrate for the subsequent adsorption of the first cationic layer. The pre-treated needles were washed with ultrapure water, dried with air, and stored in a desiccator under vacuum until further use (no longer than 2 days).

Oppositely charged polyelectrolytes were deposited via layer-by-layer assembly with intermediate washing in deionized water and air-drying between each deposition (Figure 5-1). An initial trilayer formed of PSS sandwiched in between two PEI layers [PEI/PSS/PEI] was followed by additional 4½ polyanion/polycation bilayers, consisting of PAA and PEI [$(PAA/PEI)^4$+PAA] Thus, the film profile consisted of a total of six bilayers providing carboxyl group at the last layer for the subsequent attachment of the amino-modified biotin. The incubation for each layer was as follows: PEI (3 h), PSS (30 min), PEI (16 h), PAA (15 min), PEI (15 min), PAA (15 min), PEI (15 min), PAA (15 min), PEI (15 min), PAA (3 h), PEI (15 min), PAA (15 min). All steps were performed at room temperature with mild agitation on a shaking platform. The LBL layers serve as a substrate for immobilization of biotin and the streptavidin-conjugated antibody

5.3.1.3 Anti-CD63 Antibody Immobilization

EZ-Link™ Amine-PEG2-biotin (ThermoFisher, cat. # 21346) was covalently linked to the carboxyl group of the last polyacrylic acid layer, via cross-linker chemistry mediated by 1-Ethyl-3-(3-dimethylaminopropyl) carbodiimide (EDC) [349] (ThermoFisher, cat. # 22980). Equimolar concentrations (50 mM) of amine-PEG2-biotin and freshly prepared EDC were mixed in 1:1 volume to obtain a 25 mM biotin-EDC complex mixture, which was further diluted to 5mM concentration with PBS. The needles were submerged in the 5 mM biotin-EDC linker complex solution, on a rocking platform, for 1 h at room temperature, and rinsed in 0.1% BSA in PBS. The biotinylated needles were incubated in 1 µg mL^{-1} streptavidin-conjugated anti-CD63 antibody (Abcore, cat. # AC12-0278-22) for 1 h at room temperature, with mild continuous shaking. To reduce non-specific binding, blocking was performed by incubation-shaking in 0.1% BSA for 20 min

at room temperature. The resulting CD63 antibody-coated microneedle is the ExoPRIME microprobe used for the remainder of the study and was used on the same day it was prepared (Figure 5-1) [4].

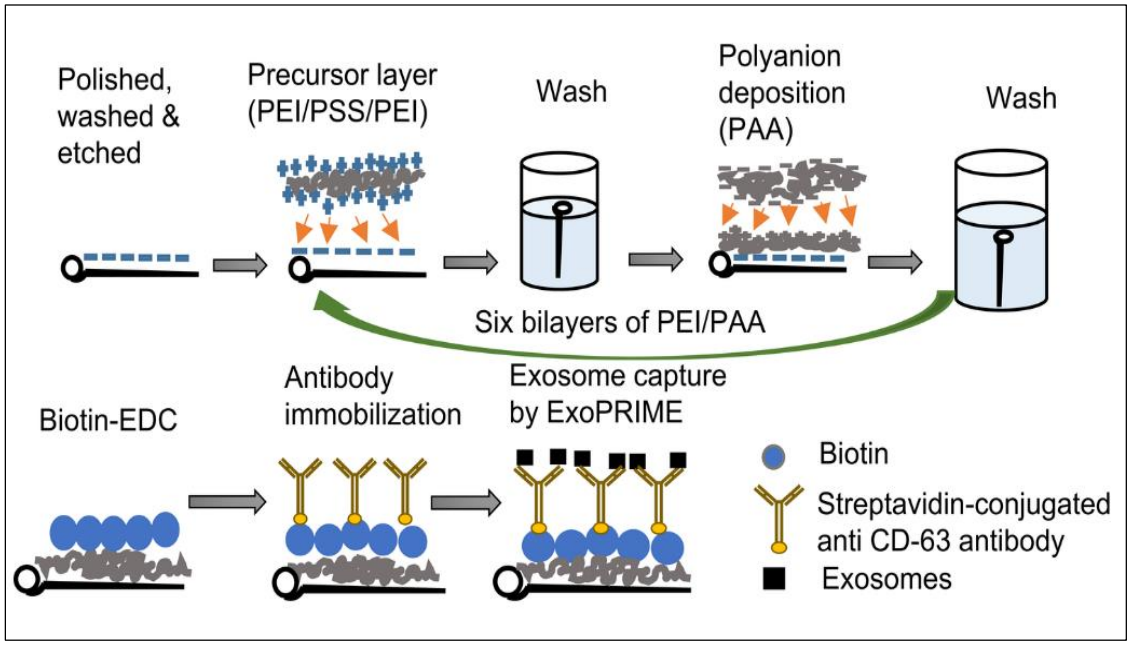

Figure 5-1 ExoPRIME probe functionalization workflow [36]

5.3.2 Evaluation of Probe Efficiency

5.3.2.1 Preparation of Conditioned Astrocyte Medium and Exosome Suspension

The biofluids used for these experiments were derived from human primary astrocytes (Sciencell, Carlsbad, CA). Countess II FL Automated Cell Counter **(**ThermoFisher Scientific**)** was used to count the cells that were seeded at a density of 2.1×10^6 cells in a T-75 flask containing 10 mL Astrocyte Medium (Sciencell, #1801), supplemented with 1% penicillin/streptomycin solution (Sciencell, #0503), 2% Fetal Bovine Serum (Sciencell), and 1% astrocyte growth supplement (Sciencell #1852). The

[4] C.D. Nwokwu, S.M. Ishraq Bari, K.H. Hutson, C. Brausell, G.G. Nestorova. ExoPRIME: Solid-phase immunoisolation and OMICS analysis of surface-marker-specific exosomal subpopulations, Talanta 236(2022):122870. https://doi.org/10.1016/j.talanta.2021.122870.

cells were grown at 37°C, 95% humidity, and 5% CO_2/air until they reached 80% confluence. All cells used for these experiments were used within a maximum of 5 passages. When the cell reached 80% confluence, the conditioned culture medium was collected and centrifuged at 2000 x g for 30 min at 4^0C to remove cellular debris. The resulting conditioned astrocyte medium (CAM) was aliquoted and stored at – 20 ^{0}C until needed. The enriched exosomal suspension (EXO) was obtained by mixing 0.5 volumes of exosome precipitation reagent (Invitrogen Total Exosome Isolation, Cat. # 4478359) and the clarified CAM, mixed well by vortexing and incubated for 16 h at 4^0C. The mixture was centrifuged at 10,000 x g for 1 h at 4^0C and the residual exosomal pellet was re-suspended in 0.2 volumes of 0.1% BSA in PBS, relative to the starting culture volume.

5.3.2.2 Exosome Immunoisolation and Quantification

The ExoPRIME microprobes were incubated in the corresponding biofluid at a 1:200 µL proportion, under a matrix of experimental conditions: biofluid type, incubation temperature, and incubation time (Table 5-1).

Table 5-1 Incubation Conditions (Biofluid Type, Incubation Temperature and Incubation Time)

16-h Incubation	**2-h Incubation**
Exosuspension at 4^0C	Exosuspension at 4^0C
Exosuspension at 22^0C	Exosuspension at 22^0C
Conditioned Medium at 4^0C	Conditioned Medium at 4^0C
Conditioned Medium at 22^0C	Conditioned Medium at 22^0C

After incubation, unadhered exosomes are washed off and steric crevices blocked using 0.1% BSA in PBS (for the exosome suspension, the diluent is the same as the blocking solution). A highly sensitive fluorescence-based enzymatic assay kit, FluoroCet (System Biosciences, FCET96A-1) was used to quantify the number of captured exosomes

according to the vendor's guideline with minor modifications to accommodate the solid-phase approach. Briefly, 5 microprobes were immersed in 60 µL PBS-diluted FluoroCet lysis in a glass microcapillary tube (Roche, cat. #04929292001). The lysis setup was placed on ice for 30 min to release exosomes captured on the surface of the microprobes. 50 µL standard or exosomal lysate, 50 µL working stock of buffer A, and 50 µL working stock of buffer B (making a 150 µL reaction volume) were mixed in each well of an opaque 96-well plate and incubated, protected from light for 20 min at room temperature. The fluorescence intensity (relative fluorescence units, RFU) was read using an Excitation: 530-570 nm and Emission: 590- 600 nm. in a Cytation 5 Cell Imaging Multi-Mode Reader. The blank for assay samples consisted of 1:2 PBS-diluted FluoroCet lysis buffer, while the blank for standard reactions was 1:2 PBS-diluted FluoroCet reaction buffer.

5.3.3 OMICS Analysis of Exosomal Cargoes

5.3.3.1 Extraction of RNA and Protein from ExoPRIME-captured Exosomes

The Total Exosome RNA and Protein Isolation Kit (cat #4478545) was used for exosomal RNA extraction. RIPA Lysis and Extraction Buffer (Biosciences, cat #786-489), mixed 7:1 with 7X protease inhibitors (Roche, Cat. # 04693124001) dissolved in deionized water, was used directly for total protein extraction. Five microprobes were submerged in 60 µL lysis/resuspension buffer in a glass microcapillary tube (Roche, Ref. 04929292001) and incubated on ice for 30 min to complete the lysis. The RNA isolation proceeded via the organic extraction technique, according to the product's guidelines, but with slight modifications. Briefly, the exosomal lysates for RNA analysis were pooled into RNase-free tubes so that each tube contained ~ 200 µL, while the number of probes per tube was recorded for eventual computation of protein concentration per probe. 1 volume of Acid-

Phenol: Chloroform was added to each sample, vortexed for 30 seconds, before centrifugation for 5 min at maximum speed (16,000 x g) at room temperature. The upper (aqueous) phase was carefully removed without disturbing the underlying organic phase and transferred to a fresh tube. 1.25 volumes 100% ethanol was added to the recovered aqueous phase and mixed thoroughly. The remaining purification steps were followed as prescribed, with multiple centrifugation and washing steps. Finally, the RNA was eluted in 100 µL pre-heated (95^{o}C) elution buffer. The concentration and quality of the RNA samples were assessed using an Agilent 2100 Bioanalyzer System with RNA Pico Chips (Lot # YH19BK30), while the protein concentration was determined using a Pierce™ BCA Protein Assay Kit (Thermo Fisher Scientific, Cat. # 23225) according to the vendor's guidelines.

5.3.3.2 MicroRNA Amplification of Enriched Exosomal RNA

The viability and integrity of probe-derived exosomal RNA were further evaluated by RT-qPCR. Hsa-miR-21-5p (Sigma Aldrich, cat. #MIRAP00047) and hsa-let-7b-5p (Sigma Aldrich, cat. #MIRAP00004) were amplified using the protocol stipulated for the MystiCq® MicroRNA® Quantitation System (Sigma-Aldrich, St. Louis, MO). Briefly, microRNA cDNA synthesis was carried out in two steps: (1) poly (A) tailing, using 3 µL of each microRNA sample in the specified 10 µL reaction volume; and (2) first-strand cDNA synthesis with the whole polyadenylated miRNA to generate a 20 µL cDNA product. The cDNA concentration was measured using Qubit 4 Fluorometer (Thermo Fisher Scientific, cat. #Q32854), and refrigerated until time for PCR amplification. Equal amounts of each cDNA template (2ng) in 1 µL suspension, was mixed with 0.4 µL 10 µM of respective MystiCq microRNA qPCR Assay Primer and 0.4 µL 10 µM MystiCq

Universal PCR Primer, and 10 µL MystiCq microRNA SYBR Green qPCR Ready-mix, and the total reaction volume made up to 20 µL with nuclease-free water. The miRNA amplification followed the vendor-recommended 2-step PCR program (in 45 cycles) on a LightScanner 32 real-time PCR instrument. The absolute threshold cycle (Ct) values were noted, and the results were represented as mean ± standard error calculated from three biological replicates ($p < 0.05$ is considered significant).

5.4 Results

5.4.1 Design and Fabrication of the ExoPRIME Microprobe

We employed a multidisciplinary approach that includes nanoscience, polymer chemistry, and immunobiology, to design, fabricate, and characterize the "smart microprobe" for the purification of antigen-specific exosomes. The ExoPRIME widget consists of an inert Serin™ stainless steel microneedle (300 µm × 30 mm) functionalized with an antibody (anti-CD63) that selectively binds to the corresponding tetraspanin embedded in the lipid bilayer of the exosomes. Layer-by-layer (LbL) assembly was applied to create the precursor layer of six alternating polyethyleneimine/polyacrylic acid bilayers $[PEI/PAA]^6$ for the immobilization of biotin to the stainless steel surface of the probe. 1-Ethyl-3-(3-dimethylaminopropyl) carbodiimide (EDC) mediated chemical linkage of amine-modified biotin to the carboxyl group of the PAA and was followed by the biotin-streptavidin covalent linkage of the CD63 antibody (Figure 5-1).

5.4.2 Evaluation of ExoPRIME's Capture Efficiency

The feasibility of the ExoPRIME to capture exosomes was assessed using conditioned astrocyte medium (CAM) and enriched exosome suspension (EXO). The impact of temperature and incubation time on the ability of the tool to capture exosomes

was evaluated as well. After incubation in a biofluid, the exosome capture efficiency was quantified using a highly sensitive fluorescence-based enzymatic assay, FluoroCet Exosome Quantification Assay, which measures the activity of exosomal cargo, acetylcholinesterase. The ExoPRIME probe was blocked with 0.1% BSA in PBS to reduce non-specific binding. Low levels of non-specific binding between the EVs and the biotin were measured and subtracted from the signal obtained using the fully functionalized probes. The fact that the ExoPRIME microprobe captured much more exosomes than a non-functionalized microneedle is indicative of enrichment of CD63-expressing exosomes.

The ExoPRIME's exosome loading capacity per microprobe was assessed under different incubation conditions, as shown in Table 5-1. The capture efficiency ranged from 3 – 24 x 10^6 exosomes per probe depending on the experimental condition. The loading capacity of the probe increased after incubation for 16 h at 4^0C in EXO suspension (24×10^6 exosomes per probe) and the efficiency decreased ~ 10 folds after 2 h at 4^0C (24×10^5 exosomes per probe). The incubation temperature has an impact on the capture capacity leading to a 2-fold efficiency reduction after incubation for 16 h at 22^0C (12×10^6 exosomes per probe). In summary, the reduced temperature with extended incubation times constitutes the most optimal parameters that ensure high probe loading capacity (Figure 5-2A). This can be easily explained by the fact that lower temperatures maintain exosome viability longer. The increased duration of the incubation increases the chances for exosomes to make contact with the immobilized antibodies. However, the 2-hour room-temperature incubation (2 h at 22^0C) of the ExoPRIME probe yielded an increased capture efficiency (12×10^6 exosomes per probe) when compared to the 4°C incubation (24×10^5 exosomes per probe). A possible reason for this phenomenon is increased collision based

on temperature-dependent molecular kinetics. At room temperature, the exosomes would move at relatively higher speeds than at refrigeration temperatures, and so, would be expected to experience more effective ‘collisions’ and interactions with the immobilized antibodies. These outcomes raise the question as to which of the two parameters is a more important determinant of efficiency. The varied interplay of time, temperature and biofluid type, thus presents exosome researchers with the flexibility to choose the combined parameters that best suit their purpose.

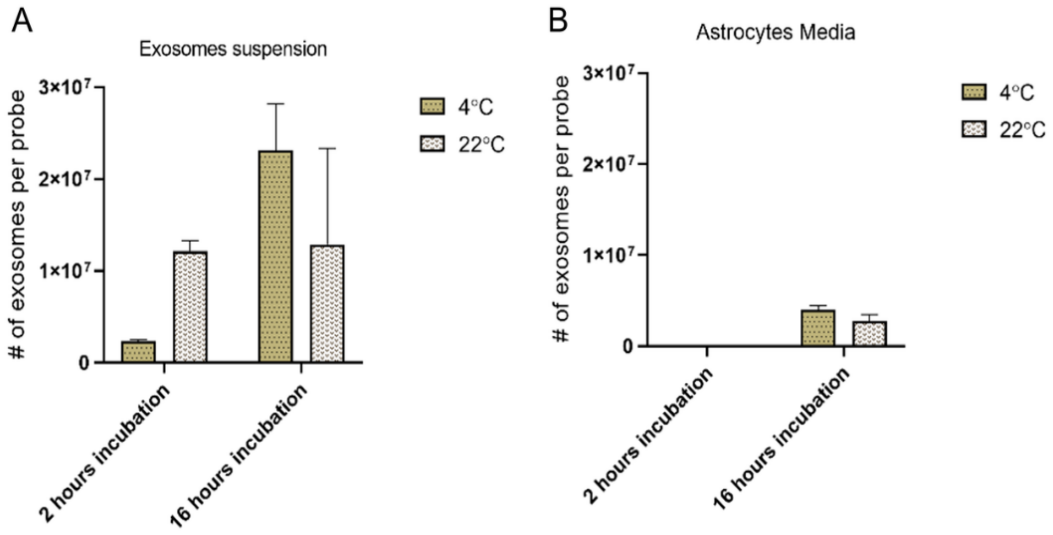

Figure 5-2 Exosome concentration obtained using ExoPRIME probe from enriched exosome suspension and astrocyte medium (n=3). The numbers of exosomes shown as isolated per microprobe are differential figures obtained from subtracting exosomes captured by negative (non-anti-CD63-functionalized, NAF) microprobes from exosomes captured by positive (biotin+anti-CD63-functionalized, BAF) microprobes [36]

At 16 h incubation, CAM-4^{0}C probes (4×10^6 exosomes per probe) bind more exosomes than CAM-22^{0}C probes (3×10^6 exosomes per probe). The CAM results are consistent with the trend obtained for EXO incubations, except for the zero-differential number of exosomes after 2 h incubation under both temperature conditions (Figure 5-2B). The CAM-2 h incubations did not generate a large enough signal to be quantified

accurately. One key factor that could account for the generally lower exosome loading capacity of the CAM probes relative to the EXO probes could be the presence of various extracellular proteins and cellular debris, which could mask antibodies and compete physically with exosomes for binding. Follow-up experiments that compared the protein concentrations of EXO versus CAM probes (Table 5-2) further support this claim of antibody sequestering by non-exosome components in the culture medium

5.4.3 Downstream Analysis of ExoPRIME-isolated Exosomes

5.4.3.1 MicroRNA and Protein Yields

Downstream analysis of the genomic and proteomic cargoes of ExoPRIME-purified exosomes was performed to further assess the feasibility of the platform for direct OMICS analysis. The antibody-functionalized probes yielded exosomal proteins from both enriched exosome suspension and conditioned medium that is sufficient for downstream analysis (Table 5-2).

Table 5-2 RNA and Protein Concentrations per ExoPRIME probe [36]

Sample	RNA (ng per probe)	Protein (ng per probe)
EXO (16 h, 4^0C)	0.54	940
CAM (16 h, 4^0C)	0.30	728

5.4.3.2 High Enrichment of Small RNAs (25 – 200 bp)

The RNA profile of the captured exosomes from the two different biofluids was assessed via capillary-based electrophoresis using Bioanalyzer 2100 RNA Pico assay. The electropherograms of the EXO and CAM samples confirm the enrichment of RNA that have fewer than 200 nucleotides, with the highest abundance observed in the range of 25

– 200 bp (small RNA) as expected for exosomal RNA samples (Figure 5-3) [5]. Total human RNA was analyzed as a positive control, alongside an RNA ladder. The narrow size distribution and particularly high enrichment of small RNAs highlight the potential use of the ExoPRIME probe in epigenetic studies involving non-coding RNAs for biomedical research and diagnostics. Herein lies the nexus between the development of this microprobe and the first prong of this project work that studied the differential expression of short regulatory RNAs (microRNA) under conditions of oxidative stress.

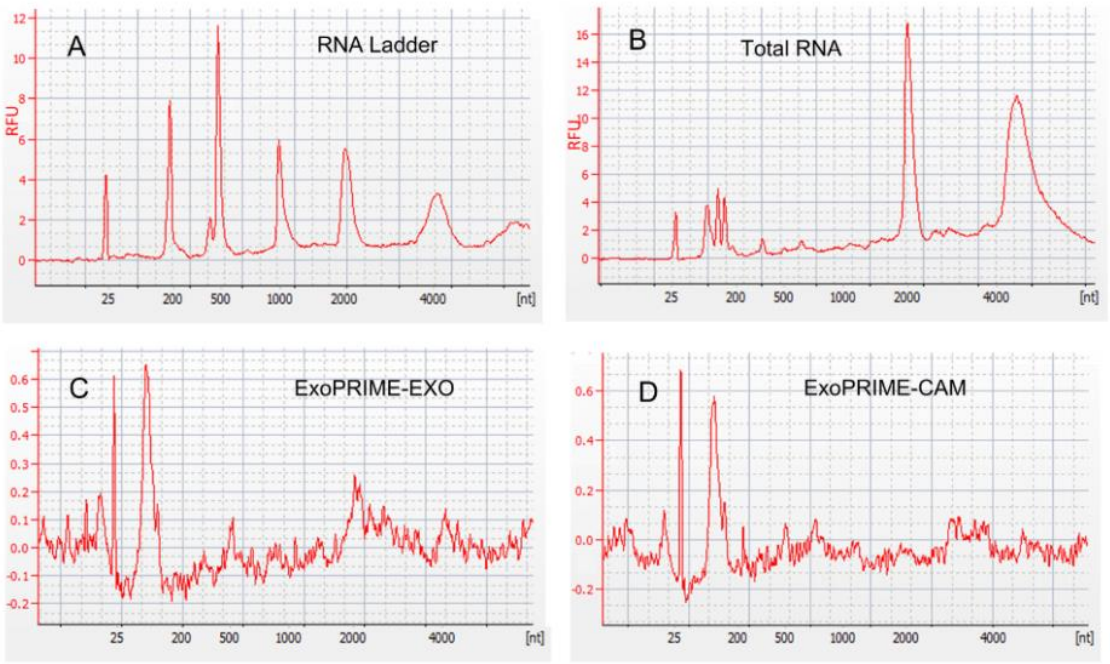

Figure 5-3 Agilent 2100 Bioanalyzer RNA analysis of (A) RNA ladder; (B) Total human RNA (3ng); (C) ExoPRIME-purified exosomal RNA from polymer-precipitated exosomes derived from human astrocytes; (D) ExoPRIME-purified exosomal RNA from exosomes directly captured from conditioned human astrocytes media. The electropherograms show the fluorescence intensity (FU) and size distribution of the RNA nucleotides (nt) [36]

[5] C.D. Nwokwu, S.M. Ishraq Bari, K.H. Hutson, C. Brausell, G.G. Nestorova. ExoPRIME: Solid-phase immunoisolation and OMICS analysis of surface-marker-specific exosomal subpopulations, Talanta 236(2022):122870. https://doi.org/10.1016/j.talanta.2021.122870.

5.4.3.3 Assessment of ExoPRIME's Diagnostic Utility

The diagnostics feasibility of the ExoPRIME technology for direct genetic analysis was evaluated using reverse transcription-quantitative PCR (RT-qPCR) of the exosomal RNA purified. The expression levels of the oxidative stress- and tumor-suppressing-associated microRNAs, miR-21 and let-7b, respectively, were measured in ExoPRIME-purified exosomes from enriched exosomal suspension and directly from conditioned astrocyte media (Figure 5-4). MiR-21 is highly expressed in astrocytes [350] and its expression is dysregulated in astrogliosis, traumatic brain injury [283], and oxidative stress [351]. MiR-let-7b has been identified as a biomarker for the early detection of cervical lesions [352]. While the mRNA targets were successfully amplified, no significant differences were detected between the EXO and CAM expression levels of both miRNAs. These results further validate the feasibility of the technology to isolate structurally intact exosomes and its application for direct genetic analysis from both enriched exosomes and cell media.

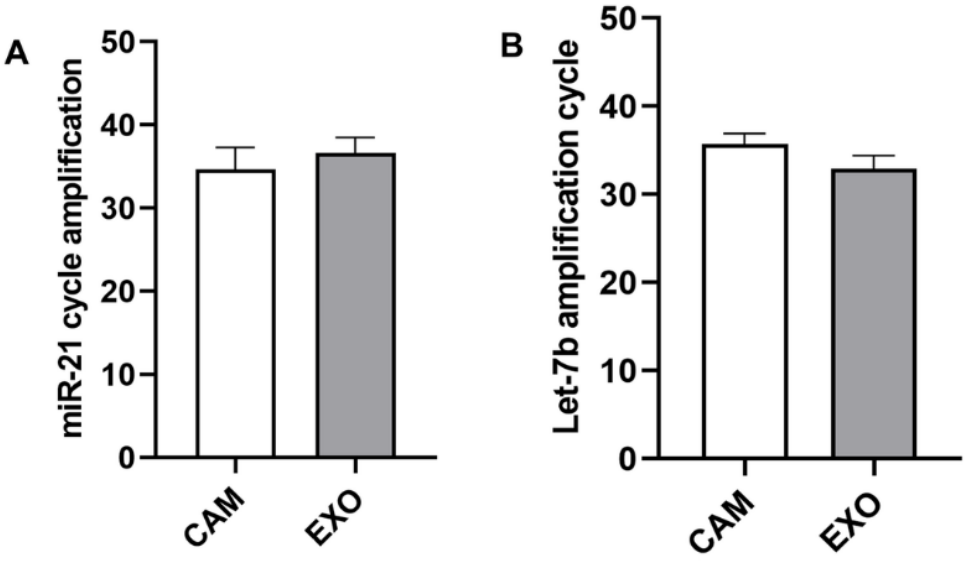

Figure 5-4 RT-qPCR amplification cycles (n=3) of (A) An oxidative stress marker, miR-21 (CAM 36.2;EXO 38.7); (B) A tumor suppressor gene, miR-let-7b (CAM 34.4; EXO 33.0), an array of 20 ExoPRIME microprobes [36]

5.5 Discussion

Circulating exosomes encapsulate genomic and proteomic cargoes that are potentially useful as cell-type-specific biomarkers for precise and non-invasive liquid biopsy [21,34,35] and targeted therapeutics delivery [353–355]. However, despite efforts to develop clinically advantageous systems for exosome purification, little has been reported on the development of solid-phase platforms for selective capture of exosomes that express the same surface marker. It has been emphasized that developing technology for the isolation of homogenous populations of exosomes will facilitate the studies of their biological function and lead to the accurate identification of biomarkers for early disease diagnostics [33].

We report a non-invasive, one-step, solid-phase, microprobe-based technology – ExoPRIME – for the direct isolation of pure exosome populations from both enriched exosome suspension and conditioned cell culture medium. The novel ExoPRIME microprobe provides direct, *in situ* enrichment of intact exosomes based on immunoaffinity, without compromising their structure by avoiding the shear strain and specimen destruction that may result from centrifugation [234]. Before deploying the ExoPRIME microprobe for exosome enrichment, structural (SEM) and fluorescence characterizations were conducted which indicated that polyelectrolyte assembly and biotin attachment were successful and serve as a good substrate for antibody immobilization. Also, EDX analysis further confirmed traces of organic materials (from the polyelectrolytes) which are not found on the plain needles (Appendix E.1).

The developed ExoPRIME microprobe technology was tested with different biofluids under various experimental conditions, and it demonstrated potential for high

capture efficiency, as well as sufficient yield of exosomal RNA and protein for downstream transcriptomic and proteomic analyses. A combination of immunofluorescence and proteomic analysis was employed to assess the specificity of the ExoPRIME's CD63+ exosome enrichment capability (Appendix E.2). Fluorescent imaging indicated distinct differences between the control and exosome-specific groups, indicating enrichment for the CD63-specific exosomal population. The proteomic profile generated by SDS-PAGE showed fewer bands with a cleaner background for the microprobe-derived exosomal protein sample compared to the traditional polymer-precipitated exosome proteins.

These results suggest that the ExoPRIME probe enriches for a homogenous exosome population in comparison with the conventional purification method. The traditional immuno-isolation system for exosome purification usually includes an enrichment step to increase the concentration and purity of collected exosomes, adding extra time and cost implications [243]. However, our novel system, with an antibody-functionalized microneedle at its core, captures antigen-specific subpopulation of exosomes directly from biofluids, eliminating the requirements for additional filtration and pre-concentration steps, and thereby cutting down costs and handling time without compromising purity and viability of exosomal cargoes. Downstream characterization of exosomal RNA lysates obtained from probe-derived exosomes indicates that the captured exosomes remain intact, with viable nucleic acid cargo (Figure 5-4).

A major advantage provided by the designed probe over other platforms is its broad dynamic range of temperature and incubation parameters that can be adjusted by the user to provide optimal results, depending on the experimental workflow. This flexibility is a desired factor for clinical and laboratory applications. Furthermore, this technology permits

the use of minimal sample volumes (≤ 200 μL). The biological sample can be reused, with an average yield recovery rate of 2×10^7 exosomes per probe from an input volume of 200 μL. The fact that the sample is not consumed in the process is especially very important for precious samples, such as cerebrospinal fluid. By bypassing the usual pre-concentration and filtration, the technology minimizes the specimen volume requirement, simplifies the workflow, providing faster sample analysis and cost savings.

Given the scalability afforded by the user-defined array of probes, the ExoPRIME Microprobe Technology also offers prospects of diagnostic profiling of multiple EV biomarkers via multiplexed analysis from the same sample. ExoPRIME has the potential for integration into an automated microfluidics workstation for exosomal RNA isolation for isothermal picomolar-range PCR detection [356], therefore, providing a potential clinical diagnostic tool at the point of care (Figure 1-3). This could enable the development of a versatile platform with a variety of biomedical applications in exosome-based disease diagnostics and assessment of therapeutic interventions. Furthermore, the ExoPRIME technology could have applications in plant exosomes research. Researchers have just begun to unravel the physiological function of plant exosomes [357,358]. The minimal invasiveness of the ExoPRIME probe could be easily exploited for plant exosomes analysis and provide useful tools in agriculture, plant-based medicine, and nutraceuticals.

CHAPTER 6

CONCLUSIONS AND FUTURE DIRECTIONS

6.1 Conclusions

6.1.1 Chapter 2 Conclusion

The present study indicates that proton and photon radiation exposure are associated with impairment of the mitochondrial populations and suppression of the base-excision repair capabilities of human astrocytes. Mitochondrial mass increased after irradiation, indicating compensatory mitochondrial activity, which further exacerbates oxidative damage (Figure 1-1). The increase in mitochondrial mass may simply serve to accelerate the increase in the frequency of DNA damages and deficient mitochondria in the overall mitochondrial population. The data reveals that photon radiation induces greater mitochondrial alteration and has a more detrimental effect on the rate of repair of oxidized adducts relative to a similar dosage of proton radiation. The findings of this study contribute to the current knowledge of the DNA repair response and mitochondrial activity in glial cells in response to radiation exposure.

Further studies should focus on the cellular mechanisms which regulate OGG1 expression to demonstrate the relationship between the enzymatic activity of the base-excision repair pathway and radiation-induced mutation.

6.1.2 Chapter 3 Conclusion

The exponential rise in chromium-related industrial products and activities exacerbates the risk of poisoning among the general population, particularly because of its ubiquity and persistence in the environment. The current research investigated the epigenetic regulation of base excision repair following exposure to sodium dichromate and oxidative stress. The intrinsic ROS vulnerability of the brain, particularly astrocytes that have a central role in CNS activity and homeostasis, informed its use as our experimental model.

The findings from this study indicate that micromolar concentrations of sodium dichromate are associated with reduced growth and distinct morphological changes, and induces accumulation of 8-OHdG adducts, as evaluated by Comet assay. Small RNA sequencing was used to identify miRNAs that are differentially expressed in human astrocytes. We report significant downregulation of multiple miRNAs (with only a small subset upregulated) in treated cells, suggesting an underlying upregulation in the transcription of their target genes. This phenomenon is attributable to the serially reported interplay between ROS signaling and the microRNA biosynthetic pathways. Functional enrichment analysis of the differentially expressed miRNAs linked many of them to molecular pathways associated with bio-signaling, cell cycle control, and DNA damage repair, especially the base excision repair mechanisms.

In conclusion, the study indicates a non-coding RNA-mediated DNA damage response (DDR) loop activation. This supports our hypothesis that oxidative stress alters the miRNA expression profile in such a way that coherent, functionally related pathways are turned on/off either singly or as an assembly complex. The miRNA candidates

identified by this study could serve as potential miRNA therapeutic targets for patients with cancer and neurodegenerative disorders.

6.1.3 Chapter 4 Conclusion

The human 8-deoxyguanosine DNA glycosylase 1 (hOGG1) is an 8-OHdG-specific base excision repair enzyme that plays an integral part in reducing the rate of mutations. Given the sodium dichromate-induced 8-OHdG accumulation and the preponderance of deregulated microRNAs that target DNA repair enzymes, as were observed in the preceding experiments, this phase of the study focused on predicting and validating specific miRNAs from our list of differentially expressed miRNAs that bind to the 3'-UTR region of the OGG1 transcript.

Based on our results, the increased genomic 8-OHdG accumulation due to ROS' oxidative burden correlates with reduced transcription and translation of hOGG1 and impairs DNA repair capabilities of the cells – a forerunner of cancer and other neurodegenerative disorders. Computational prediction analysis identified two miRNAs that selectively target hOGG1 at its 3'-UTR – miR-1248 and miR-103a – and these were validated as regulators of the hOGG1 protein via a combination of RT-qPCR, microRNA mimic or inhibitor transfection, and/or immunoprecipitation assays. As far as we know, this is the first experimentally validated assertion of these novel miRNA-mRNA pair interactions in the public domain. Inhibition of miR-1248 and miR-103a via the transfection of their inhibitors restored the increased expression levels of hOGG1 (Figure 1-2). Therefore, targeting the identified microRNAs could provide a therapeutic avenue for reducing the nuclear DNA damage in the brain caused by exposure to mutagens.

Collectively, the results from this work provide evidence that oxidative stress affects DNA repair pathways in astroglial cells through non-coding RNA-controlled mechanisms. We believe that this work has the potential for a high impact on the fields of neurotoxicity and DNA repair biology. This study provides comprehensive information regarding microRNA mediation of the genotoxic effects of sodium dichromate on the DNA repair capabilities of human astrocytes that leads to a better understanding of the epigenetic mechanisms that modulate this essential process.

6.1.4 Chapter 5 Conclusion

In this research project, we demonstrated the feasibility of a microprobe-based technology for CD63-specific exosome purification that enables solid-phase CD63-specific exosome immunopurification, and enables direct assessment of exosomal small RNA expression. The ExoPRIME tool provides a **P**recise **R**apid **I**nexpensive **M**ild (non-invasive) and **E**fficient **(**i.e. **PRIME**, from where the coinage is derived**)** alternative for exosome isolation and analysis, with an exosome capturing efficiency of 3 – 24 x 10^6 exosomes per probe depending on the experimental condition.

Overall, results from this study collectively validate the specificity and efficiency of the novel ExoPRIME microprobe technology, and thus, make a significant contribution in advancing exosomes and microvesicles research. While this novel technology is still in its developmental stages, its simplicity, scalability, tunability, affordability, portability, non-invasiveness, low sample input volume (≤ 200 µL/probe) requirement, and very importantly, its selective capture of exosomes from biological specimens, make it a promising tool for potential use in the clinical setting. The current prototype: (1) is a portable and affordable platform that does not require high amounts of antibody and large,

expensive equipment, (2) operates in situ and eliminates the time-consuming, multistep protocol for additional pre-concentration and filtration steps of the biological specimen, (3) enables selective isolation of exosomes with a high spatial resolution, (4) provides flexible options for scalability in terms of yield and speed, as desired by the user, (5) prevents consumption or destruction of specimens, thus permitting reusability multiple times, and (6) allows integration with microfluidics-based standard systems for genomic and proteomic analysis of exosomal cargoes (Figure 1-3). Thus, this direct, single-step ExoPRIME Microprobe Technology holds promise for real-time exosome sample collection which can be applied for exosome enrichment and analysis of clinical specimens.

6.2 Future Directions

The first prong of this project established two novel miRNA-mRNA pairwise interactions. Future efforts will be geared towards the validation of other putative miRNAs/mRNA target pairs within the context of DNA damage response and repair. Furthermore, preliminary data obtained show that lower doses of sodium dichromate lead to hOGG1 downregulation while increasing the concentration leads to an upregulation. This calls for more investigations into the threshold and limits of sensitivity of microRNA involvement in cellular stress response.

The future outlook of the ExoPRIME microprobe technology will focus on tests using other biofluids, and its integration with a lab-on-a-chip platform as a step towards process automation. Successful implementation of this next phase aims to provide a simple, bench-top bioanalytical system for automated high-throughput isolation and analysis of exosomes and their cargoes, with lowered technical expertise barrier for the end-user. Ultimately, the ExoPRIME microprobe technology would be useful in low-resource

clinical and laboratory settings. This important utility cannot be over-emphasized in the face of a pandemic, an epidemic outbreak, or other national health emergency scenarios, for rapid-response testing and surveillance.

APPENDIX C

SMALL RNA-Seq DATA ANALYSES [SEE COMPACT DISC]

C.6 Partek_ PCA Plot for hsa-miR-21-5p (10 µM Sodium Dichromate-Treated vs Non-Treated)

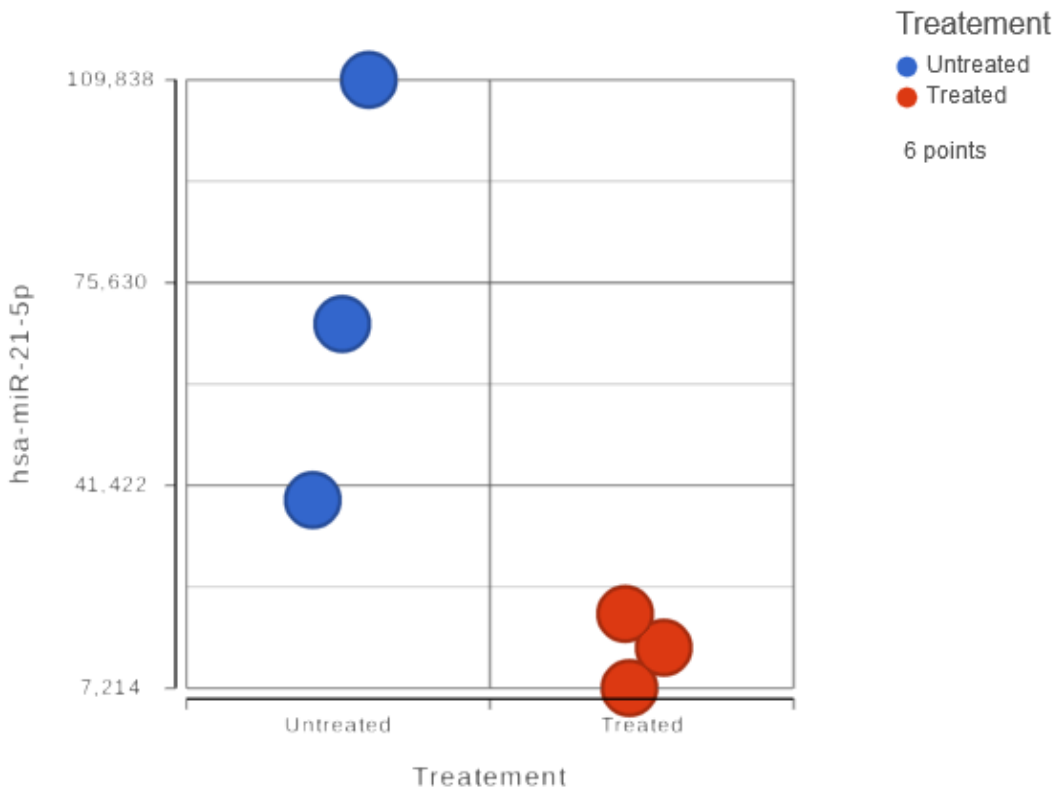

Figure C.1 PCA Plot for hsa-miR-21-5p (10 µM NaCr2O7-Treated vs Non-Treated)

C.7 Partek_PCA Plot for hsa-miR-335-5p (10 µM Sodium Dichromate-Treated vs Non-Treated)

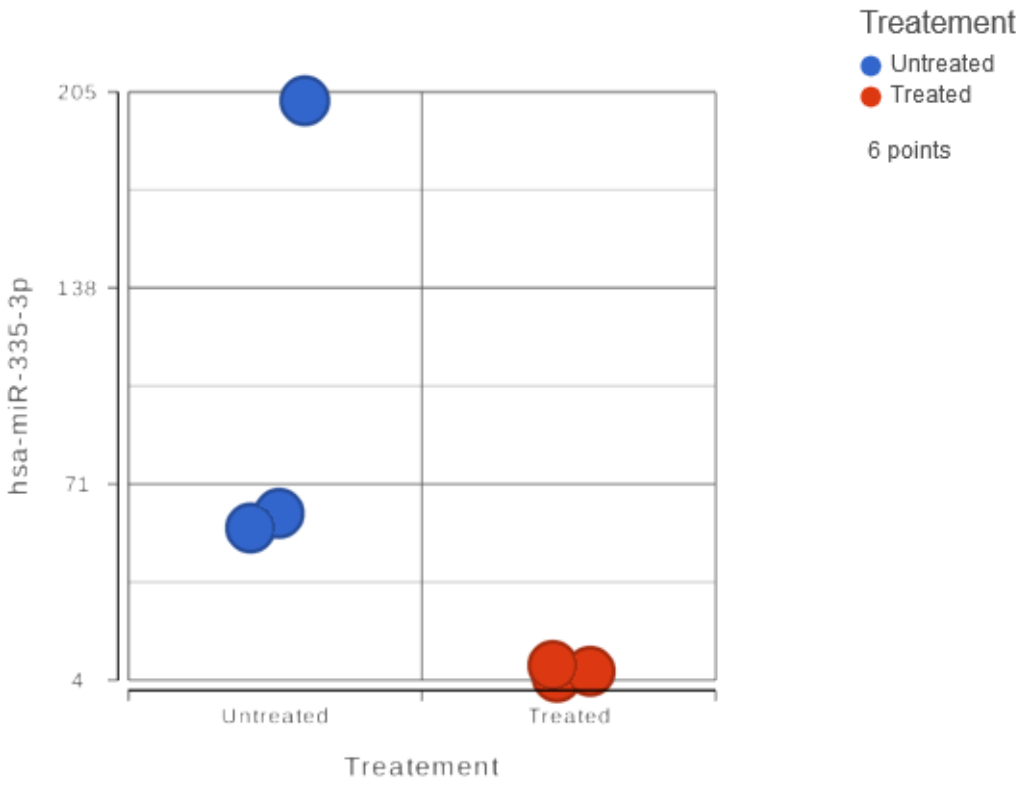

Figure C.2 PCA Plot for hsa-miR-335-5p (10 µM NaCr2O7-Treated vs Non-Treated)

APPENDIX D

VALIDATION OF PREDICTED MICRORNA TARGETS

D.1 Forward and reverse primer sequences for GAPDH and PARP-1

Table D.1 Forward and reverse primer sequences for GAPDH and PARP-1

Primer	Oligonucleotide sequences
GAPDH	F 5'– ACA TCG CTC AGA CAC CAT G – 3' R 5'– TGT AGT TGA GGT CAA TGA AGG G – 3'
PARP-1	F 5'-CGC ATA CTC CAT CCT CAG TG- 3' R 5'–GGA TCA GGG TGT AAA AGC GAT – 3'

D.2 MirTrap Vector Information

D.2.1 pMirTrap Vecor Map

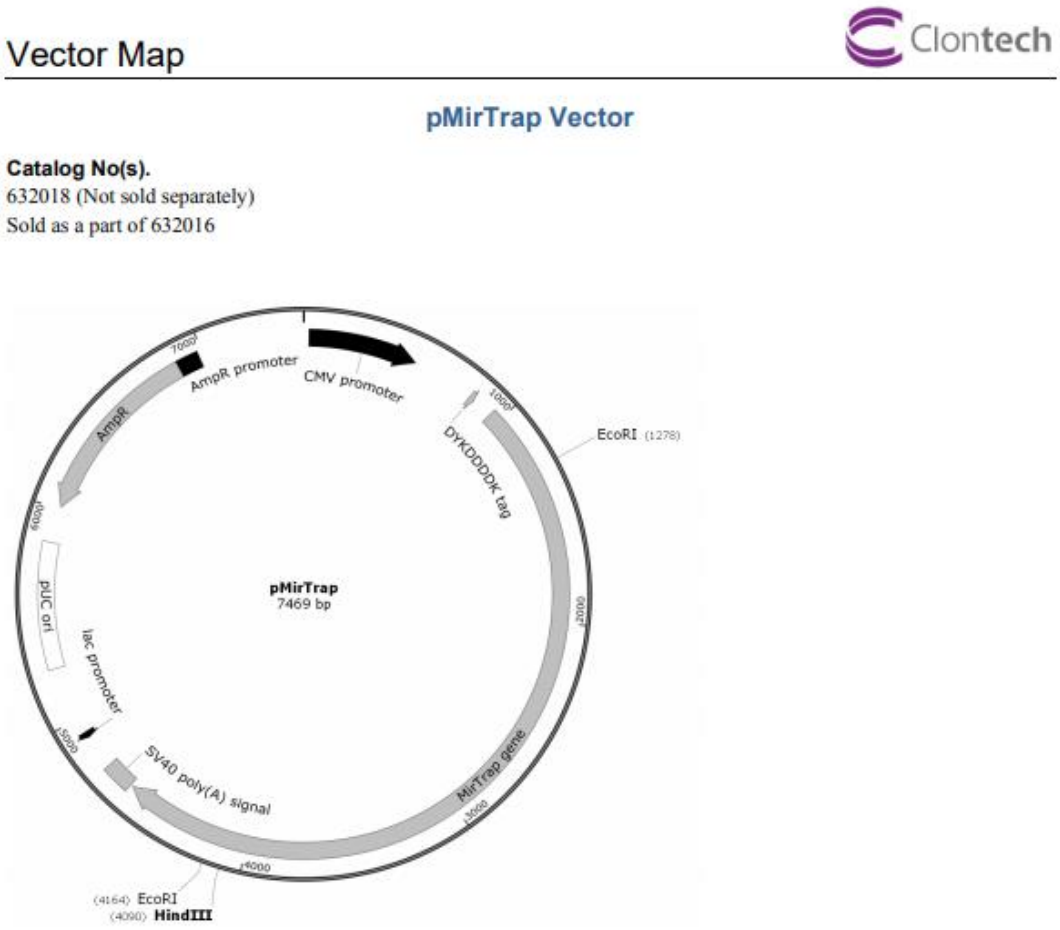

Figure D.1 pMirTrap Vector Map

D.2.2 pMirTrap Control Vector Map

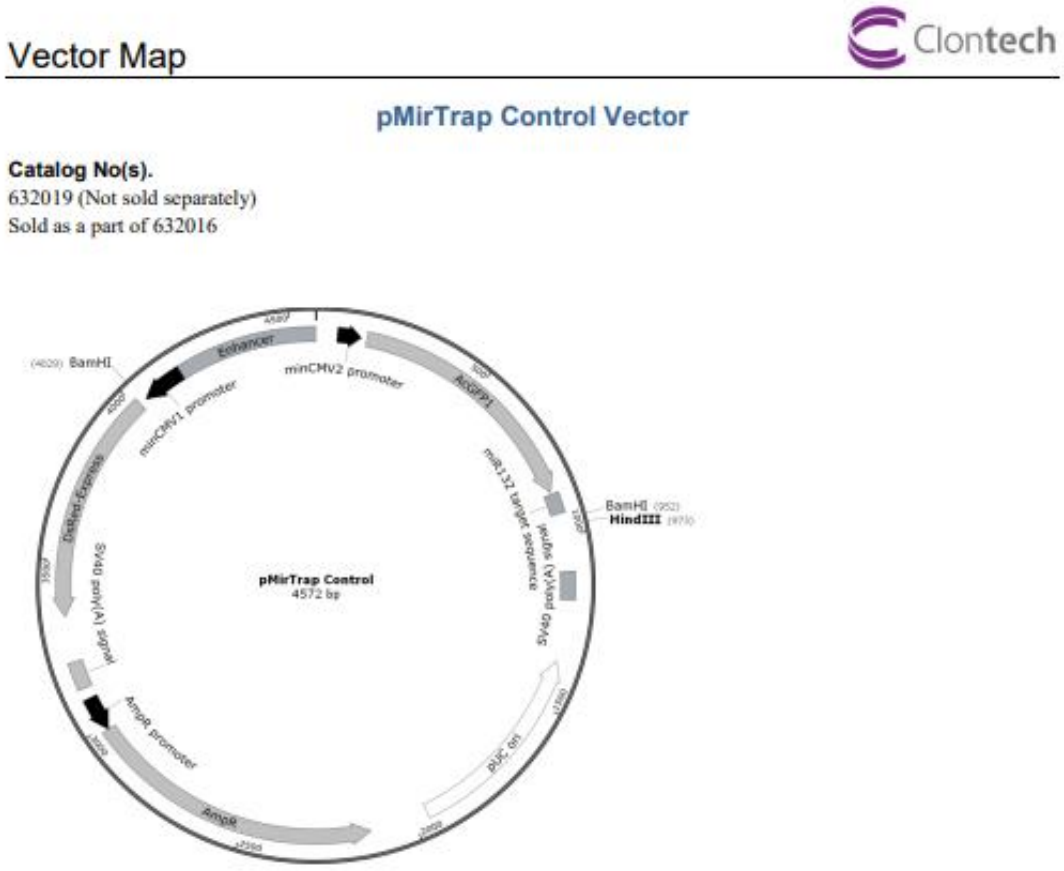

Figure D.2 pMirTrap Control Vector Map

D.3 MicroRNA Target Mining Data

D.3.1 Predicted hOGG1-targeting MicroRNAs (miRDB) – See Compact Disc

D.3.2 Predicted hOGG1-targeting MicroRNAs (miRWalk) – See Compact Disc

D.3.3 Predicted hOGG1-targeting MicroRNAs (TargetScan) – See Compact Disc

D.4 Evaluation of MirTrap Vectors Transfection Efficiency

D.4.1 Fluoresent Images of MirTrap Control Vector-Transfected Astrocytes

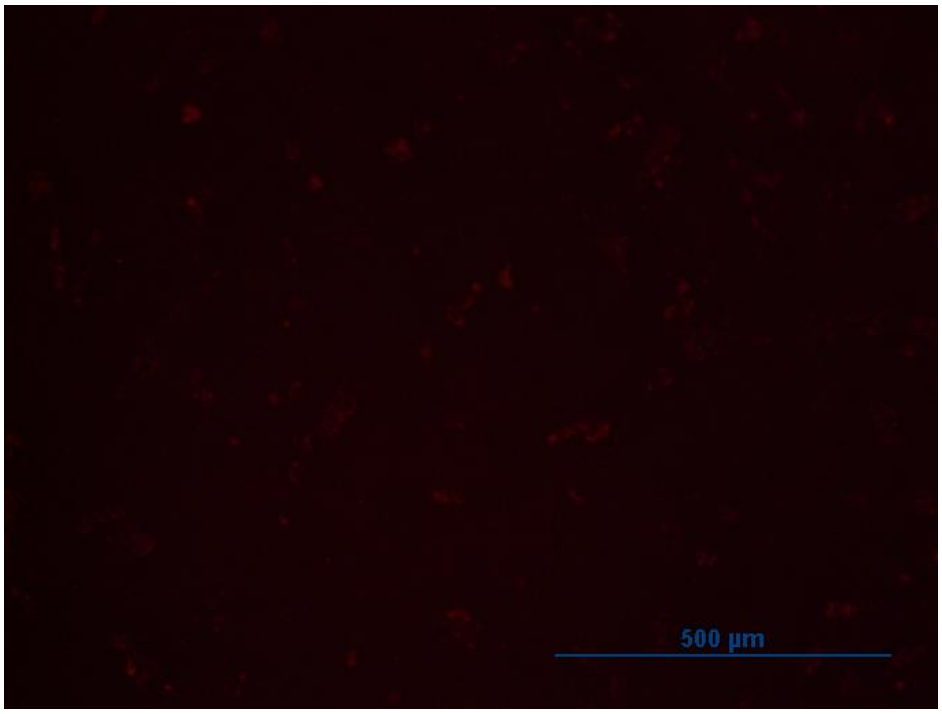

Figure D.3 Fluorescent Images at 100 ms Exposure Depicting Efficient Transfection Consistent with High Expression of DsRed Express (Red Fluorescence) with very negligible AcGFP1 Co-expression (Green Fluorescence)

D.4.2 RT-qPCR Analysis of MirTrap Control Vector-Transfected Astrocytes

Table D.2 RT-qPCR Analysis Showing Fold Enrichment of Positive (AcGFP1) and Negative (hPlod3) Controls, Relative to the GAPDH Internal Control

	Ct of AcGFP1	**Ct of hGAPDH**	**ΔCt**	**$2^{-\Delta Ct}$**	**Fold Enrichment**
Before IP Sample 1	20.71	20.27	0.44	0.74	
After IP Sample 1	24.91	26.54	-1.63	3.10	**4.20**

	Ct of AcGFP1	**Ct of hGAPDH**	**ΔCt**	**$2^{-\Delta Ct}$**	**Fold Enrichment**
Before IP Sample 2	20.27	18.79	1.48	0.36	
After IP Sample 2	25.04	26.44	-1.4	2.64	**7.36**

	Ct of AcGFP1	**Ct of hGAPDH**	**ΔCt**	**$2^{-\Delta Ct}$**	**Fold Enrichment**
Before IP Sample 3	20.81	19.65	1.16	0.45	
After IP Sample 3	23.51	26.02	-2.51	5.70	**12.73**

AcGFP1 Average Fold Enrichment = 8.10

	Ct of hPlod3	**Ct of hGAPDH**	**ΔCt**	**$2^{-\Delta Ct}$**	**Fold Enrichment**
Before IP Sample 1	23.68	20.27	3.41	0.09	
After IP Sample 1	30.61	26.54	4.07	0.06	**0.63**

	Ct of hPlod3	**Ct of hGAPDH**	**ΔCt**	**$2^{-\Delta Ct}$**	**Fold Enrichment**
Before IP Sample 2	24.03	18.79	5.24	0.03	
After IP Sample 2	30.07	26.44	3.63	0.08	**3.05**

	Ct of hPlod3	**Ct of hGAPDH**	**ΔCt**	**$2^{-\Delta Ct}$**	**Fold Enrichment**
Before IP Sample 3	24.75	19.65	5.1	0.03	
After IP Sample 3	30.41	26.02	4.39	0.05	**1.64**

hPlod3 Average Fold Enrichment = 1.77

APPENDIX E

CHARACTERIZATION OF THE EXOPRIME MICROPROBE

E.1 Structural Characterization of the LbL Precursor on the Microneedles [Excerpts from Doctoral Dissertation of S. M. Ishraq Bari][6]

E.1.1 Scanning Electron Microscopy (SEM) coupled with Energy-Dispersive X-ray Spectroscopy (EDX)

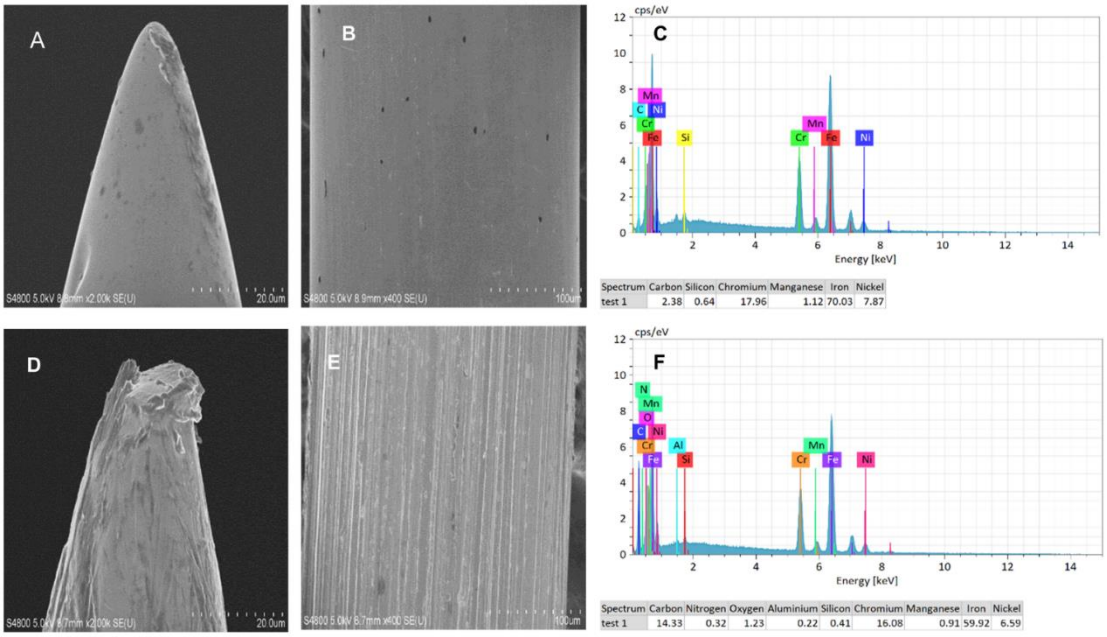

Figure E.1 SEM micrographs of the tips (left panels) and stem (middle panels) of polished plain needles (A, B) and LBL-coated microneedles (D, E), showing successful and efficient deposition polyelectrolyte bilayers. The right panels show the corresponding EDX spectra of plain (C) and LBL-coated (F) microneedles [36]

[6] C.D. Nwokwu, S.M. Ishraq Bari, K.H. Hutson, C. Brausell, G.G. Nestorova. ExoPRIME: Solid-phase immunoisolation and OMICS analysis of surface-marker-specific exosomal subpopulations, Talanta 236(2022):122870. https://doi.org/10.1016/j.talanta.2021.122870.

E.1.2 Validation of Biotin and Anti-CD63 Antibody Immobilization on the Microneedles

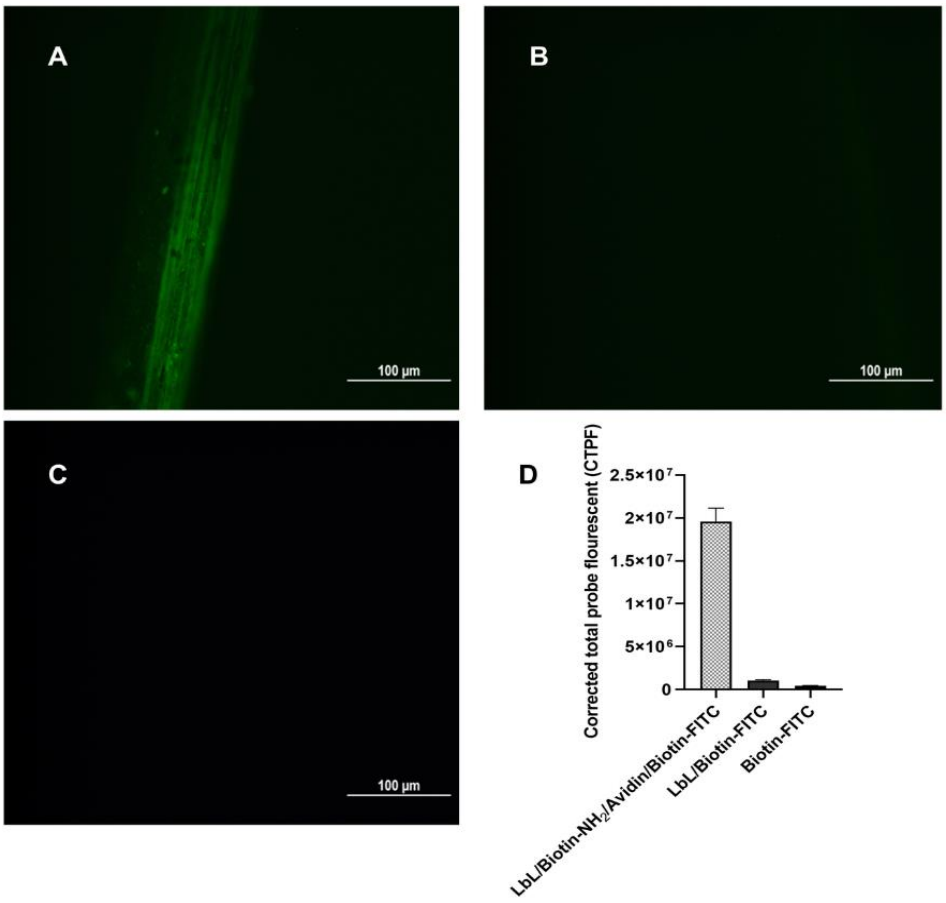

Figure E.2 Fluorescent images confirming successful LBL assembly and Biotin immobilization on microneedles: (A) LbL+Biotin-EDC+Streptavidin+Biotin-FITC; (B) LbL+Biotin-FITC; (C) Biotin-FITC. (D) ImageJ analysis of the of the CTPF of A, B, C [36]

E.2 Assessment of ExoPRIME's Specificity

[Culled from the Master's Thesis Hope K. Hutson][7]

E.2.1 Immunofluorescence Imaging of the ExoPRIME Microprobe

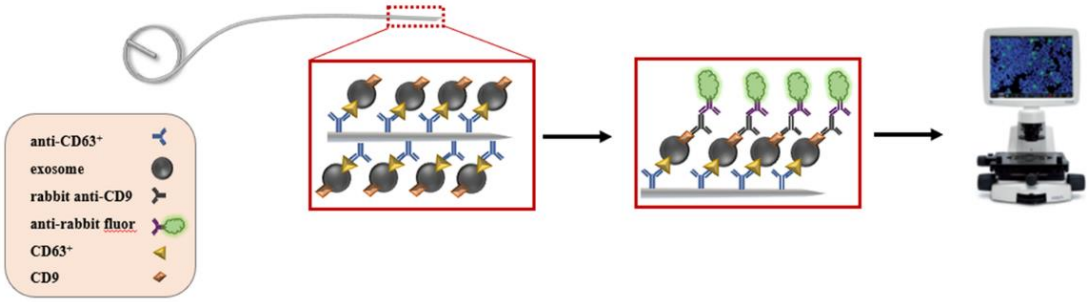

Figure E.3 Schematic of exosome immunofluorescence imaging. Exosomes are selectively captured to the surface of the ExoPRIME microprobes through antibody-specific interactions of anti-CD63 and CD63 exosomes receptors. CD9 and CD81 antibodies are used for labeling of the captured exosomes followed by detection with IgG secondary antibody conjugated to NL557 fluorophore [36]

[7] C.D. Nwokwu, S.M. Ishraq Bari, K.H. Hutson, C. Brausell, G.G. Nestorova. ExoPRIME: Solid-phase immunoisolation and OMICS analysis of surface-marker-specific exosomal subpopulations, Talanta 236(2022):122870. https://doi.org/10.1016/j.talanta.2021.122870.

E.2.2 Image J Analysis of Immunofluorescence Signal showing ExoPRIME Specificity

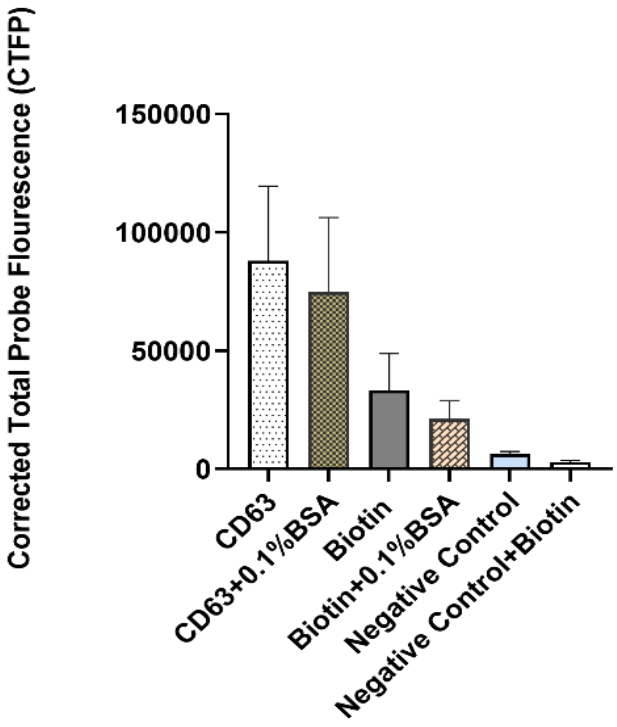

Figure E.4 CTFP Image J analysis of fluorescence signal obtained for different experimental groups (n=4) [36]

E.2.3 SDS-PAGE Gel Image confirming ExoPRIME's Enrichment Capability

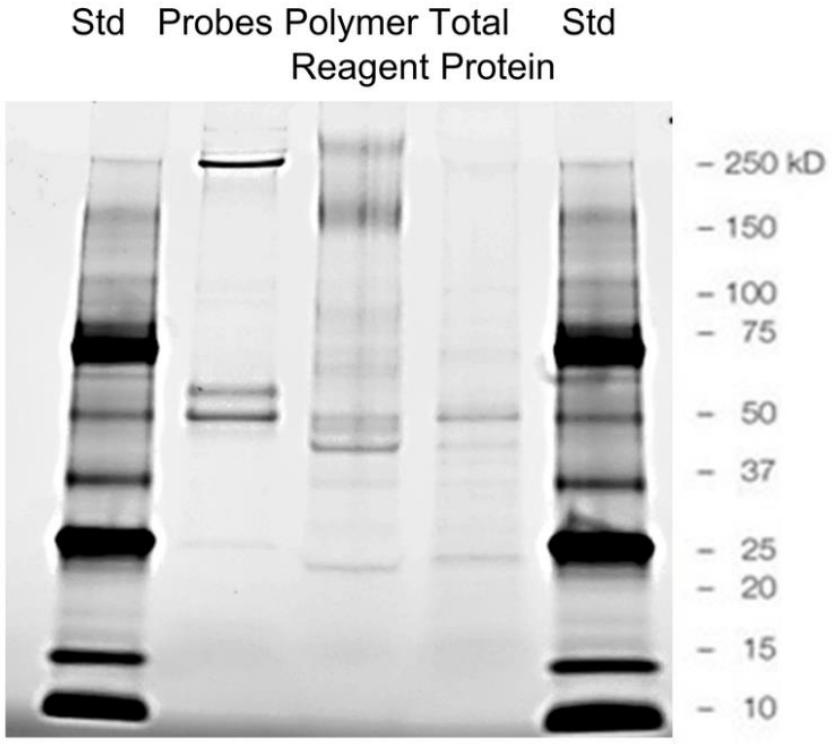

Figure E.5 Comparison of protein profile via SDS-PAGE analysis. The gel legends indicate BioRad Kalediscope™ protein standard (Std); ExoPRIME exosome (probe); polymer-percipitated exosomes (Polymer reagent); and total protein lysate (total protein) at a concentration of 20 µg per well [36]

BIBLIOGRAPHY

[1] N.Z. Borgesius, M.C. de Waard, I. van der Pluijm, A. Omrani, G.C.M. Zondag, G.T.J. van der Horst, D.W. Melton, J.H.J. Hoeijmakers, D. Jaarsma, Y. Elgersma, Accelerated Age-Related Cognitive Decline and Neurodegeneration, Caused by Deficient DNA Repair, *J. Neurosci.* 31 (2011) 12543–12553. https://doi.org/10.1523/JNEUROSCI.1589-11.2011.

[2] D. Liu, D.L. Croteau, N. Souza-Pinto, M. Pitta, J. Tian, C. Wu, H. Jiang, K. Mustafa, G. Keijzers, V.A. Bohr, M.P. Mattson, Evidence that OGG1 Glycosylase Protects Neurons against Oxidative DNA Damage and Cell Death under Ischemic Conditions, *J. Cereb. Blood Flow Metab.* 31 (2011) 680–692. https://doi.org/10.1038/jcbfm.2010.147.

[3] A. Yamamoto, Y. Nakamura, N. Kobayashi, T. Iwamoto, A. Yoshioka, H. Kuniyasu, T. Kishimoto, T. Mori, Neurons and astrocytes exhibit lower activities of global genome nucleotide excision repair than do fibroblasts, *DNA Repair* (Amst). 6 (2007) 649–657. https://doi.org/10.1016/j.dnarep.2006.12.006.

[4] F.W. Pfrieger, Synaptic Efficacy Enhanced by Glial Cells in Vitro, *Science*, 277 (1997) 1684–1687. https://doi.org/10.1126/science.277.5332.1684.

[5] M. Bélanger, I. Allaman, P.J. Magistretti, Brain Energy Metabolism: Focus on Astrocyte-Neuron Metabolic Cooperation, *Cell Metab.* 14 (2011) 724–738. https://doi.org/10.1016/j.cmet.2011.08.016.

[6] Y. Chen, R.A. Swanson, Astrocytes and Brain Injury, *J. Cereb. Blood Flow Metab.* 23 (2003) 137–149. https://doi.org/10.1097/01.WCB.0000044631.80210.3C.

[7] T.-Y. Zhao, S.-P. Zou, P.E. Knapp, Exposure to cell phone radiation up-regulates apoptosis genes in primary cultures of neurons and astrocytes, *Neurosci. Lett.* 412 (2007) 34–38. https://doi.org/10.1016/j.neulet.2006.09.092.

[8] J.K. Leach, G. Van Tuyle, P.S. Lin, R. Schmidt-Ullrich, R.B. Mikkelsen, Ionizing radiation-induced, mitochondria-dependent generation of reactive oxygen/nitrogen., *Cancer Res.* 61 (2001) 3894–901. http://www.ncbi.nlm.nih.gov/pubmed/11358802.

[9] M.T. Lin, M.F. Beal, Mitochondrial dysfunction and oxidative stress in neurodegenerative diseases, *Nature* 443 (2006) 787–795. https://doi.org/10.1038/nature05292.

[10] R. Kulkarni, B. Marples, M. Balasubramaniam, R.A. Thomas, J.D. Tucker, Mitochondrial Gene Expression Changes in Normal and Mitochondrial Mutant Cells after Exposure to Ionizing Radiation, *Radiat. Res.* 173 (2010) 635–644. https://doi.org/10.1667/RR1737.1.

[11] K.H. Hutson, K. Willis, C.D. Nwokwu, M. Maynard, G.G. Nestorova, Photon versus proton neurotoxicity: Impact on mitochondrial function and 8-OHdG base-excision repair mechanism in human astrocytes, *Neurotoxicology* 82 (2021) 158–166. https://doi.org/10.1016/j.neuro.2020.12.011.

[12] V.N. Kim, J.-W. Nam, Genomics of microRNA, *Trends Genet.* 22 (2006) 165–173. https://doi.org/10.1016/j.tig.2006.01.003.

[13] T.B. Dansen, B.M.T. Burgering, Unravelling the tumor-suppressive functions of FOXO proteins, *Trends Cell Biol.* 18 (2008) 421–429. https://doi.org/10.1016/j.tcb.2008.07.004.

[14] S. Reuter, S.C. Gupta, M.M. Chaturvedi, B.B. Aggarwal, Oxidative stress, inflammation, and cancer: How are they linked?, *Free Radic. Biol. Med.* 49 (2010) 1603–1616. https://doi.org/10.1016/j.freeradbiomed.2010.09.006.

[15] J. He, B.-H. Jiang, Interplay Between Reactive Oxygen Species and MicroRNAs in Cancer, *Curr. Pharmacol. Reports*. 2 (2016) 82–90. https://doi.org/10.1007/s40495-016-0051-4.

[16] H. Valadi, K. Ekström, A. Bossios, M. Sjöstrand, J.J. Lee, J.O. Lötvall, Exosome-mediated transfer of mRNAs and microRNAs is a novel mechanism of genetic exchange between cells, *Nat. Cell Biol.* 9 (2007) 654–659. https://doi.org/10.1038/ncb1596.

[17] Y. Men, J. Yelick, S. Jin, Y. Tian, M.S.R. Chiang, H. Higashimori, E. Brown, R. Jarvis, Y. Yang, Exosome reporter mice reveal the involvement of exosomes in mediating neuron to astroglia communication in the CNS, *Nat. Commun.* 10 (2019) 4136. https://doi.org/10.1038/s41467-019-11534-w.

[18] C. Théry, Exosomes: secreted vesicles and intercellular communications, *F1000 Biol. Rep.* 3 (2011). https://doi.org/10.3410/B3-15.

[19] T. Katsuda, N. Kosaka, T. Ochiya, The roles of extracellular vesicles in cancer biology: Toward the development of novel cancer biomarkers, *Proteomics.* 14 (2014) 412–425. https://doi.org/10.1002/pmic.201300389.

[20] Z. Zhao, Y. Yang, Y. Zeng, M. He, A microfluidic ExoSearch chip for multiplexed exosome detection towards blood-based ovarian cancer diagnosis, *Lab Chip.* 16 (2016) 489–496. https://doi.org/10.1039/C5LC01117E.

[21] J. Skog, T. Würdinger, S. van Rijn, D.H. Meijer, L. Gainche, W.T. Curry, B.S. Carter, A.M. Krichevsky, X.O. Breakefield, Glioblastoma microvesicles transport RNA and proteins that promote tumour growth and provide diagnostic biomarkers, *Nat. Cell Biol.* 10 (2008) 1470–1476. https://doi.org/10.1038/ncb1800.

[22] E.S.B. Salem, G.-C. Fan, Pathological Effects of Exosomes in Mediating Diabetic Cardiomyopathy, in: 2017: pp. 113–138. https://doi.org/10.1007/978-981-10-4397-0_8.

[23] Z. Zakeri, A. Salmaninejad, N. Hosseini, Y. Shahbakhsh, E. Fadaee, M.K. Shahrzad, S. Fadaei, MicroRNA and exosome: Key players in rheumatoid arthritis, *J. Cell. Biochem.* 120 (2019) 10930–10944. https://doi.org/10.1002/jcb.28499.

[24] J.A. Cañas, B. Sastre, J.M. Rodrigo-Muñoz, V. del Pozo, Exosomes: A new approach to asthma pathology, *Clin. Chim. Acta.* 495 (2019) 139–147. https://doi.org/10.1016/j.cca.2019.04.055.

[25] K. Mizutani, K. Kawakami, K. Horie, Y. Fujita, K. Kameyama, T. Kato, K. Nakane, T. Tsuchiya, M. Yasuda, K. Masunaga, Y. Kasuya, Y. Masuda, T. Deguchi, T. Koie, M. Ito, Urinary exosome as a potential biomarker for urinary tract infection, *Cell. Microbiol.* 21 (2019). https://doi.org/10.1111/cmi.13020.

[26] S. Saman, W. Kim, M. Raya, Y. Visnick, S. Miro, S. Saman, B. Jackson, A.C. McKee, V.E. Alvarez, N.C.Y. Lee, G.F. Hall, Exosome-associated Tau Is Secreted in Tauopathy Models and Is Selectively Phosphorylated in Cerebrospinal Fluid in Early Alzheimer Disease, *J. Biol. Chem.* 287 (2012) 3842–3849. https://doi.org/10.1074/jbc.M111.277061.

[27] M.K.S. Tang, A.S.T. Wong, Exosomes: Emerging biomarkers and targets for ovarian cancer, *Cancer Lett.* 367 (2015) 26–33. https://doi.org/10.1016/j.canlet.2015.07.014.

[28] S. Lin, Z. Yu, D. Chen, Z. Wang, J. Miao, Q. Li, D. Zhang, J. Song, D. Cui, Progress in Microfluidics-Based Exosome Separation and Detection Technologies for Diagnostic Applications, *Small.* 16 (2020) 1903916. https://doi.org/10.1002/smll.201903916.

[29] K. Yuyama, H. Sun, S. Mitsutake, Y. Igarashi, Sphingolipid-modulated Exosome Secretion Promotes Clearance of Amyloid-β by Microglia, *J. Biol. Chem.* 287 (2012) 10977–10989. https://doi.org/10.1074/jbc.M111.324616.

[30] Z. Andreu, M. YÃ¡Ã±ez-MÃ^3, Tetraspanins in Extracellular Vesicle Formation and Function, *Front. Immunol.* 5 (2014). https://doi.org/10.3389/fimmu.2014.00442.

[31] D.W. Greening, R. Xu, H. Ji, B.J. Tauro, R.J. Simpson, A Protocol for Exosome Isolation and Characterization: Evaluation of Ultracentrifugation, Density-Gradient Separation, and Immunoaffinity Capture Methods, in: 2015: pp. 179–209. https://doi.org/10.1007/978-1-4939-2550-6_15.

[32] L.-L. Yu, J. Zhu, J.-X. Liu, F. Jiang, W.-K. Ni, L.-S. Qu, R.-Z. Ni, C.-H. Lu, M.-B. Xiao, A Comparison of Traditional and Novel Methods for the Separation of Exosomes from Human Samples, *Biomed Res. Int.* 2018 (2018) 1–9. https://doi.org/10.1155/2018/3634563.

[33] J. Kowal, G. Arras, M. Colombo, M. Jouve, J.P. Morath, B. Primdal-Bengtson, F. Dingli, D. Loew, M. Tkach, C. Théry, Proteomic comparison defines novel markers to characterize heterogeneous populations of extracellular vesicle subtypes, *Proc. Natl. Acad. Sci.* 113 (2016) E968–E977. https://doi.org/10.1073/pnas.1521230113.

[34] Y.J. Piao, H.S. Kim, E.H. Hwang, J. Woo, M. Zhang, W.K. Moon, Breast cancer cell-derived exosomes and macrophage polarization are associated with lymph node metastasis, *Oncotarget*. 9 (2018) 7398–7410. https://doi.org/10.18632/oncotarget.23238.

[35] D. Chiasserini, J.R.T. van Weering, S.R. Piersma, T. V. Pham, A. Malekzadeh, C.E. Teunissen, H. de Wit, C.R. Jiménez, Proteomic analysis of cerebrospinal fluid extracellular vesicles: A comprehensive dataset, *J. Proteomics.* 106 (2014) 191–204. https://doi.org/10.1016/j.jprot.2014.04.028.

[36] C.D. Nwokwu, S.M. Ishraq Bari, K.H. Hutson, C. Brausell, G.G. Nestorova, ExoPRIME: Solid-phase immunoisolation and OMICS analysis of surface-marker-specific exosomal subpopulations, *Talanta*. 236 (2022) 122870. https://doi.org/10.1016/j.talanta.2021.122870.

[37] A.M. Khalil, M. Guttman, M. Huarte, M. Garber, A. Raj, D. Rivea Morales, K. Thomas, A. Presser, B.E. Bernstein, A. van Oudenaarden, A. Regev, E.S. Lander, J.L. Rinn, Many human large intergenic noncoding RNAs associate with chromatin-modifying complexes and affect gene expression, *Proc. Natl. Acad. Sci.* 106 (2009) 11667–11672. https://doi.org/10.1073/pnas.0904715106.

[38] R.P. Alexander, G. Fang, J. Rozowsky, M. Snyder, M.B. Gerstein, Annotating non-coding regions of the genome, *Nat. Rev. Genet.* 11 (2010) 559–571. https://doi.org/10.1038/nrg2814.

[39] M. Esteller, Non-coding RNAs in human disease, *Nat. Rev. Genet.* 12 (2011) 861–874. https://doi.org/10.1038/nrg3074.

[40] E. Lejeune, R.C. Allshire, Common ground: small RNA programming and chromatin modifications, *Curr. Opin. Cell Biol.* 23 (2011) 258–265. https://doi.org/10.1016/j.ceb.2011.03.005.

[41] J.L. Rinn, H.Y. Chang, Genome Regulation by Long Noncoding RNAs, *Annu. Rev. Biochem.* 81 (2012) 145–166. https://doi.org/10.1146/annurev-biochem-051410-092902.

[42] R. Brimacombe, W. Stiege, Structure and function of ribosomal RNA, *Biochem. J.* 229 (1985) 1–17. https://doi.org/10.1042/bj2290001.

[43] M.D. Berg, C.J. Brandl, Transfer RNAs: diversity in form and function, *RNA Biol*. 18 (2021) 316–339. https://doi.org/10.1080/15476286.2020.1809197.

[44] V. Carninci, P., Kasukawa, T., Katayama, S., Gough, J., Frith, M. C., Maeda, N., Oyama, R., Ravasi, T., Lenhard, B., Wells, C., Kodzius, R., Shimokawa, K., Bajic, V. B., Brenner, S. E., Batalov, S., Forrest, A. R., Zavolan, M., Davis, M. J., Wilming, L. G., The Transcriptional Landscape of the Mammalian Genome, *Science* 2005, 309 (5740) 1559–1563. https://doi.org/10.1126/science.1112014.

[45] E.A. Gibb, E.A. Vucic, K.S.S. Enfield, G.L. Stewart, K.M. Lonergan, J.Y. Kennett, D.D. Becker-Santos, C.E. MacAulay, S. Lam, C.J. Brown, W.L. Lam, Human Cancer Long Non-Coding RNA Transcriptomes, *PLoS One*. 6 (2011) e25915. https://doi.org/10.1371/journal.pone.0025915.

[46] J.-H. Yoon, K. Abdelmohsen, M. Gorospe, Functional interactions among microRNAs and long noncoding RNAs, *Semin. Cell Dev. Biol.* 34 (2014) 9–14. https://doi.org/10.1016/j.semcdb.2014.05.015.

[47] M.-T. Piccoli, S.K. Gupta, J. Viereck, A. Foinquinos, S. Samolovac, F.L. Kramer, A. Garg, J. Remke, K. Zimmer, S. Batkai, T. Thum, Inhibition of the Cardiac Fibroblast–Enriched lncRNA Meg3 Prevents Cardiac Fibrosis and Diastolic Dysfunction, *Circ. Res.* 121 (2017) 575–583. https://doi.org/10.1161/CIRCRESAHA.117.310624.

[48] R.C. Lee, R.L. Feinbaum, V. Ambros, The C. elegans heterochronic gene lin-4 encodes small RNAs with antisense complementarity to lin-14, *Cell*. 75 (1993) 843–854. https://doi.org/10.1016/0092-8674(93)90529-Y.

[49] N.C. Lau, An Abundant Class of Tiny RNAs with Probable Regulatory Roles in *Caenorhabditis elegans, Science* 2001, 294 (5543) 858–862. https://doi.org/10.1126/science.1065062.

[50] M. Lagos-Quintana, Identification of Novel Genes Coding for Small Expressed RNAs, *Science* 2001, 294 (5543) 853–858. https://doi.org/10.1126/science.1064921.

[51] R.C. Lee, An Extensive Class of Small RNAs in Caenorhabditis elegans, *Science* 2001, 294 (5543) 862–864. https://doi.org/10.1126/science.1065329.

[52] G. Ruvkun, The perfect storm of tiny RNAs, *Nat. Med.* 14 (2008) 1041–1045. https://doi.org/10.1038/nm1008-1041.

[53] U.A. Ørom, T. Derrien, M. Beringer, K. Gumireddy, A. Gardini, G. Bussotti, F. Lai, M. Zytnicki, C. Notredame, Q. Huang, R. Guigo, R. Shiekhattar, Long Noncoding RNAs with Enhancer-like Function in Human Cells, *Cell.* 143 (2010) 46–58. https://doi.org/10.1016/j.cell.2010.09.001.

[54] P. Carninci, Y. Hayashizaki, Noncoding RNA transcription beyond annotated genes, *Curr. Opin. Genet. Dev.* 17 (2007) 139–144. https://doi.org/10.1016/j.gde.2007.02.008.

[55] E. Korpelainen, J. Tuimala, P. Somervuo, M. Huss, G. Wong, RNA-seq Data Analysis, Chapman and Hall/CRC, 2014. https://doi.org/10.1201/b17457.

[56] N.M. Baulina, O.G. Kulakova, O.O. Favorova, MicroRNAs: The Role in Autoimmune Inflammation, *Acta Naturae.* 8 (2016) 21–33. https://doi.org/10.32607/20758251-2016-8-1-21-33.

[57] A. Osman, MicroRNAs in health and disease--basic science and clinical applications., *Clin. Lab.* 58 (2012) 393–402. http://www.ncbi.nlm.nih.gov/pubmed/22783567.

[58] D.P. Bartel, MicroRNAs: Target Recognition and Regulatory Functions, *Cell.* 136 (2009) 215–233. https://doi.org/10.1016/j.cell.2009.01.002.

[59] A.E. Pasquinelli, MicroRNAs and their targets: recognition, regulation and an emerging reciprocal relationship, *Nat. Rev. Genet.* 13 (2012) 271–282. https://doi.org/10.1038/nrg3162.

[60] A. Lauri, G. Pompilio, M.C. Capogrossi, The mitochondrial genome in aging and senescence, *Ageing Res. Rev.* 18 (2014) 1–15. https://doi.org/10.1016/j.arr.2014.07.001.

[61] S.Y. Chan, Y.-Y. Zhang, C. Hemann, C.E. Mahoney, J.L. Zweier, J. Loscalzo, MicroRNA-210 Controls Mitochondrial Metabolism during Hypoxia by Repressing the Iron-Sulfur Cluster Assembly Proteins ISCU1/2, *Cell Metab.* 10 (2009) 273–284. https://doi.org/10.1016/j.cmet.2009.08.015.

[62] H. Osada, T. Takahashi, MicroRNAs in biological processes and carcinogenesis, *Carcinogenesis.* 28 (2007) 2–12. https://doi.org/10.1093/carcin/bgl185.

[63] L. Tan, J.-T. Yu, L. Tan, Causes and Consequences of MicroRNA Dysregulation in Neurodegenerative Diseases, *Mol. Neurobiol.* 51 (2015) 1249–1262. https://doi.org/10.1007/s12035-014-8803-9.

[64] N.L. Simone, B.P. Soule, D. Ly, A.D. Saleh, J.E. Savage, W. DeGraff, J. Cook, C.C. Harris, D. Gius, J.B. Mitchell, Ionizing Radiation-Induced Oxidative Stress Alters miRNA Expression, *PLoS One.* 4 (2009) e6377. https://doi.org/10.1371/journal.pone.0006377.

[65] A. Allegra, A. ALONCI, S. CAMPO, G. PENNA, A. PETRUNGARO, D. GERACE, C. MUSOLINO, Circulating microRNAs: New biomarkers in diagnosis, prognosis and treatment of cancer (Review), *Int. J. Oncol.* 41 (2012) 1897–1912. https://doi.org/10.3892/ijo.2012.1647.

[66] T. Smith-Vikos, F.J. Slack, MicroRNAs and their roles in aging, *J. Cell Sci.* 125 (2012) 7–17. https://doi.org/10.1242/jcs.099200.

[67] G.M. Borchert, W. Lanier, B.L. Davidson, RNA polymerase III transcribes human microRNAs, *Nat. Struct. Mol. Biol.* 13 (2006) 1097–1101. https://doi.org/10.1038/nsmb1167.

[68] M. Wink, An Introduction to Molecular Biotechnology- Fundamentals, Methods and Applications, 2nd editio, lWiley-VCH, Weinheim, 2011.

[69] Y. Lee, C. Ahn, J. Han, H. Choi, J. Kim, J. Yim, J. Lee, P. Provost, O. Rådmark, S. Kim, V.N. Kim, The nuclear RNase III Drosha initiates microRNA processing, *Nature.* 425 (2003) 415–419. https://doi.org/10.1038/nature01957.

[70] R. Yi, Exportin-5 mediates the nuclear export of pre-microRNAs and short hairpin RNAs, *Genes Dev.* 17 (2003) 3011–3016. https://doi.org/10.1101/gad.1158803.

[71] E. Lund, Nuclear Export of MicroRNA Precursors, *Science* 2004, 303 (5654) 95–98. https://doi.org/10.1126/science.1090599.

[72] J.O. Westholm, E.C. Lai, Mirtrons: microRNA biogenesis via splicing, *Biochimie*. 93 (2011) 1897–1904. https://doi.org/10.1016/j.biochi.2011.06.017.

[73] T. Desvignes, P. Batzel, E. Berezikov, K. Eilbeck, J.T. Eppig, M.S. McAndrews, A. Singer, J.H. Postlethwait, miRNA Nomenclature: A View Incorporating Genetic Origins, Biosynthetic Pathways, and Sequence Variants, *Trends Genet.* 31 (2015) 613–626. https://doi.org/10.1016/j.tig.2015.09.002.

[74] S. Diederichs, D.A. Haber, Dual Role for Argonautes in MicroRNA Processing and Posttranscriptional Regulation of MicroRNA Expression, *Cell*. 131 (2007) 1097–1108. https://doi.org/10.1016/j.cell.2007.10.032.

[75] D.F. Dluzen, Y. Kim, P. Bastian, Y. Zhang, E. Lehrmann, K.G. Becker, N. Noren Hooten, M.K. Evans, MicroRNAs Modulate Oxidative Stress in Hypertension through PARP-1 Regulation, *Oxid. Med. Cell. Longev.* 2017 (2017) 1–12. https://doi.org/10.1155/2017/3984280.

[76] M.R. Fabian, N. Sonenberg, The mechanics of miRNA-mediated gene silencing: a look under the hood of miRISC, *Nat. Struct. Mol. Biol.* 19 (2012) 586–593. https://doi.org/10.1038/nsmb.2296.

[77] B. Czech, G.J. Hannon, Small RNA sorting: matchmaking for Argonautes, *Nat. Rev. Genet.* 12 (2011) 19–31. https://doi.org/10.1038/nrg2916.

[78] E. Huntzinger, E. Izaurralde, Gene silencing by microRNAs: contributions of translational repression and mRNA decay, *Nat. Rev. Genet.* 12 (2011) 99–110. https://doi.org/10.1038/nrg2936.

[79] H.A. Meijer, Y.W. Kong, W.T. Lu, A. Wilczynska, R. V. Spriggs, S.W. Robinson, J.D. Godfrey, A.E. Willis, M. Bushell, Translational Repression and eIF4A2 Activity Are Critical for MicroRNA-Mediated Gene Regulation, *Science* 2013, 340 (6128) 82–85. https://doi.org/10.1126/science.1231197.

[80] D.S. Schwarz, G. Hutvágner, T. Du, Z. Xu, N. Aronin, P.D. Zamore, Asymmetry in the Assembly of the RNAi Enzyme Complex, *Cell.* 115 (2003) 199–208. https://doi.org/10.1016/S0092-8674(03)00759-1.

[81] S.M. Hammond, Dicing and slicing, *FEBS Lett.* 579 (2005) 5822–5829. https://doi.org/10.1016/j.febslet.2005.08.079.

[82] S. Djuranovic, A. Nahvi, R. Green, miRNA-Mediated Gene Silencing by Translational Repression Followed by mRNA Deadenylation and Decay, *Science* 2012, 336 (6078) 237–240. https://doi.org/10.1126/science.1215691.

[83] S.P. Jackson, J. Bartek, The DNA-damage response in human biology and disease, *Nature*. 461 (2009) 1071–1078. https://doi.org/10.1038/nature08467.

[84] A. Ciccia, S.J. Elledge, The DNA Damage Response: Making It Safe to Play with Knives, *Mol. Cell.* 40 (2010) 179–204. https://doi.org/10.1016/j.molcel.2010.09.019.

[85] J.W. Harper, S.J. Elledge, The DNA Damage Response: Ten Years After, *Mol. Cell.* 28 (2007) 739–745. https://doi.org/10.1016/j.molcel.2007.11.015.

[86] T. Lindahl, D.E. Barnes, Repair of Endogenous DNA Damage, *Cold Spring Harb. Symp. Quant. Biol.* 65 (2000) 127–134. https://doi.org/10.1101/sqb.2000.65.127.

[87] J. Jiricny, The multifaceted mismatch-repair system, *Nat. Rev. Mol. Cell Biol.* 7 (2006) 335–346. https://doi.org/10.1038/nrm1907.

[88] M.R. Lieber, The Mechanism of Human Nonhomologous DNA End Joining, *J. Biol. Chem.* 283 (2008) 1–5. https://doi.org/10.1074/jbc.R700039200.

[89] J.H.J. Hoeijmakers, DNA Damage, Aging, and Cancer, *N. Engl. J. Med.* 361 (2009) 1475–1485. https://doi.org/10.1056/NEJMra0804615.

[90] K.W. Caldecott, Single-strand break repair and genetic disease, *Nat. Rev. Genet.* 9 (2008) 619–631. https://doi.org/10.1038/nrg2380.

[91] A. Tessitore, G. Cicciarelli, F. Del Vecchio, A. Gaggiano, D. Verzella, M. Fischietti, D. Vecchiotti, D. Capece, F. Zazzeroni, E. Alesse, MicroRNAs in the DNA damage/repair network and cancer, *Int. J. Genomics.* 2014 (2014). https://doi.org/10.1155/2014/820248.

[92] C. Rinaldi, P. Pizzul, M.P. Longhese, D. Bonetti, Sensing R-Loop-Associated DNA Damage to Safeguard Genome Stability, *Front. Cell Dev. Biol.* 8 (2021). https://doi.org/10.3389/fcell.2020.618157.

[93] J. Bartek, J. Bartkova, J. Lukas, DNA damage signalling guards against activated oncogenes and tumour progression, *Oncogene*. 26 (2007) 7773–7779. https://doi.org/10.1038/sj.onc.1210881.

[94] R.D. Wood, M. Mitchell, J. Sgouros, T. Lindahl, Human DNA repair genes, *Science* 2001, 291(5507):1284-9. https://doi.org/10.1126/science.1056154.

[95] T.A. Knijnenburg, L. Wang, M.T. Zimmermann, *et al*. Genomic and Molecular Landscape of DNA Damage Repair Deficiency across The Cancer Genome Atlas, *Cell Rep.* 23 (2018) 239-254.e6. https://doi.org/10.1016/j.celrep.2018.03.076.

[96] A.T. Natarajan, F. Palitti, DNA repair and chromosomal alterations, *Mutat. Res. Toxicol. Environ. Mutagen.* 657 (2008) 3–7. https://doi.org/10.1016/j.mrgentox.2008.08.017.

[97] Y.-J. Kim, D. M. Wilson III, Overview of Base Excision Repair Biochemistry, *Curr. Mol. Pharmacol.* 5 (2012) 3–13. https://doi.org/10.2174/1874467211205010003.

[98] H.E. Krokan, H. Nilsen, F. Skorpen, M. Otterlei, G. Slupphaug, Base excision repair of DNA in mammalian cells, *FEBS Lett.* 476 (2000) 73–77. https://doi.org/10.1016/S0014-5793(00)01674-4.

[99] J. Šebera, Y. Hattori, D. Sato, D. Řeha, R. Nencka, T. Kohno, C. Kojima, Y. Tanaka, V. Sychrovský, The mechanism of the glycosylase reaction with hOGG1 base-excision repair enzyme: concerted effect of Lys249 and Asp268 during excision of 8-oxoguanine, *Nucleic Acids Res.* 45 (2017) 5231–5242. https://doi.org/10.1093/nar/gkx157.

[100] Y. Liu, X. Lu, Non-coding RNAs in DNA damage response., *Am. J. Cancer Res.* 2 (2012) 658–75. http://www.ncbi.nlm.nih.gov/pubmed/23226613.

[101] H. Hu, R.A. Gatti, MicroRNAs: new players in the DNA damage response, *J. Mol. Cell Biol.* 3 (2011) 151–158. https://doi.org/10.1093/jmcb/mjq042.

[102] L. He, X. He, L.P. Lim, E. de Stanchina, Z. Xuan, Y. Liang, W. Xue, L. Zender, J. Magnus, D. Ridzon, A.L. Jackson, P.S. Linsley, C. Chen, S.W. Lowe, M.A. Cleary, G.J. Hannon, A microRNA component of the p53 tumour suppressor network, *Nature.* 447 (2007) 1130–1134. https://doi.org/10.1038/nature05939.

[103] C. Metheetrairut, F.J. Slack, MicroRNAs in the ionizing radiation response and in radiotherapy, *Curr. Opin. Genet. Dev.* 23 (2013) 12–19. https://doi.org/10.1016/j.gde.2013.01.002.

[104] M. Magistri, M.A. Faghihi, G. St Laurent, C. Wahlestedt, Regulation of chromatin structure by long noncoding RNAs: focus on natural antisense transcripts, *Trends Genet.* 28 (2012) 389–396. https://doi.org/10.1016/j.tig.2012.03.013.

[105] J. Pothof, N.S. Verkaik, W. van IJcken, E.A.C. Wiemer, V.T.B. Ta, G.T.J. van der Horst, N.G.J. Jaspers, D.C. van Gent, J.H.J. Hoeijmakers, S.P. Persengiev, MicroRNA-mediated gene silencing modulates the UV-induced DNA-damage response, *EMBO J.* 28 (2009) 2090–2099. https://doi.org/10.1038/emboj.2009.156.

[106] H. Hu, L. Du, G. Nagabayashi, R.C. Seeger, R.A. Gatti, ATM is down-regulated by N-Myc-regulated microRNA-421, *Proc. Natl. Acad. Sci.* 107 (2010) 1506–1511. https://doi.org/10.1073/pnas.0907763107.

[107] Y. Wang, Y. Yu, A. Tsuyada, X. Ren, X. Wu, K. Stubblefield, E.K. Rankin-Gee, S.E. Wang, Transforming growth factor-β regulates the sphere-initiating stem cell-like feature in breast cancer through miRNA-181 and ATM, *Oncogene.* 30 (2011) 1470–1480. https://doi.org/10.1038/onc.2010.531.

[108] P. Moskwa, F.M. Buffa, Y. Pan, R. Panchakshari, P. Gottipati, R.J. Muschel, J. Beech, R. Kulshrestha, K. Abdelmohsen, D.M. Weinstock, M. Gorospe, A.L. Harris, T. Helleday, D. Chowdhury, MiR-182-Mediated Downregulation of BRCA1 Impacts DNA Repair and Sensitivity to PARP Inhibitors, *Mol. Cell.* 41 (2011) 210–220. https://doi.org/10.1016/j.molcel.2010.12.005.

[109] T. Papagiannakopoulos, A. Shapiro, K.S. Kosik, MicroRNA-21 Targets a Network of Key Tumor-Suppressive Pathways in Glioblastoma Cells, *Cancer Res.* 68 (2008) 8164–8172. https://doi.org/10.1158/0008-5472.CAN-08-1305.

[110] Y.E. Choi, Y. Pan, E. Park, P. Konstantinopoulos, S. De, A. D'Andrea, D. Chowdhury, MicroRNAs down-regulate homologous recombination in the G1 phase of cycling cells to maintain genomic stability, *Elife.* 3 (2014). https://doi.org/10.7554/eLife.02445.

[111] A. Lal, Y. Pan, F. Navarro, D.M. Dykxhoorn, L. Moreau, E. Meire, Z. Bentwich, J. Lieberman, D. Chowdhury, miR-24–mediated downregulation of H2AX suppresses DNA repair in terminally differentiated blood cells, *Nat. Struct. Mol. Biol.* 16 (2009) 492–498. https://doi.org/10.1038/nsmb.1589.

[112] J.H. Chang, Y.H. Hwang, D.J. Lee, D.H. Kim, J.M. Park, H.-G. Wu, I.A. Kim, MicroRNA-203 Modulates the Radiation Sensitivity of Human Malignant Glioma Cells, *Int. J. Radiat. Oncol.* 94 (2016) 412–420. https://doi.org/10.1016/j.ijrobp.2015.10.001.

[113] C. Romilda, P. Marika, S. Alessandro, L. Enrico, B. Marina, K. Andromachi, C. Umberto, Z. Giacomo, M. Claudia, R. Massimo, F. Fabio, Oxidative DNA damage correlates with cell immortalization and mir-92 expression in hepatocellular carcinoma, *BMC Cancer.* 12 (2012) 177. https://doi.org/10.1186/1471-2407-12-177.

[114] Y.-B. Ouyang, L. Xu, S. Yue, S. Liu, R.G. Giffard, Neuroprotection by astrocytes in brain ischemia: Importance of microRNAs, *Neurosci. Lett.* 565 (2014) 53–58. https://doi.org/10.1016/j.neulet.2013.11.015.

[115] C. Piotto, A. Biscontin, C. Millino, M. Mognato, Functional validation of miRNAs targeting genes of DNA double-strand break repair to radiosensitize non-small lung cancer cells, *Biochim. Biophys. Acta - Gene Regul. Mech.* 1861 (2018) 1102–1118. https://doi.org/10.1016/j.bbagrm.2018.10.010.

[116] M. Szatkowska, R. Krupa, Regulation of DNA Damage Response and Homologous Recombination Repair by microRNA in Human Cells Exposed to Ionizing Radiation, *Cancers* (Basel). 12 (2020) 1838. https://doi.org/10.3390/cancers12071838.

[117] K.C. Miranda, T. Huynh, Y. Tay, Y.-S. Ang, W.-L. Tam, A.M. Thomson, B. Lim, I. Rigoutsos, A Pattern-Based Method for the Identification of MicroRNA Binding Sites and Their Corresponding Heteroduplexes, *Cell*. 126 (2006) 1203–1217. https://doi.org/10.1016/j.cell.2006.07.031.

[118] D. Chowdhury, Y.E. Choi, M.E. Brault, Charity begins at home: non-coding RNA functions in DNA repair, *Nat. Rev. Mol. Cell Biol.* 14 (2013) 181–189. https://doi.org/10.1038/nrm3523.

[119] R.S. Pillai, S.N. Bhattacharyya, W. Filipowicz, Repression of protein synthesis by miRNAs: how many mechanisms?, *Trends Cell Biol.* 17 (2007) 118–126. https://doi.org/10.1016/j.tcb.2006.12.007.

[120] T. Du, P.D. Zamore, Beginning to understand microRNA function, *Cell Res.* 17 (2007) 661–663. https://doi.org/10.1038/cr.2007.67.

[121] D. Didiano, O. Hobert, Perfect seed pairing is not a generally reliable predictor for miRNA-target interactions, *Nat. Struct. Mol. Biol.* 13 (2006) 849–851. https://doi.org/10.1038/nsmb1138.

[122] D.E. Kuhn, M.M. Martin, D.S. Feldman, A. V. Terry, G.J. Nuovo, T.S. Elton, Experimental validation of miRNA targets, *Methods.* 44 (2008) 47–54. https://doi.org/10.1016/j.ymeth.2007.09.005.

[123] M.M. Martin, E.J. Lee, J.A. Buckenberger, T.D. Schmittgen, T.S. Elton, MicroRNA-155 Regulates Human Angiotensin II Type 1 Receptor Expression in Fibroblasts, *J. Biol. Chem.* 281 (2006) 18277–18284. https://doi.org/10.1074/jbc.M601496200.

[124] C. Choi, J. HAN, N.T. THAO TRAN, S. YOON, G. KIM, S. SONG, Y. KIM, S. RYU, Effective experimental validation of miRNA targets using an improved linker reporter assay, *Genet. Res.* (Camb). 99 (2017) e2. https://doi.org/10.1017/S001667231600015X.

[125] M. Beitzinger, L. Peters, J.Y. Zhu, E. Kremmer, G. Meister, Identification of Human microRNA Targets From Isolated Argonaute Protein Complexes, *RNA Biol.* 4 (2007) 76–84. https://doi.org/10.4161/rna.4.2.4640.

[126] G.J. Nuovo, In situ PCR: protocols and applications. *Genome Res.* 4 (1995) S151–S167. https://doi.org/10.1101/gr.4.4.S151.

[127] A. Valoczi, Sensitive and specific detection of microRNAs by northern blot analysis using LNA-modified oligonucleotide probes, *Nucleic Acids Res*. 32 (2004) e175–e175. https://doi.org/10.1093/nar/gnh171.

[128] M. da C.G. Leitão, E.C. Coimbra, R. de C.P. de Lima, M. de L. Guimarães, S. de A. Heráclio, J. da C. Silva Neto, A.C. de Freitas, Quantifying mRNA and MicroRNA with qPCR in Cervical Carcinogenesis: A Validation of Reference Genes to Ensure Accurate Data, *PLoS One*. 9 (2014) e111021. https://doi.org/10.1371/journal.pone.0111021.

[129] Y. Zhao, J.F. Ransom, A. Li, V. Vedantham, M. von Drehle, A.N. Muth, T. Tsuchihashi, M.T. McManus, R.J. Schwartz, D. Srivastava, Dysregulation of Cardiogenesis, Cardiac Conduction, and Cell Cycle in Mice Lacking miRNA-1-2, *Cell.* 129 (2007) 303–317. https://doi.org/10.1016/j.cell.2007.03.030.

[130] M.J. Walsh, J. Cooper-Knock, J.E. Dodd, M.J. Stopford, S.R. Mihaylov, J. Kirby, P.J. Shaw, G.M. Hautbergue, Invited Review: Decoding the pathophysiological mechanisms that underlie RNA dysregulation in neurodegenerative disorders: a review of the current state of the art, *Neuropathol. Appl. Neurobiol.* 41 (2015) 109–134. https://doi.org/10.1111/nan.12187.

[131] M.N. Poy, L. Eliasson, J. Krutzfeldt, S. Kuwajima, X. Ma, P.E. MacDonald, S. Pfeffer, T. Tuschl, N. Rajewsky, P. Rorsman, M. Stoffel, A pancreatic islet-specific microRNA regulates insulin secretion, *Nature.* 432 (2004) 226–230. https://doi.org/10.1038/nature03076.

[132] J.-F. Chen, E.M. Mandel, J.M. Thomson, Q. Wu, T.E. Callis, S.M. Hammond, F.L. Conlon, D.-Z. Wang, The role of microRNA-1 and microRNA-133 in skeletal muscle proliferation and differentiation, *Nat. Genet.* 38 (2006) 228–233. https://doi.org/10.1038/ng1725.

[133] G.M. Schratt, F. Tuebing, E.A. Nigh, C.G. Kane, M.E. Sabatini, M. Kiebler, M.E. Greenberg, A brain-specific microRNA regulates dendritic spine development, *Nature.* 439 (2006) 283–289. https://doi.org/10.1038/nature04367.

[134] V. Ambros, The functions of animal microRNAs, *Nature.* 431 (2004) 350–355. https://doi.org/10.1038/nature02871.

[135] H.-W. Hwang, J.T. Mendell, MicroRNAs in cell proliferation, cell death, and tumorigenesis, *Br. J. Cancer.* 94 (2006) 776–780. https://doi.org/10.1038/sj.bjc.6603023.

[136] E. Wienholds, R.H.A. Plasterk, MicroRNA function in animal development, *FEBS Lett.* 579 (2005) 5911–5922. https://doi.org/10.1016/j.febslet.2005.07.070.

[137] K. Jakubczyk, K. Dec, J. Kałduńska, D. Kawczuga, J. Kochman, K. Janda, Reactive oxygen species - sources, functions, oxidative damage., *Pol. Merkur. Lekarski.* 48 (2020) 124–127. http://www.ncbi.nlm.nih.gov/pubmed/32352946.

[138] C.Y. Guo, L. Sun, X.P. Chen, D.S. Zhang, Oxidative stress, mitochondrial damage and neurodegenerative diseases, *Neural Regen. Res.* 8 (2013) 2003–2014. https://doi.org/10.3969/j.issn.1673-5374.2013.21.009.

[139] R.A. Perlow-Poehnelt, D.O. Zharkov, A.P. Grollman, S. Broyde, Substrate Discrimination by Formamidopyrimidine-DNA Glycosylase: Distinguishing Interactions within the Active Site †, *Biochemistry*. 43 (2004) 16092–16105. https://doi.org/10.1021/bi048747f.

[140] M.S. Cooke, M.D. Evans, M. Dizdaroglu, J. Lunec, Oxidative DNA damage: mechanisms, mutation, and disease, *FASEB J.* 17 (2003) 1195–1214. https://doi.org/10.1096/fj.02-0752rev.

[141] A. Valavanidis, T. Vlachogianni, C. Fiotakis. 8-hydroxy-2′ -deoxyguanosine (8-OHdG): A Critical Biomarker of Oxidative Stress and Carcinogenesis, *J. Environ. Sci. Heal.* Part C. 27 (2009) 120–139. https://doi.org/10.1080/10590500902885684.

[142] H. Kasai, Analysis of a form of oxidative DNA damage, 8-hydroxy-2′-deoxyguanosine, as a marker of cellular oxidative stress during carcinogenesis, *Mutat. Res. Mutat. Res.* 387 (1997) 147–163. https://doi.org/10.1016/S1383-5742(97)00035-5.

[143] S. Sentürker, B. Karahalil, M. Inal, H. Yilmaz, Hamza Müslümanoglu, G. Gedikoglu, M. Dizdaroglu, Oxidative DNA base damage and antioxidant enzyme levels in childhood acute lymphoblastic leukemia, *FEBS Lett.* 416 (1997) 286–290. https://doi.org/10.1016/S0014-5793(97)01226-X.

[144] D.C. Malins, R. Haimanot, Major alterations in the nucleotide structure of DNA in cancer of the female breast., *Cancer Res.* 51 (1991) 5430–2. http://www.ncbi.nlm.nih.gov/pubmed/1655250.

[145] M.R. Oliva, F. Ripoll, P. Muñiz, A. Iradi, R. Trullenque, V. Valls, E. Drehmer, G.T. Sáez, Genetic alterations and oxidative metabolism in sporadic colorectal tumors from a Spanish community, *Mol. Carcinog.* 18 (1997) 232–243. https://doi.org/10.1002/(SICI)1098-2744(199704)18:4<232::AID-MC7>3.0.CO;2-F.

[146] S. V. Vulimiri, X. Wu, W. Baer-Dubowska, M. de Andrade, M. Detry, M.R. Spitz, J. DiGiovanni, Analysis of aromatic DNA adducts and 7,8-dihydro-8-oxo- 2′-deoxyguanosine in lymphocyte DNA from a case–control study of lung cancer involving minority populations, *Mol. Carcinog.* 27 (2000) 34. https://doi.org/10.1002/(SICI)1098-2744(200001)27:1<34::AID-MC6>3.3.CO;2-7.

[147] J. Zhang, G. Perry, M.A. Smith, D. Robertson, S.J. Olson, D.G. Graham, T.J. Montine, Parkinson's Disease Is Associated with Oxidative Damage to Cytoplasmic DNA and RNA in Substantia Nigra Neurons, *Am. J. Pathol.* 154 (1999) 1423–1429. https://doi.org/10.1016/S0002-9440(10)65396-5.

[148] A.M.S. Lezza, P. Mecocci, A. Cormio, M.F. Beal, A. Cherubini, P. Cantatore, U. Senin, M.N. Gadaleta, Area-Specific Differences in OH8dG and mtDNA4977 Levels in Alzheimer Disease Patients and Aged Controls, *J. Anti. Aging. Med.* 2 (1999) 209–216. https://doi.org/10.1089/rej.1.1999.2.209.

[149] D. Thomas, A.D. Scot, R. Barbey, M. Padula, S. Boiteux, Inactivation of OGG1 increases the incidence of G · C→T · A transversions in Saccharomyces cerevisiae : evidence for endogenous oxidative damage to DNA in eukaryotic cells, *Mol. Gen. Genet.* 254 (1997) 171–178. https://doi.org/10.1007/s004380050405.

[150] A.J. Lee, Interindividual Variability in Response to Sodium Dichromate-Induced Oxidative DNA Damage: Role of the Ser326Cys Polymorphism in the DNA-Repair Protein of 8-Oxo-7,8-Dihydro-2'-Deoxyguanosine DNA Glycosylase 1, *Cancer Epidemiol. Biomarkers Prev.* 14 (2005) 497–505. https://doi.org/10.1158/1055-9965.EPI-04-0295.

[151] A. Magenta, C. Cencioni, P. Fasanaro, G. Zaccagnini, S. Greco, G. Sarra-Ferraris, A. Antonini, F. Martelli, M.C. Capogrossi, miR-200c is upregulated by oxidative stress and induces endothelial cell apoptosis and senescence via ZEB1 inhibition, *Cell Death Differ.* 18 (2011) 1628–1639. https://doi.org/10.1038/cdd.2011.42.

[152] V.A. Bohr, O.P. Ottersen, T. Tønjum, Genome instability and DNA repair in brain, ageing and neurological disease, *Neuroscience.* 145 (2007) 1183–1186. https://doi.org/10.1016/j.neuroscience.2007.03.015.

[153] C. Lu, D. Zhou, Q. Wang, W. Liu, F. Yu, F. Wu, C. Chen, Crosstalk of MicroRNAs and Oxidative Stress in the Pathogenesis of Cancer, *Oxid. Med. Cell. Longev.* 2020 (2020) 1–13. https://doi.org/10.1155/2020/2415324.

[154] N. Soudani, A. Troudi, I. Ben Amara, H. Bouaziz, T. Boudawara, N. Zeghal, Ameliorating effect of selenium on chromium (VI)-induced oxidative damage in the brain of adult rats, *J. Physiol. Biochem.* 68 (2012) 397–409. https://doi.org/10.1007/s13105-012-0152-4.

[155] R. Lewis, Occupational Exposures: Metals. In: Current Occupational & Environmental Medicine, 3rd Ed., Lange Medical Books/McGraw-Hill Companies, Inc., 2004.

[156] M.M. Aruldhas, S. Subramanian, P. Sekar, G. Vengatesh, G. Chandrahasan, P. Govindarajulu, M.A. Akbarsha, Chronic chromium exposure-induced changes in testicular histoarchitecture are associated with oxidative stress: study in a non-human primate (*Macaca radiata* Geoffroy), *Hum. Reprod.* 20 (2005) 2801–2813. https://doi.org/10.1093/humrep/dei148.

[157] D. Bagchi, J. Balmoori, M. Bagchi, X. Ye, C.B. Williams, S.J. Stohs, Comparative effects of TCDD, endrin, naphthalene and chromium (VI) on oxidative stress and tissue damage in the liver and brain tissues of mice, *Toxicology.* 175 (2002) 73–82. https://doi.org/10.1016/S0300-483X(02)00062-8.

[158] US Environmental Protection Agencey (EPA), Toxicological Review of Trivalent Chromium. CAS No. 16065-83-1. In support of Summary Information on the Integrated Risk Information System (IRIS). U.S. Environmental Protection Agency, Washington, D.C., (1998). https://doi.org/https://iris.epa.gov/static/pdfs/0028tr.pdf.

[159] Agency for Toxic Substances and Disease Registry (ATSDR). Toxicological profile for Chromium CAS#: 7440-47-3. Atlanta, GA: U.S. Department of Health and Human Services, Public Health Service., (2020). https://doi.org/http://www.atsdr.cdc.gov/toxprofiles/tp.asp?id=62&tid=17.

[160] J.A. Fagliano, J. Savrin, I. Udasin, M. Gochfeld, Community Exposure and Medical Screening near Chromium Waste Sites in New Jersey, *Regul. Toxicol. Pharmacol*. 26 (1997) S13–S22. https://doi.org/10.1006/rtph.1997.1134.

[161] T. Becquer, C. Quantin, M. Sicot, J.. Boudot, Chromium availability in ultramafic soils from New Caledonia, *Sci. Total Environ.* 301 (2003) 251–261. https://doi.org/10.1016/S0048-9697(02)00298-X.

[162] World Health Organization (WHO), "Chromium (Environmental Health Criteria 61) International Programme on Chemical Safety". Geneva, Switzerlands, (1990).

[163] Z.H. Stern, A. H., Yu, C. H., Black, K., Lin, L., Lioy, P. J., Gochfeld, M., & Fan, Hexavalent chromium in house dust--a comparison between an area with historic contamination from chromate production and background locations, *Sci. Total Environ.* 408 (2010) 4993–4998. https://doi.org/https://doi.org/10.1016/j.scitotenv.2010.07.035.s.

[164] N. Papassiopi, A. Kontoyianni, K. Vaxevanidou, A. Xenidis, Assessment of chromium biostabilization in contaminated soils using standard leaching and sequential extraction techniques, *Sci. Total Environ.* 407 (2009) 925–936. https://doi.org/10.1016/j.scitotenv.2008.09.020.

[165] S.S. Wise, A.L. Holmes, J.P. Wise, Sr., Hexavalent Chromium-Induced DNA Damage and Repair Mechanisms, *Rev. Environ. Health.* 23 (2008). https://doi.org/10.1515/REVEH.2008.23.1.39.

[166] H.E. Bryant, S. Ying, T. Helleday, Homologous recombination is involved in repair of chromium-induced DNA damage in mammalian cells, *Mutat. Res. Mol. Mech. Mutagen.* 599 (2006) 116–123. https://doi.org/10.1016/j.mrfmmm.2006.02.001.

[167] J. Messer, M. Reynolds, L. Stoddard, A. Zhitkovich, Causes of DNA single-strand breaks during reduction of chromate by glutathione in vitro and in cells, *Free Radic. Biol. Med.* 40 (2006) 1981–1992. https://doi.org/10.1016/j.freeradbiomed.2006.01.028.

[168] G. Quievryn, M. Goulart, J. Messer, A. Zhitkovich, Reduction of Cr(VI) by cysteine: Significance in human lymphocytes and formation of DNA damage in reactions with variable reduction rates, *Mol. Cell. Biochem*. 2001 2221. 222 (2001) 107–118. https://doi.org/10.1023/A:1017923609175.

[169] T.J. O'Brien, B.R. Brooks, S.R. Patierno, Nucleotide excision repair functions in the removal of chromium-induced DNA damage in mammalian cells, *Mol. Cell. Biochem.* 279 (2005) 85–95. https://doi.org/10.1007/s11010-005-8225-0.

[170] S.R. Ha, L., Ceryak, S., & Patierno, Generation of S phase-dependent DNA double-strand breaks by Cr(VI) exposure: involvement of ATM in Cr(VI) induction of -H2AX, *Carcinogenesis.* 25 (2004) 2265–2274. https://doi.org/10.1093/carcin/bgh242.

[171] M. Valko, H. Morris, M. Cronin, Metals, Toxicity and Oxidative Stress, *Curr. Med. Chem.* 12 (2005) 1161–1208. https://doi.org/10.2174/0929867053764635.

[172] Z. Fang, M. Zhao, H. Zhen, L. Chen, P. Shi, Z. Huang, Genotoxicity of Tri- and Hexavalent Chromium Compounds In Vivo and Their Modes of Action on DNA Damage In Vitro, *PLoS One.* 9 (2014) e103194. https://doi.org/10.1371/journal.pone.0103194.

[173] G. Anger, J. Halstenberg, K. Hochgeschwender, C. Scherhag, U. Korallus, H. Knopf, P. Schmidt, M. Ohlinger, Chromium Compounds, in: *Ullmann's Encycl. Ind. Chem*., Wiley-VCH Verlag GmbH & Co. KGaA, Weinheim, Germany, 2000. https://doi.org/10.1002/14356007.a07_067.

[174] F. Freeman, Encyclopedia of Reagents for Organic Synthesis, J. Wiley & Sons, New York, 2004. https://doi.org/10.1002/047084289X.

[175] V. Balachandar, M. Arun, S. Mohana Devi, P. Velmurugan, P. Manikantan, A. Karthick Kumar, K. Sasikala, C. Venkatesan, Evaluation of the genetic alterations in direct and indirect exposures of hexavalent chromium [Cr(VI)] in leather tanning industry workers North Arcot District, South India, *Int. Arch. Occup. Environ. Health.* 83 (2010) 791–801. https://doi.org/10.1007/s00420-010-0562-y.

[176] International Agency for Research on Cancer (IARC), Chromium, nickel and welding., *IARC Monogr. Eval. Carcinog. Risks to Humans*. 49 (1990) 1–648. http://www.ncbi.nlm.nih.gov/pubmed/2232124.

[177] A.J. Lee, N.J. Hodges, J.K. Chipman, Modified comet assay as a biomarker of sodium dichromate-induced oxidative DNA damage: Optimization and reproducibility, *Biomarkers.* 9 (2004) 103–115. https://doi.org/10.1080/13547500410001704891.

[178] J.K. Hodges, N.J. and Chipman, Down-regulation of the DNA-repair endonuclease 8-oxo-guanine DNA glycosylase 1 (hOGG1) by sodium dichromate in cultured human A549 lung carcinoma cells, *Carcinogenesis.* 23 (2002) 55–60. https://doi.org/10.1093/carcin/23.1.55.

[179] M. Goulart, M.C. Batoréu, A.S. Rodrigues, A. Laires, J. Rueff, Lipoperoxidation products and thiol antioxidants in chromium exposed workers, *Mutagenesis*. 20 (2005) 311–315. https://doi.org/10.1093/mutage/gei043.

[180] K.E.. Iztleuov E.M, Iztleuov M.K, Prenatal effects of potassium dichromate and their correction in the offspring of rats Medicine and Public Health: materials of the IV International Scientific Conference (Kazan, May M422016), *Kazan Young Sci*. (2016) 23–26.

[181] A. Campbell, The role of aluminum and copper on neuroinflammation and Alzheimer's disease, *J. Alzheimer's Dis.* 10 (2006) 165–172. https://doi.org/10.3233/JAD-2006-102-304.

[182] D.K.B. Egemberdieva R.E, Kismanova G.N, Dosmambetova S.K, Microelement composition and morphological characteristics of the brain of rats when exposed to chemical compounds. Questions of morphology and clinic, *Almaty.* 12 (2004) 412–424.

[183] M. Travacio, J. María Polo, S. Llesuy, Chromium(VI) induces oxidative stress in the mouse brain, *Toxicology.* 150 (2000) 137–146. https://doi.org/10.1016/S0300-483X(00)00254-7.

[184] S. Rezapoor, A. Shirazi, S. Abbasi, J. Bazzaz, P. Izadi, H. Rezaeejam, M. Valizadeh, F. Soleimani-Mohammadi, M. Najafi, Modulation of radiation-induced base excision repair pathway gene expression by melatonin, *J. Med. Phys.* 42 (2017) 245. https://doi.org/10.4103/jmp.JMP_9_17.

[185] E.I. Azzam, J.-P. Jay-Gerin, D. Pain, Ionizing radiation-induced metabolic oxidative stress and prolonged cell injury, *Cancer Lett.* 327 (2012) 48–60. https://doi.org/10.1016/j.canlet.2011.12.012.

[186] W.W.-Y. Kam, R.B. Banati, Effects of ionizing radiation on mitochondria., *Free Radic. Biol. Med.* 65 (2013) 607–619. https://doi.org/10.1016/j.freeradbiomed.2013.07.024.

[187] S. Xu, Z. Zhou, L. Zhang, Z. Yu, W. Zhang, Y. Wang, X. Wang, M. Li, Y. Chen, C. Chen, M. He, G. Zhang, M. Zhong, Exposure to 1800 MHz radiofrequency radiation induces oxidative damage to mitochondrial DNA in primary cultured neurons, *Brain Res.* 1311 (2010) 189–196. https://doi.org/10.1016/j.brainres.2009.10.062.

[188] F.M. Yakes, B. Van Houten, Mitochondrial DNA damage is more extensive and persists longer than nuclear DNA damage in human cells following oxidative stress, *Proc. Natl. Acad. Sci.* 94 (1997) 514–519. https://doi.org/10.1073/pnas.94.2.514.

[189] R. Mohan, D. Grosshans, Proton therapy – Present and future, *Adv. Drug Deliv. Rev.* 109 (2017) 26–44. https://doi.org/10.1016/j.addr.2016.11.006.

[190] B.A. Greenberger, M.B. Pulsifer, D.H. Ebb, S.M. MacDonald, R.M. Jones, W.E. Butler, M.S. Huang, K.J. Marcus, J.A. Oberg, N.J. Tarbell, T.I. Yock, Clinical Outcomes and Late Endocrine, Neurocognitive, and Visual Profiles of Proton Radiation for Pediatric Low-Grade Gliomas, *Int. J. Radiat. Oncol.* 89 (2014) 1060–1068. https://doi.org/10.1016/j.ijrobp.2014.04.053.

[191] J. Jhaveri, E. Cheng, S. Tian, Z. Buchwald, M. Chowdhary, Y. Liu, T.W. Gillespie, J.J. Olson, A.Z. Diaz, A. Voloschin, B.R. Eaton, I.R. Crocker, M.W. McDonald, W.J. Curran, K.R. Patel, Proton vs. Photon Radiation Therapy for Primary Gliomas: An Analysis of the National Cancer Data Base, *Front. Oncol.* 8 (2018). https://doi.org/10.3389/fonc.2018.00440.

[192] L. Gong, J. Gu, J. Ge, X. Wu, C. Zhang, C. Yang, W. Weng, G. Gao, J. Feng, Q. Mao, Differential radiation response between normal astrocytes and glioma cells revealed by comparative transcriptome analysis, *Onco. Targets. Ther.* Volume 10 (2017) 5755–5764. https://doi.org/10.2147/OTT.S144002.

[193] Y. Tamari, G. Kashino, H. Mori, Acquisition of radioresistance by IL-6 treatment is caused by suppression of oxidative stress derived from mitochondria after γ-irradiation, *J. Radiat. Res.* 58 (2017) 412–420. https://doi.org/10.1093/jrr/rrw084.

[194] J. Rzeszowska-Wolny, W.M. Przybyszewski, M. Widel, Ionizing radiation-induced bystander effects, potential targets for modulation of radiotherapy, *Eur. J. Pharmacol.* 625 (2009) 156–164. https://doi.org/10.1016/j.ejphar.2009.07.028.

[195] G. Minniti, D. Traish, S. Ashley, A. Gonsalves, M. Brada, Risk of Second Brain Tumor after Conservative Surgery and Radiotherapy for Pituitary Adenoma: Update after an Additional 10 Years, *J. Clin. Endocrinol. Metab.* 90 (2005) 800–804. https://doi.org/10.1210/jc.2004-1152.

[196] H. Balloni, Role of Radiotherapy in High Grade Glioma, in: Prim. Intracranial Tumors, *IntechOpen*, 2019. https://doi.org/10.5772/intechopen.80923.

[197] C. Lawson, J.M. Vicencio, D.M. Yellon, S.M. Davidson, Microvesicles and exosomes: new players in metabolic and cardiovascular disease, *J. Endocrinol.* 228 (2016) R57–R71. https://doi.org/10.1530/JOE-15-0201.

[198] Y. Jia, Z. Ni, H. Sun, C. Wang, Microfluidic Approaches Toward the Isolation and Detection of Exosome Nanovesicles, *IEEE Access.* 7 (2019) 45080–45098. https://doi.org/10.1109/ACCESS.2019.2907123.

[199] J.K. Jaiswal, N.W. Andrews, S.M. Simon, Membrane proximal lysosomes are the major vesicles responsible for calcium-dependent exocytosis in nonsecretory cells, *J. Cell Biol.* 159 (2002) 625–635. https://doi.org/10.1083/jcb.200208154.

[200] L.F. Bátiz, M.A. Castro, P. V. Burgos, Z.D. Velásquez, R.I. Muñoz, C.A. Lafourcade, P. Troncoso-Escudero, U. Wyneken, Exosomes as Novel Regulators of Adult Neurogenic Niches, *Front. Cell. Neurosci.* 9 (2016). https://doi.org/10.3389/fncel.2015.00501.

[201] D. Fitzner, M. Schnaars, D. van Rossum, G. Krishnamoorthy, P. Dibaj, M. Bakhti, T. Regen, U.-K. Hanisch, M. Simons, Selective transfer of exosomes from oligodendrocytes to microglia by macropinocytosis, *J. Cell Sci.* 124 (2011) 447–458. https://doi.org/10.1242/jcs.074088.

[202] J.C. Contreras-Naranjo, H.-J. Wu, V.M. Ugaz, Microfluidics for exosome isolation and analysis: enabling liquid biopsy for personalized medicine, *Lab Chip*. 17 (2017) 3558–3577. https://doi.org/10.1039/C7LC00592J.

[203] S.-C. Guo, S.-C. Tao, H. Dawn, Microfluidics-based on-a-chip systems for isolating and analysing extracellular vesicles, *J. Extracell. Vesicles.* 7 (2018) 1508271. https://doi.org/10.1080/20013078.2018.1508271.

[204] M.C. Deregibus, V. Cantaluppi, R. Calogero, M. Lo Iacono, C. Tetta, L. Biancone, S. Bruno, B. Bussolati, G. Camussi, Endothelial progenitor cell–derived microvesicles activate an angiogenic program in endothelial cells by a horizontal transfer of mRNA, *Blood*. 110 (2007) 2440–2448. https://doi.org/10.1182/blood-2007-03-078709.

[205] M.N. Madison, R.J. Roller, C.M. Okeoma, Human semen contains exosomes with potent anti-HIV-1 activity, *Retrovirology*. 11 (2014) 102. https://doi.org/10.1186/s12977-014-0102-z.

[206] T.F. Hiemstra, P.D. Charles, T. Gracia, S.S. Hester, L. Gatto, R. Al-Lamki, R.A. Floto, Y. Su, J.N. Skepper, K.S. Lilley, F.E. Karet Frankl, Human Urinary Exosomes as Innate Immune Effectors, *J. Am. Soc. Nephrol.* 25 (2014) 2017–2027. https://doi.org/10.1681/ASN.2013101066.

[207] A. Michael, S. Bajracharya, P. Yuen, H. Zhou, R. Star, G. Illei, I. Alevizos, Exosomes from human saliva as a source of microRNA biomarkers, *Oral Dis.* 16 (2010) 34–38. https://doi.org/10.1111/j.1601-0825.2009.01604.x.

[208] J.M. Street, P.E. Barran, C.L. Mackay, S. Weidt, C. Balmforth, T.S. Walsh, R.T. Chalmers, D.J. Webb, J.W. Dear, Identification and proteomic profiling of exosomes in human cerebrospinal fluid, *J. Transl. Med.* 10 (2012) 5. https://doi.org/10.1186/1479-5876-10-5.

[209] S. Keerthikumar, D. Chisanga, D. Ariyaratne, H. Al Saffar, S. Anand, K. Zhao, M. Samuel, M. Pathan, M. Jois, N. Chilamkurti, L. Gangoda, S. Mathivanan, ExoCarta: A Web-Based Compendium of Exosomal Cargo, *J. Mol. Biol*. 428 (2016) 688–692. https://doi.org/10.1016/j.jmb.2015.09.019.

[210] M. Pathan, P. Fonseka, S. V Chitti, T. Kang, R. Sanwlani, J. Van Deun, A. Hendrix, S. Mathivanan, Vesiclepedia 2019: a compendium of RNA, proteins, lipids and metabolites in extracellular vesicles, *Nucleic Acids Res.* 47 (2019) D516–D519. https://doi.org/10.1093/nar/gky1029.

[211] R.J. Lobb, M. Becker, S. Wen Wen, C.S.F. Wong, A.P. Wiegmans, A. Leimgruber, A. Möller, Optimized exosome isolation protocol for cell culture supernatant and human plasma, *J. Extracell. Vesicles.* 4 (2015) 27031. https://doi.org/10.3402/jev.v4.27031.

[212] M. Logozzi, A. De Milito, L. Lugini, M. Borghi, L. Calabrò, M. Spada, M. Perdicchio, M.L. Marino, C. Federici, E. Iessi, D. Brambilla, G. Venturi, F. Lozupone, M. Santinami, V. Huber, M. Maio, L. Rivoltini, S. Fais, High Levels of Exosomes Expressing CD63 and Caveolin-1 in Plasma of Melanoma Patients, *PLoS One*. 4 (2009) e5219. https://doi.org/10.1371/journal.pone.0005219.

[213] S.J. Gould, A.M. Booth, J.E.K. Hildreth, The Trojan exosome hypothesis, *Proc. Natl. Acad. Sci.* 100 (2003) 10592–10597. https://doi.org/10.1073/pnas.1831413100.

[214] T. Templin, S.A. Amundson, D.J. Brenner, L.B. Smilenov, Whole mouse blood microRNA as biomarkers for exposure to ?-rays and 56 Fe ions, *Int. J. Radiat. Biol*. 87 (2011) 653–662. https://doi.org/10.3109/09553002.2010.549537.

[215] R. Sullivan, F. Saez, J. Girouard, G. Frenette, Role of exosomes in sperm maturation during the transit along the male reproductive tract, *Blood Cells, Mol. Dis.* 35 (2005) 1–10. https://doi.org/10.1016/j.bcmd.2005.03.005.

[216] U. Gehrmann, T.I. Näslund, S. Hiltbrunner, P. Larssen, S. Gabrielsson, Harnessing the exosome-induced immune response for cancer immunotherapy, *Semin. Cancer Biol.* 28 (2014) 58–67. https://doi.org/10.1016/j.semcancer.2014.05.003.

[217] C. Guay, R. Regazzi, Exosomes as new players in metabolic organ cross-talk, *Diabetes, Obes. Metab.* 19 (2017) 137–146. https://doi.org/10.1111/dom.13027.

[218] E. Levy, Exosomes in the Diseased Brain: First Insights from In vivo Studies, *Front. Neurosci.* 11 (2017). https://doi.org/10.3389/fnins.2017.00142.

[219] R. Kalluri, The biology and function of exosomes in cancer, *J. Clin. Invest.* 126 (2016) 1208–1215. https://doi.org/10.1172/JCI81135.

[220] T. Aung, B. Chapuy, D. Vogel, D. Wenzel, M. Oppermann, M. Lahmann, T. Weinhage, K. Menck, T. Hupfeld, R. Koch, L. Trumper, G.G. Wulf, Exosomal evasion of humoral immunotherapy in aggressive B-cell lymphoma modulated by ATP-binding cassette transporter A3, *Proc. Natl. Acad. Sci.* 108 (2011) 15336–15341. https://doi.org/10.1073/pnas.1102855108.

[221] R. Kalluri, V.S. LeBleu, The biology , function , and biomedical applications of exosomes, *Science*, 367 (6478) (2020) eaau6977. https://doi.org/10.1126/science.aau6977.

[222] Y. Zhang, J. Bi, J. Huang, Y. Tang, S. Du, P. Li, Exosome: A Review of Its Classification, Isolation Techniques, Storage, Diagnostic and Targeted Therapy Applications, *Int. J. Nanomedicine.* Volume 15 (2020) 6917–6934. https://doi.org/10.2147/IJN.S264498.

[223] A.G. Bader, D. Brown, M. Winkler, The Promise of MicroRNA Replacement Therapy: Figure 1., *Cancer Res.* 70 (2010) 7027–7030. https://doi.org/10.1158/0008-5472.CAN-10-2010.

[224] J.K.W. Lam, M.Y.T. Chow, Y. Zhang, S.W.S. Leung, siRNA Versus miRNA as Therapeutics for Gene Silencing, *Mol. Ther. - Nucleic Acids.* 4 (2015) e252. https://doi.org/10.1038/mtna.2015.23.

[225] L. Barile, G. Vassalli, Exosomes: Therapy delivery tools and biomarkers of diseases, *Pharmacol. Ther.* 174 (2017) 63–78. https://doi.org/10.1016/j.pharmthera.2017.02.020.

[226] J. Liao, Y. Song, C. Liu, D. Li, H. Zheng, B. Lu, Dual-drug delivery based charge-conversional polymeric micelles for enhanced cellular uptake and combination therapy, *Polym. Chem.* 10 (2019) 5879–5893. https://doi.org/10.1039/C9PY01105F.

[227] K. O'Brien, K. Breyne, S. Ughetto, L.C. Laurent, X.O. Breakefield, RNA delivery by extracellular vesicles in mammalian cells and its applications, *Nat. Rev. Mol. Cell Biol.* 21 (2020) 585–606. https://doi.org/10.1038/s41580-020-0251-y.

[228] X. Zhu, M. Badawi, S. Pomeroy, D.S. Sutaria, Z. Xie, A. Baek, J. Jiang, O.A. Elgamal, X. Mo, K. La Perle, J. Chalmers, T.D. Schmittgen, M.A. Phelps, Comprehensive toxicity and immunogenicity studies reveal minimal effects in mice following sustained dosing of extracellular vesicles derived from HEK293T cells, *J. Extracell. Vesicles.* 6 (2017) 1324730. https://doi.org/10.1080/20013078.2017.1324730.

[229] R.J. Buckanovich, D. Sasaroli, A. O'Brien-Jenkins, J. Botbyl, R. Hammond, D. Katsaros, R. Sandaltzopoulos, L.A. Liotta, P.A. Gimotty, G. Coukos, Tumor Vascular Proteins As Biomarkers in Ovarian Cancer, *J. Clin. Oncol.* 25 (2007) 852–861. https://doi.org/10.1200/JCO.2006.08.8583.

[230] Y.H. Park, H.W. Shin, A.R. Jung, O.S. Kwon, Y.-J. Choi, J. Park, J.Y. Lee, Prostate-specific extracellular vesicles as a novel biomarker in human prostate cancer, *Sci. Rep.* 6 (2016) 30386. https://doi.org/10.1038/srep30386.

[231] J. Fauré, G. Lachenal, M. Court, J. Hirrlinger, C. Chatellard-Causse, B. Blot, J. Grange, G. Schoehn, Y. Goldberg, V. Boyer, F. Kirchhoff, G. Raposo, J. Garin, R. Sadoul, Exosomes are released by cultured cortical neurones, *Mol. Cell. Neurosci*. 31 (2006) 642–648. https://doi.org/10.1016/j.mcn.2005.12.003.

[232] T.F. Bruce, T.J. Slonecki, L. Wang, S. Huang, R.R. Powell, R.K. Marcus, Exosome isolation and purification via hydrophobic interaction chromatography using a polyester, capillary-channeled polymer fiber phase, *Electrophoresis*. 40 (2019) 571–581. https://doi.org/10.1002/elps.201800417.

[233] R. Hou, Y. Li, Z. Sui, H. Yuan, K. Yang, Z. Liang, L. Zhang, Y. Zhang, Advances in exosome isolation methods and their applications in proteomic analysis of biological samples, *Anal. Bioanal. Chem.* 411 (2019) 5351–5361. https://doi.org/10.1007/s00216-019-01982-0.

[234] M.A. Livshits, E. Khomyakova, E.G. Evtushenko, V.N. Lazarev, N.A. Kulemin, S.E. Semina, E. V. Generozov, V.M. Govorun, Isolation of exosomes by differential centrifugation: Theoretical analysis of a commonly used protocol, *Sci. Rep.* 5 (2015) 17319. https://doi.org/10.1038/srep17319.

[235] E. Zeringer, T. Barta, M. Li, A. V. Vlassov, Strategies for Isolation of Exosomes, *Cold Spring Harb. Protoc.* 2015 (2015) pdb.top074476. https://doi.org/10.1101/pdb.top074476.

[236] T. Yamashita, Y. Takahashi, M. Nishikawa, Y. Takakura, Effect of exosome isolation methods on physicochemical properties of exosomes and clearance of exosomes from the blood circulation, *Eur. J. Pharm. Biopharm.* 98 (2016) 1–8. https://doi.org/10.1016/j.ejpb.2015.10.017.

[237] M.Y. Konoshenko, E.A. Lekchnov, A. V. Vlassov, P.P. Laktionov, Isolation of Extracellular Vesicles: General Methodologies and Latest Trends, *Biomed Res. Int*. 2018 (2018) 1–27. https://doi.org/10.1155/2018/8545347.

[238] A.H. Gheinani, M. Vögeli, U. Baumgartner, E. Vassella, A. Draeger, F.C. Burkhard, K. Monastyrskaya, Improved isolation strategies to increase the yield and purity of human urinary exosomes for biomarker discovery, *Sci. Rep.* 8 (2018) 3945. https://doi.org/10.1038/s41598-018-22142-x.

[239] L. Doyle, M. Wang, Overview of Extracellular Vesicles, Their Origin, Composition, Purpose, and Methods for Exosome Isolation and Analysis, *Cells.* 8 (2019) 727. https://doi.org/10.3390/cells8070727.

[240] K. Boriachek, M.K. Masud, C. Palma, H.-P. Phan, Y. Yamauchi, M.S.A. Hossain, N.-T. Nguyen, C. Salomon, M.J.A. Shiddiky, Avoiding Pre-Isolation Step in Exosome Analysis: Direct Isolation and Sensitive Detection of Exosomes Using Gold-Loaded Nanoporous Ferric Oxide Nanozymes, *Anal. Chem.* 91 (2019) 3827–3834. https://doi.org/10.1021/acs.analchem.8b03619.

[241] M.F. Peterson, N. Otoc, J.K. Sethi, A. Gupta, T.J. Antes, Integrated systems for exosome investigation, *Methods.* 87 (2015) 31–45. https://doi.org/10.1016/j.ymeth.2015.04.015.

[242] M.P. Oksvold, A. Neurauter, K.W. Pedersen, Magnetic Bead-Based Isolation of Exosomes, in: 2015: pp. 465–481. https://doi.org/10.1007/978-1-4939-1538-5_27.

[243] N. Zarovni, A. Corrado, P. Guazzi, D. Zocco, E. Lari, G. Radano, J. Muhhina, C. Fondelli, J. Gavrilova, A. Chiesi, Integrated isolation and quantitative analysis of exosome shuttled proteins and nucleic acids using immunocapture approaches, *Methods*. 87 (2015) 46–58. https://doi.org/10.1016/j.ymeth.2015.05.028.

[244] A.T. Reiner, K.W. Witwer, B.W.M. van Balkom, J. de Beer, C. Brodie, R.L. Corteling, S. Gabrielsson, M. Gimona, A.G. Ibrahim, D. de Kleijn, C.P. Lai, J. Lötvall, H.A. del Portillo, I.G. Reischl, M. Riazifar, C. Salomon, H. Tahara, W.S. Toh, M.H.M. Wauben, V.K. Yang, Y. Yang, R.W.Y. Yeo, H. Yin, B. Giebel, E. Rohde, S.K. Lim, Concise Review: Developing Best-Practice Models for the Therapeutic Use of Extracellular Vesicles, *Stem Cells Transl. Med.* 6 (2017) 1730–1739. https://doi.org/10.1002/sctm.17-0055.

[245] A. Liga, A.D.B. Vliegenthart, W. Oosthuyzen, J.W. Dear, M. Kersaudy-Kerhoas, Exosome isolation: a microfluidic road-map, *Lab Chip*. 15 (2015) 2388–2394. https://doi.org/10.1039/C5LC00240K.

[246] R.T. Davies, J. Kim, S.C. Jang, E.-J. Choi, Y.S. Gho, J. Park, Microfluidic filtration system to isolate extracellular vesicles from blood, *Lab Chip*. 12 (2012) 5202. https://doi.org/10.1039/c2lc41006k.

[247] S.M. Santana, M.A. Antonyak, R.A. Cerione, B.J. Kirby, Microfluidic isolation of cancer-cell-derived microvesicles from hetergeneous extracellular shed vesicle populations, *Biomed. Microdevices.* 16 (2014) 869–877. https://doi.org/10.1007/s10544-014-9891-z.

[248] K. Lee, H. Shao, R. Weissleder, H. Lee, Acoustic Purification of Extracellular Microvesicles, *ACS Nano*. 9 (2015) 2321–2327. https://doi.org/10.1021/nn506538f.

[249] G. Raposo, W. Stoorvogel, Extracellular vesicles: Exosomes, microvesicles, and friends, *J. Cell Biol.* 200 (2013) 373–383. https://doi.org/10.1083/jcb.201211138.

[250] X. Li, A.L. Corbett, E. Taatizadeh, N. Tasnim, J.P. Little, C. Garnis, M. Daugaard, E. Guns, M. Hoorfar, I.T.S. Li, Challenges and opportunities in exosome research—Perspectives from biology, engineering, and cancer therapy, *APL Bioeng.* 3 (2019) 011503. https://doi.org/10.1063/1.5087122.

[251] Y. Chen, Q. Zhu, L. Cheng, Y. Wang, M. Li, Q. Yang, L. Hu, D. Lou, J. Li, X. Dong, L.P. Lee, F. Liu, Exosome detection via the ultrafast-isolation system: EXODUS, *Nat. Methods*. 18 (2021) 212–218. https://doi.org/10.1038/s41592-020-01034-x.

[252] A. Mateos-Maroto, I. Abelenda-Núñez, F. Ortega, R.G. Rubio, E. Guzmán, Polyelectrolyte Multilayers on Soft Colloidal Nanosurfaces: A New Life for the Layer-By-Layer Method, *Polymers* (Basel). 13 (2021) 1221. https://doi.org/10.3390/polym13081221.

[253] Y. Lvov, K. Ariga, I. Ichinose, T. Kunitake, Assembly of Multicomponent Protein Films by Means of Electrostatic Layer-by-Layer Adsorption, *J. Am. Chem. Soc.* 117 (1995) 6117–6123. https://doi.org/10.1021/ja00127a026.

[254] S. Kudaibergenov, G. Tatykhanova, N. Bakranov, R. Tursunova, Layer-by-Layer Thin Films and Coatings Containing Metal Nanoparticles in Catalysis, in: Thin Film Process. - Artifacts Surf. Phenom. Technol. Facet., *InTech*, 2017. https://doi.org/10.5772/67215.

[255] J. Schmitt, T. Gruenewald, G. Decher, P.S. Pershan, K. Kjaer, M. Loesche, Internal structure of layer-by-layer adsorbed polyelectrolyte films: a neutron and x-ray reflectivity study, *Macromolecules.* 26 (1993) 7058–7063. https://doi.org/10.1021/ma00077a052.

[256] V. V. Tsukruk, V.N. Bliznyuk, D. Visser, A.L. Campbell, T.J. Bunning, W.W. Adams, Electrostatic Deposition of Polyionic Monolayers on Charged Surfaces †, *Macromolecules*. 30 (1997) 6615–6625. https://doi.org/10.1021/ma961897g.

[257] G. Lvov, Y. M., & Decher, Assembly of multilayer ordered films by alternating adsorption of oppositely charged macromolecules, *Crystallogr. Reports.* 39 (1994) 628–647. https://doi.org/Bibcode: 1994CryRp..39..628L.

[258] G. Decher, Fuzzy Nanoassemblies: Toward Layered Polymeric Multicomposites, *Science* 1997, 277 (5330) 1232–1237. https://doi.org/10.1126/science.277.5330.1232.

[259] L.L. del Mercato, M.M. Ferraro, F. Baldassarre, S. Mancarella, V. Greco, R. Rinaldi, S. Leporatti, Biological applications of LbL multilayer capsules: From drug delivery to sensing, *Adv. Colloid Interface Sci.* 207 (2014) 139–154. https://doi.org/10.1016/j.cis.2014.02.014.

[260] M. Erhola, S. Toyokuni, K. Okada, T. Tanaka, H. Hiai, H. Ochi, K. Uchida, T. Osawa, M.M. Nieminen, H. Alho, P. Kellokumpu-Lehtinen, Biomarker evidence of DNA oxidation in lung cancer patients: association of urinary 8-hydroxy-2′-deoxyguanosine excretion with radiotherapy, chemotherapy, and response to treatment, *FEBS Lett.* 409 (1997) 287–291. https://doi.org/10.1016/S0014-5793(97)00523-1.

[261] R. Alan Mitteer, Y. Wang, J. Shah, S. Gordon, M. Fager, P.-P. Butter, H. Jun Kim, C. Guardiola-Salmeron, A. Carabe-Fernandez, Y. Fan, Proton beam radiation induces DNA damage and cell apoptosis in glioma stem cells through reactive oxygen species., *Sci. Rep.* 5 (2015) 13961. https://doi.org/10.1038/srep13961.

[262] Y.H. Han, S.H. Kim, S.Z. Kim, W.H. Park, Carbonyl cyanide p-(trifluoromethoxy) phenylhydrazone (FCCP) as an O2− generator induces apoptosis via the depletion of intracellular GSH contents in Calu-6 cells, *Lung Cancer.* 63 (2009) 201–209. https://doi.org/10.1016/j.lungcan.2008.05.005.

[263] M. Collado, M. Serrano, Senescence in tumours: evidence from mice and humans, *Nat. Rev. Cancer.* 10 (2010) 51–57. https://doi.org/10.1038/nrc2772.

[264] J.-W. Hyun, G.-J. Cheon, H.-S. Kim, Y.-S. Lee, E.-Y. Choi, B.-H. Yoon, J.-S. Kim, M.-H. Chung, Radiation sensitivity depends on OGG1 activity status in human leukemia cell lines, *Free Radic. Biol. Med.* 32 (2002) 212–220. https://doi.org/10.1016/S0891-5849(01)00793-6.

[265] N.C. de Souza-Pinto, L. Eide, B.A. Hogue, T. Thybo, T. Stevnsner, E. Seeberg, A. Klungland, V.A. Bohr, Repair of 8-oxodeoxyguanosine lesions in mitochondrial dna depends on the oxoguanine dna glycosylase (OGG1) gene and 8-oxoguanine accumulates in the mitochondrial dna of OGG1-defective mice., *Cancer Res.* 61 (2001) 5378–81. http://www.ncbi.nlm.nih.gov/pubmed/11454679.

[266] N.U. Ahmed, M. UEDA, O. NIKAIDO, T. OSAWA, M. ICHIHASHI, High levels of 8-hydroxy-2′-deoxyguanosine appear in normal human epidermis after a single dose of ultraviolet radiation, *Br. J. Dermatol.* 140 (1999) 226–231. https://doi.org/10.1111/j.1365-2133.1999.02653.x.

[267] H.J.T. A D Haegele, P Wolfe, X-radiation induces 8-hydroxy-2'-deoxyguanosine formation in vivo in rat mammary gland DNA, *Carcinogenesis.* 19 (1998) 1319–1321. https://doi.org/10.1093/carcin/19.7.1319.

[268] H.G. Claycamp, K.-K. Ho, Background and Radiation-induced 8-hydroxy-2′-deoxyguanosine in γ-irradiated Escherichia Coli, *Int. J. Radiat. Biol.* 63 (1993) 597–607. https://doi.org/10.1080/09553009314450781.

[269] P.-C. Pao, D. Patnaik, L.A. Watson, F. Gao, L. Pan, J. Wang, C. Adaikkan, J. Penney, H.P. Cam, W.-C. Huang, L. Pantano, A. Lee, A. Nott, T.X. Phan, E. Gjoneska, S. Elmsaouri, S.J. Haggarty, L.-H. Tsai, HDAC1 modulates OGG1-initiated oxidative DNA damage repair in the aging brain and Alzheimer's disease, *Nat. Commun.* 11 (2020) 2484. https://doi.org/10.1038/s41467-020-16361-y.

[270] L. Tinaburri, M. D'Errico, S. Sileno, R. Maurelli, P. Degan, A. Magenta, E. Dellambra, miR-200a Modulates the Expression of the DNA Repair Protein OGG1 Playing a Role in Aging of Primary Human Keratinocytes, *Oxid. Med. Cell. Longev.* 2018 (2018) 1–17. https://doi.org/10.1155/2018/9147326.

[271] T. Yamamori, H. Yasui, M. Yamazumi, Y. Wada, Y. Nakamura, H. Nakamura, O. Inanami, Ionizing radiation induces mitochondrial reactive oxygen species production accompanied by upregulation of mitochondrial electron transport chain function and mitochondrial content under control of the cell cycle checkpoint, *Free Radic. Biol. Med.* 53 (2012) 260–270. https://doi.org/10.1016/j.freeradbiomed.2012.04.033.

[272] M. Ott, V. Gogvadze, S. Orrenius, B. Zhivotovsky, Mitochondria, oxidative stress and cell death, *Apoptosis.* 12 (2007) 913–922. https://doi.org/10.1007/s10495-007-0756-2.

[273] S.M.E. Nugent, C.E. Mothersill, C. Seymour, B. McClean, F.M. Lyng, J.E.J. Murphy, Increased Mitochondrial Mass in Cells with Functionally Compromised Mitochondria after Exposure to both Direct γ Radiation and Bystander Factors, *Radiat. Res.* 168 (2007) 134–142. https://doi.org/10.1667/RR0769.1.

[274] H.-C. Lee, P.-H. Yin, C.-W. Chi, Y.-H. Wei, Increase in mitochondrial mass in human fibroblasts under oxidative stress and during replicative cell senescence., *J. Biomed. Sci.* 9 (2002) 517–26. https://doi.org/10.1007/BF02254978.

[275] F.J. Iborra, H. Kimura, P.R. Cook, The functional organization of mitochondrial genomes in human cells., *BMC Biol.* 2 (2004) 9. https://doi.org/10.1186/1741-7007-2-9.

[276] R.-K. Bai, L.-J.C. Wong, Simultaneous Detection and Quantification of Mitochondrial DNA Deletion(s), Depletion, and Over-Replication in Patients with Mitochondrial Disease, *J. Mol. Diagnostics.* 7 (2005) 613–622. https://doi.org/10.1016/S1525-1578(10)60595-8.

[277] B.M. Gyori, G. Venkatachalam, P.S. Thiagarajan, D. Hsu, M.-V. Clement, OpenComet: An automated tool for comet assay image analysis, *Redox Biol.* 2 (2014) 457–465. https://doi.org/10.1016/j.redox.2013.12.020.

[278] A.Y. Xiao, M.R. Maynard, C.G. Piett, Z.D. Nagel, J.S. Alexander, C.G. Kevil, M. V. Berridge, C.B. Pattillo, L.R. Rosen, S. Miriyala, L. Harrison, Sodium sulfide selectively induces oxidative stress, DNA damage, and mitochondrial dysfunction and radiosensitizes glioblastoma (GBM) cells., *Redox Biol.* 26 (2019) 101220. https://doi.org/10.1016/j.redox.2019.101220.

[279] P. Inc., Partek® Flow® (Version 10.0) [Computer software], (2020). https://www.partek.com/partek-flow/.

[280] L. Chang, G. Zhou, O. Soufan, J. Xia, miRNet 2.0: network-based visual analytics for miRNA functional analysis and systems biology, *Nucleic Acids Res.* 48 (2020) W244–W251. https://doi.org/10.1093/nar/gkaa467.

[281] J. Tchou, V. Bodepudi, S. Shibutani, I. Antoshechkin, J. Miller, A.P. Grollman, F. Johnson, Substrate specificity of Fpg protein. Recognition and cleavage of oxidatively damaged DNA, *J. Biol. Chem.* 269 (1994) 15318–15324. https://doi.org/10.1016/s0021-9258(17)36608-5.

[282] A.F. Palazzo, T.R. Gregory, The Case for Junk DNA, *PloS Genet.* 10 (2014). https://doi.org/10.1371/journal.pgen.1004351.

[283] P. Lei, Y. Li, X. Chen, S. Yang, J. Zhang, Microarray based analysis of microRNA expression in rat cerebral cortex after traumatic brain injury, *Brain Res.* 1284 (2009) 191–201. https://doi.org/10.1016/j.brainres.2009.05.074.

[284] Y. Luo, L. Tong, H. Meng, W. Zhu, L. Guo, T. Wei, J. Zhang, MiR-335 regulates the chemo-radioresistance of small cell lung cancer cells by targeting PARP-1, *Gene*. 600 (2017) 9–15. https://doi.org/10.1016/j.gene.2016.11.031.

[285] Y. Chen, X. Wang, miRDB : an online database for prediction of functional microRNA targets, *Nucleic Acids Res.* 48 (2020) 127–131. https://doi.org/10.1093/nar/gkz757.

[286] D. Szklarczyk, A.L. Gable, D. Lyon, A. Junge, S. Wyder, J. Huerta-cepas, M. Simonovic, N.T. Doncheva, J.H. Morris, P. Bork, L.J. Jensen, C. Von Mering, STRING v11 : protein – protein association networks with increased coverage , supporting functional discovery in genome-wide experimental datasets, *Nucleic Acids Res.* 47 (2019) 607–613. https://doi.org/10.1093/nar/gky1131.

[287] K. Saraste, Antti; Pulkki, Morphologic and biochemical hallmarks of apoptosis, *Cardiovasc. Res.* 45 (2000) 528–537. https://pubmed.ncbi.nlm.nih.gov/10728374/.

[288] J.M. Matés, F.M. Sánchez-Jiménez, Role of reactive oxygen species in apoptosis: Implications for cancer therapy, *Int. J. Biochem. Cell Biol.* 32 (2000) 157–170. https://doi.org/10.1016/S1357-2725(99)00088-6.

[289] K. Daeho, I.-H. Choi, Hydrogen Peroxide Upregulates TNF-Related Apoptosis-Inducing Ligand (TRAIL) Expression in Human AstroglialCells, and Augments Apoptosis of T Cells, *Yonsei Med. J.* 47 (2006) 551–557.

[290] T.L. Denning, H. Takaishi, S.E. Crowe, I. Boldogh, A. Jevnikar, P.B. Ernst, Oxidative stress induces the expression of Fas and Fas ligand and apoptosis in murine intestinal epithelial cells, *Free Radic. Biol. Med.* 33 (2002) 1641–1650. https://doi.org/10.1016/S0891-5849(02)01141-3.

[291] I.H. Kwon, D., Choi, C., Lee, J., Kim, K. O., Kim, J. D., Kim, S. J., & Choi, Hydrogen peroxide triggers the expression of Fas/FasL in astrocytoma cell lines and augments apoptosis, *J. Neuroimmunol.* 113 (2001) 1–9. https://doi.org/10.1016/S0165-5728(00)00321-0.

[292] Z. Ungvari, Z. Tucsek, D. Sosnowska, P. Toth, T. Gautam, A. Podlutsky, A. Csiszar, G. Losonczy, M.N. Valcarcel-Ares, W.E. Sonntag, A. Csiszar, Aging-Induced Dysregulation of Dicer1-Dependent MicroRNA Expression Impairs Angiogenic Capacity of Rat Cerebromicrovascular Endothelial Cells, *Journals Gerontol. Ser. A Biol. Sci. Med. Sci.* 68 (2013) 877–891. https://doi.org/10.1093/gerona/gls242.

[293] M. Mitre, A. Mariga, M. V Chao, HHS Public Access, *Clinical science,* 131 (2017) 13–23. https://doi.org/10.1042/CS20160044.Neurotrophin.

[294] V. Fiorini, F.; Bagchi, D.; Le Hir, H.; Croquette, Human Upf1 is a highly processive RNA helicase and translocase with RNP remodelling activities, *Nat. Commun.* 6 (2015) 1–10. https://doi.org/10.1038/ncomms8581.

[295] M.M. Kucherenko, H.R. Shcherbata, miRNA targeting and alternative splicing in the stress response - Events hosted by membrane-less compartments, *J. Cell Sci.* 131 (2018). https://doi.org/10.1242/jcs.202002.

[296] E. Gobbini, C. Cassani, M. Villa, D. Bonetti, M. Longhese, Functions and regulation of the MRX complex at DNA double-strand breaks, *Microb. Cell.* 3 (2016) 329–337. https://doi.org/10.15698/mic2016.08.517.

[297] A.N. Blackford, S.P. Jackson, ATM, ATR, and DNA-PK: The Trinity at the Heart of the DNA Damage Response, *Mol. Cell.* 66 (2017) 801–817. https://doi.org/10.1016/j.molcel.2017.05.015.

[298] F. d'Adda di Fagagna, A direct role for small non-coding RNAs in DNA damage response, *Trends Cell Biol.* 24 (2014) 171–178. https://doi.org/10.1016/j.tcb.2013.09.008.

[299] S. Francia, M. Cabrini, V. Matti, A. Oldani, F. d'Adda di Fagagna, DICER, DROSHA and DNA damage-response RNAs are necessary for the secondary recruitment of DNA damage response factors, *J. Cell Sci.* (2016). https://doi.org/10.1242/jcs.182188.

[300] E.D. Koval, C. Shaner, P. Zhang, X. Maine, K. Fischer, J. Tay, B.N. Chau, G.F. Wu, T.M. Miller, Method for widespread microRNA-155 inhibition prolongs survival in ALS-model mice, *Hum. Mol. Genet.* 22 (2013) 4127–4135. https://doi.org/10.1093/hmg/ddt261.

[301] A. Junker, M. Krumbholz, S. Eisele, H. Mohan, F. Augstein, R. Bittner, H. Lassmann, H. Wekerle, R. Hohlfeld, E. Meinl, MicroRNA profiling of multiple sclerosis lesions identifies modulators of the regulatory protein CD47, *Brain*. 132 (2009) 3342–3352. https://doi.org/10.1093/brain/awp300.

[302] P.I.D. Urso, O.F.D. Urso, C. Storelli, M. Mallardo, C.D. Gianfreda, A. Montinaro, A. Cimmino, C. Pietro, S. Marsigliante, miR-155 is up-regulated in primary and secondary glioblastoma and promotes tumour growth by inhibiting GABA receptors, *Int. J. Oncol.* (2012) 228–234. https://doi.org/10.3892/ijo.2012.1420.

[303] J.L. Parks, L. Mcneill, M. Frey, A.D. Eaton, A. Haghani, L. Ramirez, M. Edwards, Determination of total chromium in environmental water samples, *Water Res.* 38 (2004) 2827–2838. https://doi.org/10.1016/j.watres.2004.04.024.

[304] A.J. Lee, N.J. Hodges, J.K. Chipman, Interindividual variability in response to sodium dichromate-induced oxidative DNA damage: Role of the Ser326Cys polymorphism in the DNA-repair protein of 8-oxo-7,8-dihydro-2′-deoxyguanosine DNA glycosylase 1, *Cancer Epidemiol. Biomarkers Prev.* 14 (2005) 497–505. https://doi.org/10.1158/1055-9965.EPI-04-0295.

[305] K. Brandhuber, P., Frey, M., McGuire, M.J., Chao, P-F., Seidel, C., Amy, G., Yoon, J., McNeill, L.S., Banerjee, Low-Level Hexavalent Chromium Treatment Options: Bench-Scale Evaluation, *Am. Water Work. Assoc. Res. Found.* Report No. (2004).

[306] H. Lai, L.S. McNeill, Chromium Redox Chemistry in Drinking Water Systems, *J. Environ. Eng.* 132 (2006) 842–851. https://doi.org/10.1061/(ASCE)0733-9372(2006)132:8(842).

[307] ATSDR, ToxGuide for Chromium, 2012. https://www.atsdr.cdc.gov/toxguides/toxguide-7.pdf.

[308] X.A. Cambronne, R. Shen, P.L. Auer, R.H. Goodman, Capturing microRNA targets using an RNA-induced silencing complex (RISC)-trap approach, *Proc. Natl. Acad. Sci.* 109 (2012) 20473–20478. https://doi.org/10.1073/pnas.1218887109.

[309] C. Sticht, C. De La Torre, A. Parveen, N. Gretz, miRWalk: An online resource for prediction of microRNA binding sites, *PLoS One.* 13 (2018) e0206239. https://doi.org/10.1371/journal.pone.0206239.

[310] Y. Chen, X. Wang, miRDB: an online database for prediction of functional microRNA targets, *Nucleic Acids Res.* 48 (2020) D127–D131. https://doi.org/10.1093/nar/gkz757.

[311] V. Agarwal, G.W. Bell, J.-W. Nam, D.P. Bartel, Predicting effective microRNA target sites in mammalian mRNAs, *Elife.* 4 (2015). https://doi.org/10.7554/eLife.05005.

[312] K. Nishioka, T. Ohtsubo, H. Oda, T. Fujiwara, D. Kang, K. Sugimachi, Y. Nakabeppu, Expression and Differential Intracellular Localization of Two Major Forms of Human 8-Oxoguanine DNA Glycosylase Encoded by Alternatively Spliced OGG1 mRNAs, *Mol. Biol. Cell.* 10 (1999) 1637–1652. https://doi.org/10.1091/mbc.10.5.1637.

[313] B.P. Lewis, C.B. Burge, D.P. Bartel, Conserved Seed Pairing, Often Flanked by Adenosines, Indicates that Thousands of Human Genes are MicroRNA Targets, *Cell.* 120 (2005) 15–20. https://doi.org/10.1016/j.cell.2004.12.035.

[314] D. Betel, A. Koppal, P. Agius, C. Sander, C. Leslie, Comprehensive modeling of microRNA targets predicts functional non-conserved and non-canonical sites, *Genome Biol.* 11 (2010) R90. https://doi.org/10.1186/gb-2010-11-8-r90.

[315] R.C. Friedman, K.K.-H. Farh, C.B. Burge, D.P. Bartel, Most mammalian mRNAs are conserved targets of microRNAs, *Genome Res.* 19 (2008) 92–105. https://doi.org/10.1101/gr.082701.108.

[316] J. Lai, H. Yang, Y. Zhu, M. Ruan, Y. Huang, Q. Zhang, MiR-7-5p-mediated downregulation of PARP1 impacts DNA homologous recombination repair and resistance to doxorubicin in small cell lung cancer, *BMC Cancer.* 19 (2019) 1–9. https://doi.org/10.1186/s12885-019-5798-7.

[317] N. Noren Hooten, K. Kompaniez, J. Barnes, A. Lohani, M.K. Evans, Poly(ADP-ribose) polymerase 1 (PARP-1) binds to 8-oxoguanine-DNA glycosylase (OGG1), *J. Biol. Chem.* 286 (2011) 44679–44690. https://doi.org/10.1074/jbc.M111.255869.

[318] M. Masè, M. Grasso, L. Avogaro, E. D'Amato, F. Tessarolo, A. Graffigna, M.A. Denti, F. Ravelli, Selection of reference genes is critical for miRNA expression analysis in human cardiac tissue. A focus on atrial fibrillation, *Sci. Rep.* 7 (2017) 41127. https://doi.org/10.1038/srep41127.

[319] C. Morata-Tarifa, M. Picon-Ruiz, C. Griñan-Lison, H. Boulaiz, M. Perán, M.A. Garcia, J.A. Marchal, Validation of suitable normalizers for miR expression patterns analysis covering tumour heterogeneity, *Sci. Rep.* 7 (2017) 39782. https://doi.org/10.1038/srep39782.

[320] K.J. Livak, T.D. Schmittgen, Analysis of Relative Gene Expression Data Using Real-Time Quantitative PCR and the 2−ΔΔCT Method, *Methods.* 25 (2001) 402–408. https://doi.org/10.1006/meth.2001.1262.

[321] Y. Luo, L. Tong, H. Meng, W. Zhu, L. Guo, T. Wei, J. Zhang, MiR-335 regulates the chemo-radioresistance of small cell lung cancer cells by targeting PARP-1, *Gene.* 600 (2017) 9–15. https://doi.org/10.1016/j.gene.2016.11.031.

[322] H. Bu, S. Wedel, M. Cavinato, P. Jansen-Dürr, MicroRNA Regulation of Oxidative Stress-Induced Cellular Senescence, *Oxid. Med. Cell. Longev.* 2017 (2017) 1–12. https://doi.org/10.1155/2017/2398696.

[323] D.M. Hardbower, T. de Sablet, R. Chaturvedi, K.T. Wilson, Chronic inflammation and oxidative stress, *Gut Microbes.* 4 (2013) 475–481. https://doi.org/10.4161/gmic.25583.

[324] B. Mateescu, L. Batista, M. Cardon, T. Gruosso, Y. de Feraudy, O. Mariani, A. Nicolas, J.-P. Meyniel, P. Cottu, X. Sastre-Garau, F. Mechta-Grigoriou, miR-141 and miR-200a act on ovarian tumorigenesis by controlling oxidative stress response, *Nat. Med.* 17 (2011) 1627–1635. https://doi.org/10.1038/nm.2512.

[325] Subrata Kumar Biswas, Does the Interdependence between Oxidative Stress and Inflammation Explain the Antioxidant Paradox?, *Oxidative Med. Celluar Longev.* 5698931 (2016) 1–9. https://doi.org/10.1155/2016/5698931.

[326] K.H. Hutson, K. Willis, C.D. Nwokwu, M. Maynard, G.G. Nestorova, Neurotoxicology Photon versus proton neurotoxicity : Impact on mitochondrial function and 8-OHdG base-excision repair mechanism in human astrocytes, *Neurotoxicology.* 82 (2021) 158–166. https://doi.org/10.1016/j.neuro.2020.12.011.

[327] J. Konovalova, D. Gerasymchuk, I. Parkkinen, P. Chmielarz, Interplay between MicroRNAs and Oxidative Stress in Neurodegenerative Diseases, *Int. J. Mol. Sci.*, 2019, *20*(23), 6055. https://doi.org/10.3390/ijms20236055 (2019).

[328] Y. Wang, T. Taniguchi, MicroRNAs and DNA damage response, *Cell Cycle.* 12 (2013) 32–42. https://doi.org/10.4161/cc.23051.

[329] V. Sharma, T. Misteli, Non-coding RNAs in DNA damage and repair, *FEBS Lett.* 587 (2013) 1832–1839. https://doi.org/10.1016/j.febslet.2013.05.006.

[330] E. Touati, V. Michel, J.-M. Thiberge, P. Ave, M. Huerre, F. Bourgade, A. Klungland, A. Labigne, Deficiency in OGG1 Protects against Inflammation and Mutagenic Effects Associated with H. pylori Infection in Mouse, *Helicobacter.* 11 (2006) 494–505. https://doi.org/10.1111/j.1523-5378.2006.00442.x.

[331] S.S. Hébert, K. Horré, L. Nicolaï, B. Bergmans, A.S. Papadopoulou, A. Delacourte, B. De Strooper, MicroRNA regulation of Alzheimer's Amyloid precursor protein expression, *Neurobiol. Dis.* 33 (2009) 422–428. https://doi.org/10.1016/j.nbd.2008.11.009.

[332] N. Patel, D. Hoang, N. Miller, S. Ansaloni, Q. Huang, J.T. Rogers, J.C. Lee, A.J. Saunders, MicroRNAs can regulate human APP levels, *Mol. Neurodegener.* 3 (2008) 10. https://doi.org/10.1186/1750-1326-3-10.

[333] N.N. Hooten, M. Fitzpatrick, W.H. Wood, S. De, N. Ejiogu, Y. Zhang, J.A. Mattison, K.G. Becker, A.B. Zonderman, K. Michele, Age-related changes in microRNA levels in serum, *Aging* (Albany. NY). 5 (2013) 725–740. https://doi.org/10.18632/aging.100603.

[334] R.P.L. Panganiban, M.H. Pinkerton, S.Y. Maru, S.J. Jefferson, A.N. Roff, F.T. Ishmael, Differential microRNA epression in asthma and the role of miR-1248 in regulation of IL-5., *Am. J. Clin. Exp. Immunol.* 1 (2012) 154–65. http://www.ncbi.nlm.nih.gov/pubmed/23885321.

[335] S.-I. Jang, M. Tandon, L. Teos, C. Zheng, B.M. Warner, I. Alevizos, Dual function of miR-1248 links interferon induction and calcium signaling defects in Sjögren's syndrome, *EBioMedicine.* 48 (2019) 526–538. https://doi.org/10.1016/j.ebiom.2019.09.010.

[336] T. Yang, M. Li, H. Li, P. Shi, J. Liu, M. Chen, Downregulation of circEPSTI1 represses the proliferation and invasion of non-small cell lung cancer by inhibiting TRIM24 via miR-1248 upregulation, *Biochem. Biophys. Res. Commun.* 530 (2020) 348–354. https://doi.org/10.1016/j.bbrc.2020.06.106.

[337] Raga Krishnakumar; W. Lee Kraus, PARP-1 Regulates Chromatin Structure and Transcription Through a KDM5B-Dependent Pathway, *Mol. Cell.* 39 (2010) 736–749. https://doi.org/10.1016/j.molcel.2010.08.014.

[338] N.A. Lebedeva, N.I. Rechkunova, A. V. Endutkin, O.I. Lavrik, Apurinic/Apyrimidinic Endonuclease 1 and Tyrosyl-DNA Phosphodiesterase 1 Prevent Suicidal Covalent DNA-Protein Crosslink at Apurinic/Apyrimidinic Site, *Front. Cell Dev. Biol.* 8 (2021). https://doi.org/10.3389/fcell.2020.617301.

[339] A. Sinha, S. Katyal, T.M. Kauppinen, PARP-DNA trapping ability of PARP inhibitors jeopardizes astrocyte viability: Implications for CNS disease therapeutics, *Neuropharmacology.* 187 (2021) 108502. https://doi.org/10.1016/j.neuropharm.2021.108502.

[340] V.B. Sampson, S. Yoo, A. Kumar, N.S. Vetter, E.A. Kolb, MicroRNAs and Potential Targets in Osteosarcoma: Review, *Front. Pediatr.* 3 (2015). https://doi.org/10.3389/fped.2015.00069.

[341] B. Zuo, J. Zhu, J. Li, C. Wang, X. Zhao, G. Cai, Z. Li, J. Peng, P. Wang, C. Shen, Y. Huang, J. Xu, X. Zhang, X. Chen, microRNA-103a Functions as a Mechanosensitive microRNA to Inhibit Bone Formation Through Targeting Runx2, *J. Bone Miner. Res.* 30 (2015) 330–345. https://doi.org/10.1002/jbmr.2352.

[342] S. Moncini, A. Salvi, P. Zuccotti, G. Viero, A. Quattrone, S. Barlati, G. De Petro, M. Venturin, P. Riva, The Role of miR-103 and miR-107 in Regulation of CDK5R1 Expression and in Cellular Migration, *PLoS One.* 6 (2011) e20038. https://doi.org/10.1371/journal.pone.0020038.

[343] P.K. Bischof, O., & Puvvula, It Takes Four to Tango: Long Noncoding RNA PANDA, SAF-A, Polycomb Repressive Complexes and NF-Y in Senescence Regulation, *RNA Dis.* (2015). https://doi.org/10.14800/rd.855.

[344] P.T.. Went, A. Lugli, S. Meier, M. Bundi, M. Mirlacher, G. Sauter, S. Dirnhofer, Frequent EpCam protein expression in human carcinomas, *Hum. Pathol.* 35 (2004) 122–128. https://doi.org/10.1016/j.humpath.2003.08.026.

[345] L.P. Lim, N.C. Lau, P. Garrett-Engele, A. Grimson, J.M. Schelter, J. Castle, D.P. Bartel, P.S. Linsley, J.M. Johnson, Microarray analysis shows that some microRNAs downregulate large numbers of target mRNAs, *Nature.* 433 (2005) 769–773. https://doi.org/10.1038/nature03315.

[346] D.D. Taylor, C. Gercel-Taylor, MicroRNA signatures of tumor-derived exosomes as diagnostic biomarkers of ovarian cancer, *Gynecol. Oncol.* 110 (2008) 13–21. https://doi.org/10.1016/j.ygyno.2008.04.033.

[347] Y. Ma, J. Dong, S. Bhattacharjee, S. Wijeratne, M.L. Bruening, G.L. Baker, Increased Protein Sorption in Poly(acrylic acid)-Containing Films through Incorporation of Comb-Like Polymers and Film Adsorption at Low pH and High Ionic Strength, *Langmuir.* 29 (2013) 2946–2954. https://doi.org/10.1021/la305137m.

[348] Y. Lvov, K. Ariga, I. Ichinose, T. Kunitake, Molecular film assembly via layer-by-layer adsorption of oppositely charged macromolecules (linear polymer, protein and clay) and concanavalin A and glycogen, *Thin Solid Films.* 284–285 (1996) 797–801. https://doi.org/10.1016/S0040-6090(95)08449-5.

[349] N.G. Welch, J.A. Scoble, B.W. Muir, P.J. Pigram, Orientation and characterization of immobilized antibodies for improved immunoassays (Review), *Biointerphases.* 12 (2017) 02D301. https://doi.org/10.1116/1.4978435.

[350] V. Sahni, A. Mukhopadhyay, V. Tysseling, A. Hebert, D. Birch, T.L. Mcguire, S.I. Stupp, J.A. Kessler, BMPR1a and BMPR1b Signaling Exert Opposing Effects on Gliosis after Spinal Cord Injury, *J. Neurosci.* 30 (2010) 1839–1855. https://doi.org/10.1523/JNEUROSCI.4459-09.2010.

[351] S.S. Yildirim, D. Akman, D. Catalucci, B. Turan, Relationship Between Downregulation of miRNAs and Increase of Oxidative Stress in the Development of Diabetic Cardiac Dysfunction: Junctin as a Target Protein of miR-1, *Cell Biochem. Biophys.* 67 (2013) 1397–1408. https://doi.org/10.1007/s12013-013-9672-y.

[352] J.O. Okoye, A.A. Ngokere, C.C. Onyenekwe, C.A. Erinle, Comparable expression of miR-let-7b, miR-21, miR-182, miR-145, and p53 in serum and cervical cells: Diagnostic implications for early detection of cervical lesions., *Int. J. Health Sci.* (Qassim). 13 (2019) 29–38. http://www.ncbi.nlm.nih.gov/pubmed/31341453.

[353] L. Duan, L. Xu, X. Xu, Z. Qin, X. Zhou, Y. Xiao, Y. Liang, J. Xia, Exosome-mediated delivery of gene vectors for gene therapy., *Nanoscale.* 13 (2021) 1387–1397. https://doi.org/10.1039/d0nr07622h.

[354] G.G. Shetgaonkar, S.M. Marques, C.E.M. DCruz, R.J.A. Vibhavari, L. Kumar, R.K. Shirodkar, Exosomes as cell-derivative carriers in the diagnosis and treatment of central nervous system diseases, *Drug Deliv. Transl. Res.* (2021). https://doi.org/10.1007/s13346-021-01026-0.

[355] J. Wang, W. Tang, M. Yang, Y. Yin, H. Li, F. Hu, L. Tang, X. Ma, Y. Zhang, Y. Wang, Inflammatory tumor microenvironment responsive neutrophil exosomes-based drug delivery system for targeted glioma therapy, *Biomaterials.* 273 (2021) 120784. https://doi.org/10.1016/j.biomaterials.2021.120784.

[356] G. Dong, J. Dai, L. Jin, H. Shi, F. Wang, C. Zhou, B. Zheng, Y. Guo, D. Xiao, A rapid room-temperature DNA amplification and detection strategy based on nicking endonuclease and catalyzed hairpin assembly, *Anal. Methods*. 11 (2019) 2537–2541. https://doi.org/10.1039/C9AY00507B.

[357] B.D. Rutter, R.W. Innes, Extracellular Vesicles Isolated from the Leaf Apoplast Carry Stress-Response Proteins, *Plant Physiol.* 173 (2017) 728–741. https://doi.org/10.1104/pp.16.01253.

[358] Q. Cai, L. Qiao, M. Wang, B. He, F.-M. Lin, J. Palmquist, S.-D. Huang, H. Jin, Plants send small RNAs in extracellular vesicles to fungal pathogen to silence virulence genes, *Science* (2018). *360* (6393) 1126–1129. https://doi.org/10.1126/science.aar4142.